Assessing the feasibility of utilising tidal stream energy for green ammonia production

Honora Driscoll

Supervisor: Professor René Bañares-Alcántara

A thesis submitted for the degree of
Doctor of Philosophy

New College
Department of Engineering Science
University of Oxford

2026

Abstract

The climate crisis is driving policy makers, energy companies and chemical industries to accelerate the transition from conventional high-carbon ammonia to low-carbon and zero-carbon (green) ammonia. Ammonia is produced on a vast scale globally and is predominantly used for fertilizers but has a potential use as an energy vector and maritime fuel. Utilising variable renewable energy (typically onshore solar or wind) for green ammonia production requires expensive energy storage. Tidal stream energy is a novel energy source for green ammonia production and could be an ideal energy source, given its phasing potential and predictability. This thesis presents the first analysis of green ammonia production using tidal stream energy and the first analysis of green hydrogen and ammonia production using tidal phasing.

A levelized cost of ammonia (LCOA) reduction of up to 18% can be realised for offshore green ammonia production when tidal stream energy is added to offshore wind energy in the Pentland Firth, a high-energy tidal stream energy site. Tidal stream energy is competitive against (or, at least, an ideal complement to) offshore wind energy for onshore green ammonia production in six tidal hotspots around the world, despite offshore wind being a cheaper energy resource.

Tidal stream energy in the Pentland Firth (UK), the Alderney Race (UK), and the Minas Passage (Canada) can deliver an LCOA competitive with conventional green ammonia today. Tidal phasing reduces the LCOA by 6% in the English Channel, with onshore green ammonia production. However, both nearby and high-energy turbine locations are likely required for the phased tidal stream energy LCOA to be competitive with conventional green ammonia or conventional fossil fuel-based ammonia. The predictability aspect of tidal stream energy is

likely to be its most significant advantage over other renewable sources for green ammonia production.

Acknowledgements

Firstly, I am very grateful to my supervisor, Professor René Bañares-Alcántara, for all his encouragement and support throughout the DPhil. I am thankful to have had Holywell House as a place to work, and to have met many welcoming people there. I am also thankful for the colleagues I have met through the women in engineering (WiE) network.

Outside of engineering, I have frequented New College and the Catholic Chaplaincy, which have been essential places of friendship and community.

Without the support of my family, the DPhil would not have been possible. I am grateful for the privilege to have had the opportunity to study at the University of Oxford and do a DPhil in a subject which I am passionate about.

Contents

Chapter 1: Introduction

2020 USD is used in the thesis unless otherwise stated. The GBP to USD exchange rate used is 1.2832 USD/GBP [1] (for 2020). The thesis uses metric units. Moreover, all references to the unit of mass, 1 tonne/ton/t, refer to 1000 kg. The capacity factor is defined as the mean power in a time frame compared to the rated power, with a maximum value of 1 and a minimum value of 0. Unless otherwise stated, the capacity factor refers to an annual value in this thesis.

1.1. Context: Importance of Green Ammonia

This section outlines why it is essential to decarbonise conventional ammonia production, and why ammonia is such an important chemical globally.

1.1.1. Conventional ammonia production

Ammonia (NH_3) is produced via the Haber-Bosch process (est. 1908), and has previously been used for fertilizer and explosives production, which has allowed billions of people to have food but unfortunately has also led to millions dying in wars [2]. Ammonia is conventionally produced from fossil fuels (brown ammonia). In particular, 72% of ammonia is currently produced from natural gas (grey ammonia) and 22% from coal (black ammonia) [3]. The process schematic for ammonia production via natural gas is shown in Figure 1.1(A). The scale and impact of ammonia production is vast - ammonia is the second most produced chemical in the world and accounts for 1% of global greenhouse emissions [3]. In 2020, ammonia production accounted for 5% of global industrial carbon dioxide emissions, and 35% of the global chemical sector's carbon dioxide emissions [4]. Moreover, conventional ammonia production is the most carbon dioxide emissions intensive process per tonne of product, compared to steel, cement, methanol, and other high value chemicals [4]. Ammonia's uses are rapidly expanding from fertilizer and explosives production to use as an energy storage vector, as a hydrogen carrier, for power generation and as a maritime fuel [3].

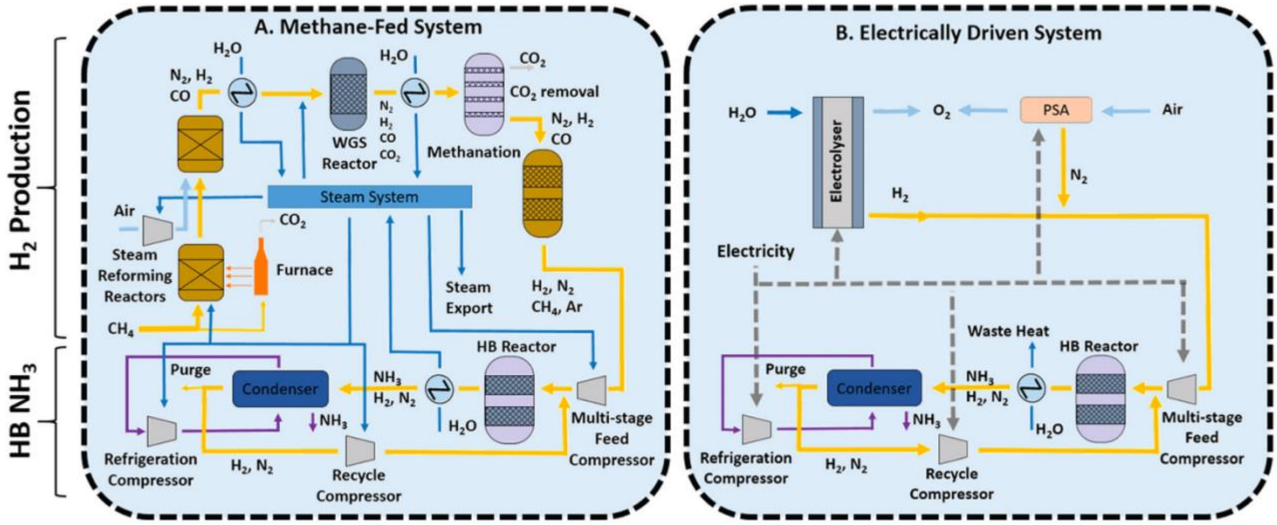

Figure 1.1: Schematic of ammonia production via natural gas (A) and production of green ammonia (B). Reproduced from Ref. [5]

1.1.2. Green ammonia

Since conventional ammonia production has such a large greenhouse gas footprint, it is clear that ammonia production must change in line with the current climate crisis so as to ensure countries meet their net zero targets. New uses of ammonia, as well as an increase in population, will markedly increase global ammonia demand to 688 Mt in 2050 (estimated under a 1.5° temperature increase scenario) from 183 Mt in 2020 [3]. However, current ammonia production methods are not sustainable, with near exclusive production from fossil fuels (i.e. natural gas, coal, heavy fuel oil and naphtha) and negligible production (0.02 Mt/year) from renewable energy (green ammonia) [3]. Conversely, a global green ammonia production capacity of 566 Mt is expected in 2050 (under the 1.5° scenario) [3], i.e. 82% of global ammonia demand in 2050. Thus, the green ammonia production rate must increase rapidly.

Using entirely renewable energy, hydrogen (produced via electrolysis) and nitrogen (produced via air separation) react to form green ammonia (via the Haber-Bosch process) [6]. The process schematic for green ammonia production is shown in Figure 1.1(B). Production of hydrogen via electrolysis allows for more agile production of ammonia, suited for variable renewable energy, compared to using methane reforming reactors, which require more stages as shown in Figure 1.1 [5]. Electrolysis-produced hydrogen is at a lower pressure compared to the conventional Haber-Bosch operating pressure (~150 bar [5]), introducing the need for a new, highly active catalyst for ammonia production under these conditions e.g. Ru (the conventional Fe is significantly less active at low pressures) [7]. Power-to-ammonia is a subgroup of power-to-x systems (where x is hydrogen [8], ammonia [9], methanol, gas [10], methane [11], etc.).

However, there is a gap in knowledge and lack of proved feasibility of variable renewable energy-powered green ammonia plants on a commercial scale (> 500 kt/a) [4]. Today, the LCOA for green ammonia is between 720-1,400 USD/t [3], which is higher than the historical LCOA for conventional ammonia (200-600 USD/t) [12]. For green ammonia to be cost competitive with ammonia produced via natural gas, it has been estimated that electrolyser costs of < 400 USD/kW, electricity prices of < 40 USD/MWh or high natural gas prices of > 34 USD/MWh are required [4].

1.1.3. Ammonia as an energy storage vector

Long-term energy storage is essential for a practical shift to renewable energy from fossil fuels, given the intermittency of renewables [13], yet widespread usage of chemical energy storage vectors is still developing [14]. A cheap, abundant, energy dense (gravimetrically and volumetrically) energy storage vector that can be produced using entirely renewable electricity and used without releasing greenhouse gas emissions is desirable [13]. Thus, carbon-containing energy storage vectors are not desirable (although they are relatively abundant and energy dense). Carbon-free energy storage media include aluminium, hydrogen and ammonia and carbon-containing energy storage media include ethanol, methanol, diesel, gasoline and LPG [15]. Green hydrogen has received immense investment in recent months, particularly in the US, with 7 billion USD allocated for seven clean hydrogen hubs and 1 billion USD allocated for a Clean Hydrogen Electrolysis Program [16].

The properties and variety of uses of ammonia are summarised in a policy briefing by the Royal Society [17]: ammonia has a higher volumetric energy density than hydrogen and is much cheaper to store and transport. On a volume basis, liquid ammonia contains 50% extra hydrogen compared to liquid hydrogen. Ammonia can be transported and cracked back to hydrogen as and when desired for use, e.g. in a PEM fuel cell to produce electricity. Alternatively, ammonia can be used as a transport fuel, directly in combustion engines (e.g. in the shipping industry) or in fuel cells (solid oxide or alkaline). Cesaro et al. [12] studied the use of ammonia for power - ammonia can be combusted in a combined cycle gas turbine to produce electricity via pure ammonia, an ammonia-hydrogen mix or pure hydrogen (produced from ammonia cracking). Transporting ammonia to ultimately produce energy allows ammonia to function as a chemical energy vector.

Ammonia can also be used to store energy. For example, when a variable renewable energy source supplies energy above demand, the excess energy could be used to produce ammonia (instead of curtailing the excess energy) [18]. This ammonia could be sold or converted back to energy, as explained previously, if the renewable energy source cannot meet demand (e.g. at night for solar power or at low wind speeds for wind power).

1.2. Objectives

Green ammonia is ammonia produced using renewable energy, with no direct carbon dioxide emissions. The green ammonia production process is not fully flexible [3], so a steady energy input is ideal. However, renewable energy is usually variable which means expensive energy storage and flexibility (ramping) are required to produce ammonia with the Haber-Bosch process [19]. The Haber-Bosch process can operate at as low as 10-30% of rated capacity [3]. However, the ramp-up rate is slow and thus costly - Fasihi et al. [20] use ramp up and down limits of 2% per hour and 20% per hour respectively.

Planned green ammonia production is dominated by solar and onshore wind (given their low electricity cost [17]), but there is no existing or planned green ammonia production from tidal stream energy [3], despite its desirable predictability. Compared to wind or solar, a predictable power source ensures that less buffer storage is required for ammonia production. Tidal stream power can be accurately forecast far into the future [21]. Tidal stream energy also has the potential to be phased [22] to produce a more consistent power profile (exploiting the difference in the timing of currents in nearby locations). Thus, the **predictability** and **phasing potential** of tidal stream energy make it a unique energy resource for green ammonia production. This thesis aims to assess the feasibility of utilising tidal stream energy for green ammonia production.

Land availability concerns ensure that utilising offshore energy sources for ammonia production onshore or offshore could be attractive [23]. If ammonia is produced onshore, an expensive and inefficient cable from the offshore renewable energy source to the onshore production location is required for electricity transmission [18]. If ammonia is produced offshore, a platform is required near the offshore renewable energy source to produce ammonia, and ammonia is sent to shore, either via ship at around 0.5 USD/t/100 km or via pipeline at 2 USD/t/100 km [24].

Utilising both wind and solar generally gives a high capacity factor (up to 60-70%) and lower ammonia cost compared to utilising wind or solar individually (capacity factor 20-60%) [18], [3]. Thus, combining offshore energy sources could help to enable cost-effective green ammonia.

Tidal stream energy is compared to offshore wind energy as offshore wind energy is a more established and cheaper offshore energy technology [21], but is not predictable in the long and medium term and does not have local phasing potential.

The three objectives of this research are:

1. **To show that tidal stream energy is a useful energy source for green ammonia production.**
2. **To show that tidal stream phasing is beneficial for green ammonia production.**
3. **To show that tidal stream energy is complementary to offshore wind energy for green ammonia production.**

The thesis provides novel research in the areas of green ammonia production from tidal stream energy and tidal phasing for green ammonia and hydrogen production.

1.3. Chapter outline

The literature review in Chapter 2 explores the potential offshore energy sources for green ammonia production, onshore and offshore green ammonia production literature, and explains why tidal stream energy could be promising for green ammonia production, including an explanation of tidal phasing.

The first research chapter, Chapter 3, is a case study on the Pentland Firth. Offshore green ammonia production is focused on, and both offshore wind energy and tidal stream energy are used as energy inputs to a green ammonia plant. This chapter assesses whether tidal stream energy can decrease the levelized cost of ammonia (LCOA) when combined with offshore wind energy. This chapter addresses research objectives 1 and 3. The chapter is the basis of the first-author journal paper, entitled "Technoeconomic evaluation of offshore green ammonia production using tidal and wind energy: a case study" [25].

The second research chapter, Chapter 4, assesses the effect of tidal phasing on onshore green ammonia production, with a case study in the English Channel. The effect of tidal phasing on green hydrogen production is used as a comparison to green ammonia. This chapter addresses research objectives 1 and 2 and is the basis of a first-author conference paper [26]. Turbine locations are selected based on the minimum coefficient of variation of the aggregate power profile. This method is the third method of local tidal phasing for green fuel production presented by the author and was chosen for its accuracy and simplicity. The two other methods, using correlation coefficients and using a genetic algorithm, are presented in two first-author journal papers [27] and [28].

The third and final research chapter, Chapter 5, assesses the benefit of tidal stream energy for onshore green ammonia production in several tidal hotspots around the world, in comparison to the use of offshore wind energy. This chapter implements the main findings from the previous two research chapters in more locations worldwide and is the most realistic in its modelling of tidal stream energy (as wake and blockage effects are incorporated). This chapter addresses research objectives 1 and 3.

The conclusion, Chapter 6, discusses the thesis as a whole, states the main findings and limitations and makes suggestions for further work.

References

[1] "Average Sterling exchange rate: US Dollar," Office for National Statistics. Accessed: Sep. 23, 2025. [Online]. Available: https://www.ons.gov.uk/economy/nationalaccounts/balanceofpayments/timeseries/auss/diop

[2] J. W. Erisman, M. A. Sutton, J. Galloway, Z. Klimont, and W. Winiwarter, "How a century of ammonia synthesis changed the world," *Nat. Geosci.*, vol. 1, no. 10, pp. 636–639, 2008.

[3] IRENA and AEA, "Innovation Outlook: Renewable Ammonia," International Renewable Energy Agency, Abu Dhabi, Ammonia Energy Association, Brooklyn, 2022. [Online]. Available: https://www.irena.org/publications/2022/May/Innovation-Outlook-Renewable-Ammonia

[4] International Energy Agency, "Ammonia Technology Roadmap: Towards more sustainable nitrogen fertiliser production," Paris, France, 2021. [Online]. Available: https://iea.blob.core.windows.net/assets/6ee41bb9-8e81-4b64-8701-2acc064ff6e4/AmmoniaTechnologyRoadmap.pdf

[5] C. Smith, A. K. Hill, and L. Torrente-Murciano, "Current and future role of Haber–Bosch ammonia in a carbon-free energy landscape," *Energy Environ. Sci.*, vol. 13, no. 2, pp. 331–344, 2020.

[6] E. R. Morgan, J. F. Manwell, and J. G. McGowan, "Sustainable Ammonia Production from U.S. Offshore Wind Farms: A Techno-Economic Review," *ACS Sustain. Chem. Eng.*, vol. 5, no. 11, pp. 9554–9567, 2017.

[7] L. Ye, R. Nayak-Luke, R. Bañares-Alcántara, and E. Tsang, "Reaction: '"Green"' Ammonia Production," *Chem*, vol. 3, no. 5, pp. 709–714, 2017.

[8] L. Weimann, P. Gabrielli, A. Boldrini, G. J. Kramer, and M. Gazzani, "Optimal

hydrogen production in a wind-dominated zero-emission energy system," *Adv. Appl. Energy*, vol. 3, p. 100032, 2021.

[9] J. Ikäheimo, J. Kiviluoma, R. Weiss, and H. Holttinen, "Power-to-ammonia in future North European 100 % renewable power and heat system," *Int. J. Hydrogen Energy*, vol. 43, no. 36, pp. 17295–17308, 2018.

[10] A. Crivellari and V. Cozzani, "Offshore renewable energy exploitation strategies in remote areas by power-to-gas and power-to- liquid conversion," *Int. J. Hydrogen Energy*, vol. 45, no. 4, pp. 2936–2953, 2020.

[11] H. Blanco, W. Nijs, J. Ruf, and A. Faaij, "Potential of Power-to-Methane in the EU energy transition to a low carbon system using cost optimization," *Appl. Energy*, vol. 232, pp. 323–340, 2018.

[12] Z. Cesaro, M. Ives, R. Nayak-Luke, M. Mason, and R. Bañares-Alcántara, "Ammonia to power: Forecasting the levelized cost of electricity from green ammonia in large-scale power plants," *Appl. Energy*, vol. 282, p. 116009, 2021.

[13] K. A. Trowell, S. Goroshin, D. L. Frost, and J. M. Bergthorson, "Aluminum and its role as a recyclable, sustainable carrier of renewable energy," *Appl. Energy*, vol. 275, p. 115112, 2020.

[14] Z. Cesaro, R. M. Nayak-Luke, and R. Bañares-Alcántara, "Chapter 2 - Energy Storage Technologies: Power-to-X," in *Techno-Economic Challenges of Green Ammonia as an Energy Vector*, A. Valera-Medina and R. Banares-Alcantara, Eds., Academic Press, 2021, pp. 15–26.

[15] E. R. Morgan, "Fuel Production Systems for Remote Areas via an Aluminum Energy Vector," *Energy & Fuels*, vol. 32, no. 9, pp. 9033–9042, 2018.

[16] "Biden-Harris Administration Announces Regional Clean Hydrogen Hubs to Drive Clean Manufacturing and Jobs," The White House. Accessed: Nov. 02, 2022. [Online].

Available: https://www.whitehouse.gov/briefing-room/statements-releases/2023/10/13/biden-harris-administration-announces-regional-clean-hydrogen-hubs-to-drive-clean-manufacturing-and-jobs/

[17] The Royal Society, "Ammonia: zero-carbon fertiliser, fuel and energy store," London, UK, 2020. [Online]. Available: https://royalsociety.org/-/media/policy/projects/green-ammonia/green-ammonia-policy-briefing.pdf

[18] N. Salmon and R. Bañares-Alcántara, "Green ammonia as a spatial energy vector: a review," *Sustain. Energy Fuels*, vol. 5, no. 11, pp. 2814–2839, 2021.

[19] N. Salmon and R. Bañares-Alcántara, "Impact of grid connectivity on cost and location of green ammonia production: Australia as a case study," *Energy Environ. Sci.*, vol. 14, no. 12, pp. 6655–6671, 2021.

[20] M. Fasihi, R. Weiss, J. Savolainen, and C. Breyer, "Global potential of green ammonia based on hybrid PV-wind power plants," *Appl. Energy*, vol. 294, p. 116170, 2021.

[21] D. Coles, A. Angeloudis, D. Greaves, G. Hastie, M. Lewis, L. Mackie, J. McNaughton, J. Miles, S. Neill, M. Piggott, D. Risch, B. Scott, C. Sparling, T. Stallard, P. Thies, S. Walker, D. White, R. Willden, and B. Williamson, "A review of the UK and British Channel Islands practical tidal stream energy resource," *Proc. R. Soc. A*, vol. 477, no. 2255, p. 20210469, 2021.

[22] S. P. Neill, M. R. Hashemi, and M. J. Lewis, "Optimal phasing of the European tidal stream resource using the greedy algorithm with penalty function," *Energy*, vol. 73, pp. 997–1006, 2014.

[23] N. Salmon and R. Bañares-Alcántara, "Offshore green ammonia synthesis," *Nat. Synth.*, vol. 2, no. 7, pp. 604–611, 2023.

[24] N. Salmon, R. Bañares-Alcántara, and R. Nayak-Luke, "Optimization of green ammonia distribution systems for intercontinental energy transport," *iScience*, vol. 24,

no. 8, p. 102903, 2021.

[25] H. Driscoll, N. Salmon, and R. Bañares-Alcántara, “Technoeconomic evaluation of offshore green ammonia production using tidal and wind energy: a case study,” *Energy Sources, Part A Recover. Util. Environ. Eff.*, vol. 45, no. 3, pp. 7222–7244, 2023.

[26] H. Driscoll, C. Palazzi, and R. Bañares-Alcántara, “The Role of Tidal Stream Energy in Green Ammonia and Green Hydrogen Production in The English Channel,” in *OCEANS 2024 - Halifax*, 2024, pp. 1–4.

[27] H. Driscoll, N. Salmon, and R. Bañares-Alcántara, “Exploiting the temporal characteristics of tidal stream power for green ammonia production,” *Renew. Energy*, vol. 226, p. 120377, 2024.

[28] H. Driscoll, N. Salmon, and R. Bañares-Alcántara, “Optimal phasing of tidal stream power around the British Isles and within the English Channel for green ammonia production,” *Renew. Energy*, vol. 241, p. 122335, 2025.

Chapter 2: Literature review

To appreciate the significance of ammonia production from offshore energy sources, the broader context will be first established and a review of previous work in this area will be conducted. Appropriate renewable energy sources for green ammonia production will be discussed, with an emphasis on offshore renewable energy sources. Then, a thorough review of previous work on ammonia produced offshore (and onshore) from offshore energy sources will be conducted. In addition, the concept of tidal phasing is described, and a critical review of tidal phasing literature is conducted. Finally, wake and blockage effects are outlined in the context of their impact on tidal stream power production. The ultimate aims of this literature review are to determine appropriate offshore energy sources to produce ammonia and to establish why this is of importance on a local and global scale, particularly in this time of climate crisis.

2.1. Methods of offshore energy production

The potential of several offshore energy sources is discussed as a background to the next section (Section 2.2. Production of green ammonia).

2.1.1. Introduction to offshore energy sources for green ammonia production

A common way to produce green ammonia is through onshore solar and/or onshore wind energy, given their low cost [1]. There is also academic and commercial interest in green ammonia production from offshore energy (mainly offshore wind), as described in section 2.2. Determining suitable offshore renewable energy sources for ammonia production worldwide is of great importance because of land availability reasons. An appropriate energy source for green ammonia production should be reliable to enable steady-state ammonia synthesis and able to provide sufficient power to deliver electricity for ammonia production [2]. Several days may be required to get back to appropriate reaction conditions to produce ammonia after stopping production [3], so energy interruptions should be avoided or minimised.

According to Thyssenkrupp, small-scale green ammonia plants produce 50-300 tons/day of ammonia [4], which corresponds to around 25-150 MW of power input [2]. Thus, an appropriate offshore energy source for green ammonia production should be able to provide > 25 MW of power.

The key details of the most relevant offshore energy sources are discussed in this section. Figure 2.1 displays the schematics of the six offshore energy sources that are focussed on, and Table 2.1 displays their worldwide potential electricity production. Offshore wind has the largest worldwide electricity potential as shown in Table 2.1. However, for successful ammonia production offshore, other factors such as the reliability and the technological maturity of the energy source must also be taken into account.

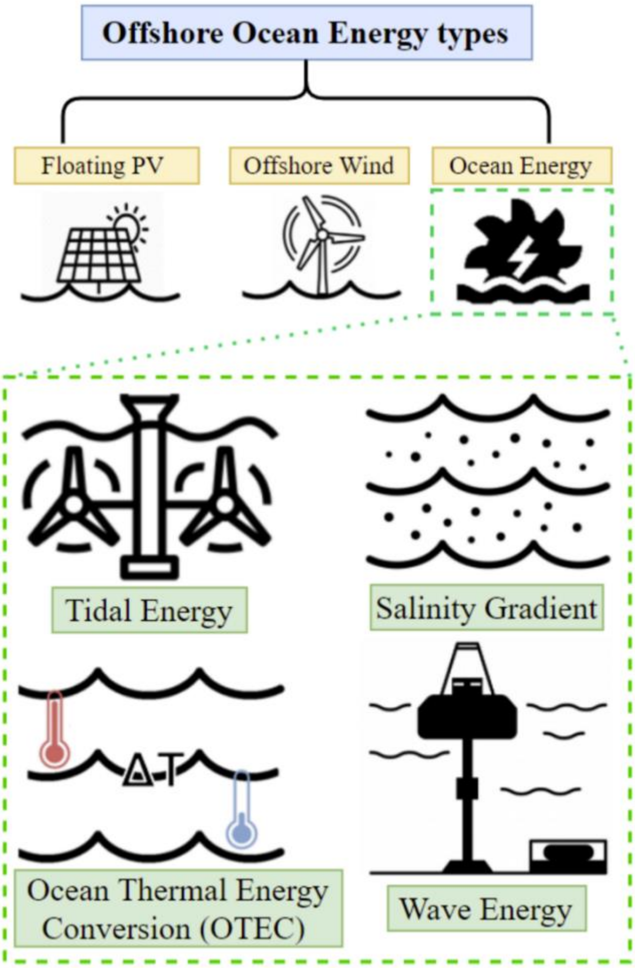

Figure 2.1: The six offshore energy sources discussed in this section [5]

Table 2.1: Worldwide potential electricity production from different offshore energy sources

Energy source	***TWh/year***	***Reference***
Wave Power	8,000-80,000	[6]
Osmotic (Salinity Gradient)	2,000	[6]
OTEC (Ocean Thermal Energy Conversion)	10,000	[6]
Tidal Stream	800	[6]
Offshore Wind (total technical potential)	420,000	[7]
Offshore Wind in water depths of < 60 m (technical potential)	87,000	[7]
Offshore Wind in water depths of > 60 m (technical potential)	330,000	[7]
Floating solar on freshwater man-made reservoirs	520-5,200	[8]

2.1.2. Wave power

Wave power was originally researched in the 18th century, and the primary patent in this area was granted in 1799 [9]. Worldwide wave power potential is shown in Table 2.1- a small fraction of this potential power is utilised at present [10]. Moreover, compared to nearshore wave energy, offshore wave energy has a higher wave power potential but is less exploitable and would require a longer, more expensive, transmission line to land and to the grid [11].

Compared to other renewable energy sources, wave energy has the largest energy density and is very predictable [12]. However, wave energy harvesting is less developed compared to other renewable energies [11]. There are many different wave power devices, including power absorbers, overtopping devices, oscillating water columns, attenuators, oscillating wave surge converters, submerged pressure differential devices, rotating mass devices and bulge head wave energy converters [11].

2.1.3. Osmotic power

Seawater and freshwater have a salinity gradient which can be exploited to generate power [13]. In an osmotic power plant (Figure 2.2), freshwater transfers across a semi-permeable membrane to dilute seawater as a result of osmosis, increasing the pressure of the seawater [14]. The pressurised seawater turns a turbine, generating power. Some of the pressurised seawater is used to increase the pressure of the seawater entering the membrane in a pressure exchanger [14].

Osmotic power can be utilised wherever freshwater and saltwater meet and is particularly of use in coastal regions. Moreover, osmotic power is not subject to intermittency, i.e. osmotic power can be operated continuously. A major difficulty with utilising the vast potential of osmotic power (displayed in Table 2.1) is scaling up the membrane to millions of m^2 for commercial use [13].

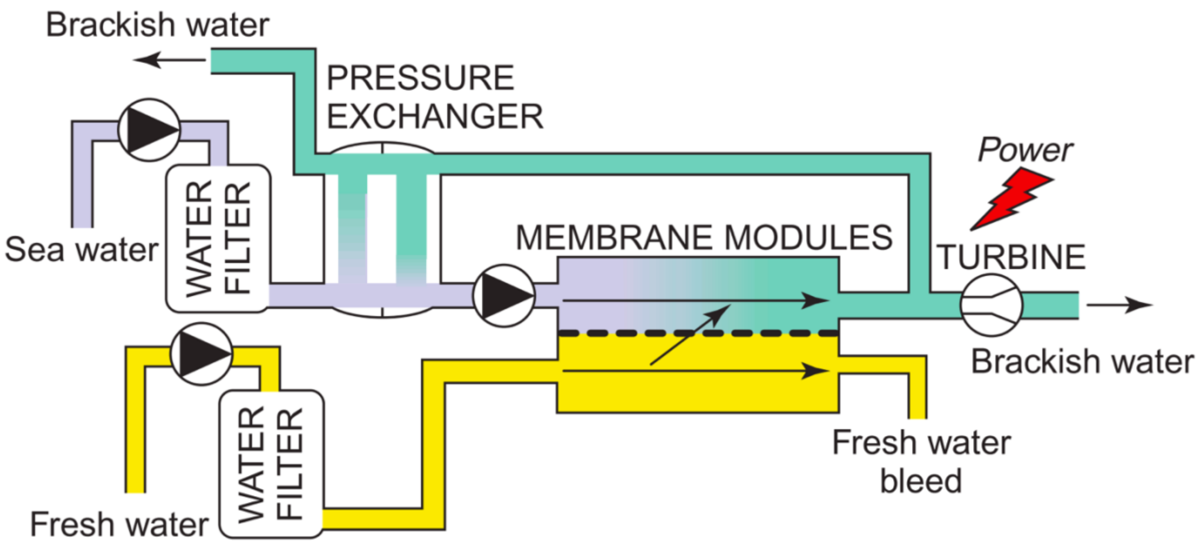

Figure 2.2: Osmotic power plant schematic [14]

2.1.4. OTEC

Ocean thermal energy conversion (OTEC) harnesses the difference in temperature (> 20°C) between the hotter surface ocean water and colder water below to generate power via a heat engine [15]. Herrera et al. [16] recently published a review, in which the economic viability of OTEC was evaluated: OTEC technology has a prohibitively large infrastructure and installation cost and a prohibitively small efficiency of 3-9% and yet the source of energy (the ocean) is practically unbounded. Effective use of OTEC to produce electricity is mostly confined to equatorial latitudes. Moreover, if desalinated water can be sold from OTEC plants, as well as electricity or ammonia (on ammonia OTEC plant-ships), it may increase the plant's viability.

2.1.5. Tidal Power

Tidal power is split into tidal range and tidal stream, of which the latter is the more heavily researched given the smaller price of installation and minimal negative effect on the surrounding environment [17][18]. Tidal range power exploits the water level variation with the tides and tidal stream power exploits the kinetic energy from tidal currents. Within tidal stream energy, usually tidal turbines are used but other, less common, technologies are also researched e.g. oscillating hydrofoils or tidal kites. The most common type of tidal turbine is an axial turbine, with cross-flow turbines second (Figure 2.3) [18]. The thesis focuses on the axial turbine – hereafter referred to as 'tidal turbine'. Tidal stream energy in the UK has a large practical resource potential of between 11.5-15 GW [19], [20].

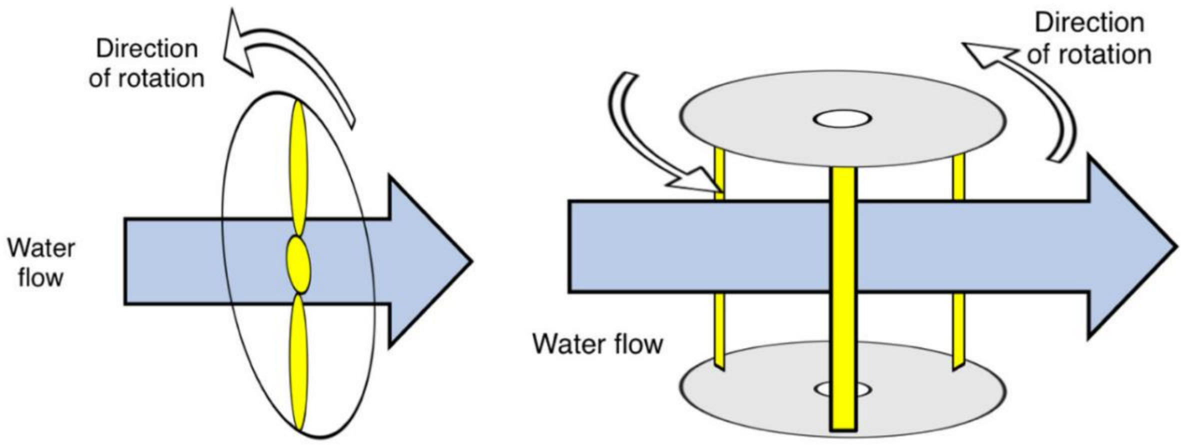

Figure 2.3: Axial turbine (left) and cross-flow turbine (right) [18].

The extractable power, P, from a turbine is:

$$P = \frac{1}{2}\rho A C_p u^3$$

where ρ is density of water, A is device swept area, C_p is turbine power coefficient, u is the free-stream flow speed [18].

Tidal turbines are a very promising technology, they are similar to wind turbines although they are powered by strong tidal currents, and since water is over 800 times denser than air, the blade diameter is shorter [21], [22]. Figure 2.4 shows the evolution of tidal turbines in recent years. Due to their high power capacity, the two turbine types that should be highlighted are the AR2000, a fixed-bottom 2 MW turbine (second from the right), and the Orbital O2, a floating 2 MW turbine (first from the right) [23].

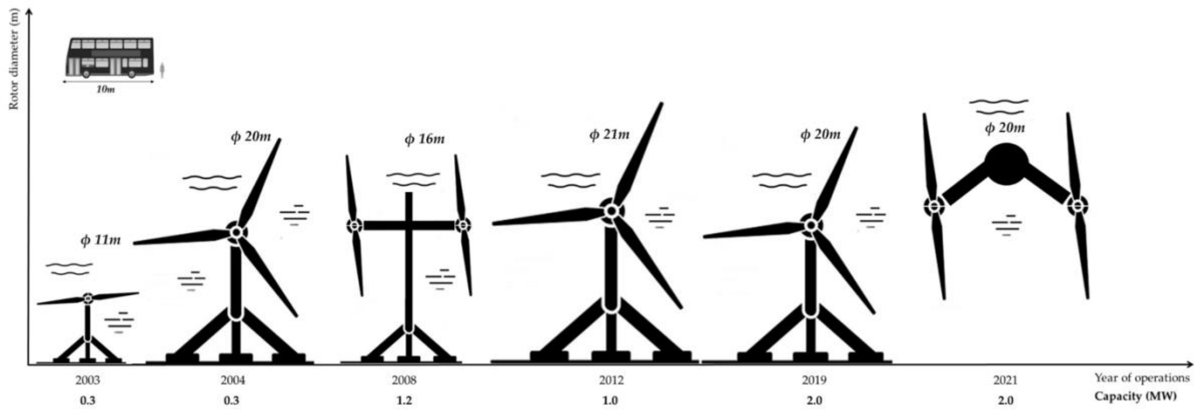

Figure 2.4: Evolution of tidal turbines [23]. Ø refers to rotor diameter.

Coles et al. [19] recently reviewed the potential of tidal stream energy implementation in the UK – the financial and practical assessment is discussed here.

In the UK today, the levelized cost of energy (LCOE) is 240 GBP/MWh for tidal stream energy and 80 GBP/MWh for offshore wind energy. Moreover, by 2031 in the UK, the predicted LCOE for tidal stream energy is 150 GBP/MWh, which is still three times larger than offshore wind (LCOE of around 50 GBP/MWh). However, the predictability of tidal energy is financially appealing, especially since there is a rise in variable renewable energy on the grid which will require supply-demand balancing and significant storage.

From a practical point of view, tidal turbines have a lower variation in capacity factor than wind turbines. For example, tidal turbines have a ±10% variation within a year. Additionally, tidal turbines do not pose a significant risk to the surrounding marine environment (i.e. minimal or no habitat disruption or marine life collisions with turbines) [19].

The Pentland Firth in Scotland is an exceptionally good tidal stream location, as explained in section 3.1.1. Water depths in the Pentland Firth are between 30 m and around 80 m, which are relatively shallow [24].

According to Almoghayer et al., to use tidal turbines effectively the tidal turbine type should be chosen appropriately for the area of operation, and both the array configuration and power regulation should be optimized [25]. In section 2.4., the tidal array layout is discussed in more detail, as it is an integral part of tidal power extraction.

The turbine power curve incorporates both the cut-in velocity and the rated velocity, and it will differ depending on the type of turbine. If the power curve for a specific turbine is not known, a standardised power curve is valuable. Lewis et al. [26] determined a standardised power curve from 14 of the most relevant tidal-stream turbines (Figure 2.5).

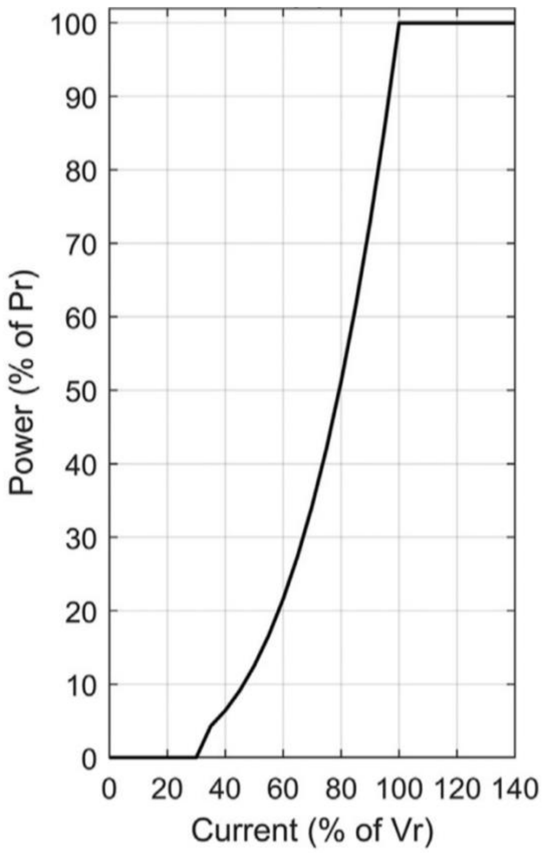

Figure 2.5: Standardised tidal turbine power curve, adapted from [26]. Vr is rated speed and Pr is rated power.

The global deployment capacity of tidal stream energy is currently very low. The active installed tidal stream capacity around the world is 10.1 MW in the UK, 1.7 MW in China, 1.29 MW in the Netherlands, 1 MW in France, 0.7 MW in Canada, and 0.5 MW in Japan [27]. Thus, the UK has the largest active installed tidal stream capacity in the world (66% of the global total). In September 2023, 53.04 MW of tidal stream capacity was secured in Scotland and Wales in the Contracts for Difference (CfD) Allocation Round 5 at a strike price of £198.00/MWh, for delivery between 2026-2028 [28]. Moreover, in September 2024, a further 28 MW was outlined in Allocation Round 6 at £172.00/MWh, for delivery by 2029 [29]. Thus, the recent investment in tidal stream energy in the UK proves that it is an important renewable energy technology and that large-scale deployment is possible.

Remarkably, there is no active installed tidal stream capacity in the US, although 5.08 MW is under development [27]. The main tidal stream energy hotspots in the US are in the Salish Sea, Washington [30], the Cook Inlet, Alaska [31] and the Western Passage, Maine [32]. The Salish Sea and the Western Passage are both on the US/Canada border (bordering Vancouver Island and the Bay of Fundy, respectively). The main global tidal stream energy hotspots are shown in Figure 2.6.

Figure 2.6: Global tidal stream energy hotspots [27].

The energy resource estimate (in GW) of tidal stream energy in the UK will be constant or locally increase slightly with climate change [33]. However, climate change will either lower the offshore wind energy resource in the UK or make it more variable, or both [34]. Large-scale tidal stream energy extraction can affect marine current patterns (both accelerating and decelerating) and tidal elevation (both increasing and decreasing) [33]. In some locations, the increase in tidal elevation due to climate change can be counteracted by the decrease in tidal elevation due to tidal energy extraction, such as the east coast of the UK, which is beneficial for coastal defence [33].

2.1.6. Wind Energy

Wind energy is a key technology to help avoid the worst effects of climate change but is not a silver bullet. Wind energy made up 6-7 % of worldwide electricity in 2021 [35]. Furthermore, installed capacity of wind is expected to be between 5,000-8,200 GW by 2050 [35].

The large and stable wind speeds offshore compared to onshore are attractive for offshore wind exploitation and subsequent power generation e.g. using floating offshore wind turbines [36]. Moreover, there are abundant regions in the ocean that are suitable and untapped for offshore wind development [37]. The larger wind speeds over the ocean compared to the land are partly due to the lower surface roughness of water [36]. Within offshore wind, fixed-bottom structures are the most common type of structure which operate at water depths of < 60 m, additionally floating structures can operate at water depths of > 60 m [38], but are currently more expensive than fixed-bottom turbines [39].

Offshore wind is variable on different time scales – sub-hourly, hourly, diurnally, seasonally (winter versus summer), interannually [43], and across multiple decades [44]. The hourly variability of wind is particularly important to note due to the ramping constraints of the Haber-Bosch (addressed in Section E.9 of Appendix E). Moreover, wind droughts (low wind speeds for a sustained interval of time) can occur, which could last for a number of weeks [45].

The LCOE of wind energy has reduced rapidly over recent years, and by 2050, compared to 2019, fixed-bottom offshore wind and onshore wind are expected to decrease by up to 49% and 37% respectively [39]. Moreover, offshore wind is projected to cost < 50 USD/MWh by 2050 worldwide [39]. Offshore wind is more expensive than onshore wind due to more complicated planning, construction, maintenance and grid connection [37]. However, mass deployment of offshore wind can reduce the cost of electricity from wind, which is economically attractive on a national scale [40].

Several other factors must be considered when implementing offshore wind or other forms of offshore energy. For example, the seafood industry may be adversely affected by offshore wind since fishing locations may have to be relocated [40]. The wider impacts of producing wind turbines must also be considered, such as the availability of large quantities of input materials (concrete, steel and iron, polymer materials, fiberglass, etc.) [41]. Moreover, wind turbines can last around 25 years [42] and up to 90 % of a wind turbine is recyclable at present [35].

2.1.7. Floating Solar

Solar energy has enormous worldwide potential to provide renewable electricity. Competing uses for land has motivated the use of floating photovoltaic (FPV) systems on water as opposed to land-based solar energy [46]. FPV systems have a high efficiency due to convection cooling from the surrounding water [47]. FPV systems have been applied almost exclusively to freshwater locations, and seldom to oceans. However, oceans occupy 70% of global area [47], so the resource potential for ocean FPV is likely to be significantly larger than for freshwater FPV (Table 2.1). Saltwater corrosion and constant wave and wind loads require the ocean FPV structure to be made of strong materials, for example HDPE or galvanized steel [47].

2.2. Production of green ammonia

To understand the current landscape of ammonia production from offshore energy sources, a review of previous work is conducted and gaps in the literature are discussed.

2.2.1. OTEC ammonia plant-ships

The first idea of producing ammonia offshore by harnessing the energy from the ocean was published in the 1970s [15]. In summary, the power required for the process is entirely from OTEC and the ammonia is produced on a plant-ship which has a concrete hull and the platform moves at ~0.5 knot. Ammonia OTEC plant-ships would produce ammonia via the Haber-Bosch process and the reactants, hydrogen and nitrogen, would be produced via water electrolysis and air separation, respectively. Subsequent research has not led to any commercial or large-scale pilot OTEC plants, partially due to the high LCOE [48].

George and Richards of the Applied Physics Laboratory in Johns Hopkins University produced a detailed 40 MW OTEC plant design of a slow moving plant-ship which forms an "energy-intensive product" [49]. Panchal et al. [50] built on the design of George and Richards' plant-ship where the overall cost of ammonia production is 1,066 USD/ton (2005 USD). Moreover, the design of a satellite plant-ship arrangement was reported by Panchal et al. whereby separate OTEC plants deliver energy to a single 2,000-3,000 ton/day ammonia plant (using solid-state ammonia synthesis rather than Haber-Bosch) and the ammonia cost is 755 USD/ton (2005 USD).

2.2.2. Production of ammonia onshore from offshore wind

The first techno-economic analysis of ammonia produced via offshore wind was in 2013 in a Ph.D thesis by Morgan [51], with onshore ammonia production and grid support. Morgan and co-workers have done further research in this area, including looking at ammonia production from wind on a small island in the Gulf of Maine to make the island less reliant on diesel for boats and for electricity [52]. However, this model is fairly unrealistic given the cost of boat engine conversion (to ammonia) and inadequate infrastructure on the island to facilitate the wind turbine and ammonia plant construction (e.g. roads) [52]. Morgan et al. [2] later presented a simple, steady-state model of a grid-supported offshore wind powered ammonia plant in the Gulf of Maine whereby the LCOA is 1,224 USD/ton (2010 USD), which is not cost competitive with conventional ammonia, and the ammonia is produced onshore. The design of the offshore wind farm could be more detailed, e.g. by factoring in the depth of the water which affects the cost and type of the wind turbine platform [38] (the wind farm modelled is "generic", not designed for the Gulf of Maine specifically [2]).

2.2.3. Production of ammonia offshore from offshore energy

Producing ammonia offshore from offshore energy has scarcely been researched, apart from a handful of offshore wind (and solar) production studies. Most notably, Salmon and Bañares-Alcántara [53] determined locations worldwide which could economically produce green ammonia offshore via offshore wind and solar while factoring land limitations and infrastructure requirements. This work illustrated that, due to the UK's low land availability, offshore ammonia production is particularly attractive for the UK – up to 100% of its ammonia could be produced offshore. Wang et al. [54] performed a detailed design optimization for offshore ammonia production, which determined the scenarios in which the Levelized Cost of Ammonia (LCOA), using offshore wind, is competitive with a reference green ammonia LCOA from 2020. However, this work did not consider specific geographical locations, rather an average of Pacific, Atlantic, and Gulf offshore regions. Thommessen et al. [55] present an offshore ammonia energy hub system powered by offshore wind and located in the North Sea.

The efficiency of ammonia production, storage and transport is estimated. This study does not perform an optimization or thorough cost analysis of the energy hub or wind turbine; for example, they do not report platform cost.

The fourth notable paper is by Parmar et al. [3] who look at an ammonia plant-ship, with several ammonia synthesis plants, powered by offshore wind off the coast of Massachusetts (this paper was based on a Master's Thesis by Parmar [56]). When there are low periods of power from offshore wind, ammonia can be combusted to facilitate plant idling (as there is no grid connection). The optimized scenario is when two ammonia synthesis plants are used whereby the LCOA is 1,566 USD/ton (2018 USD) which is clearly too high for commercial use, furthermore, only around 67.5% of the capacity (300 tons/day, 330 days a year) is produced annually. The dimensions of the plant-ship were based on Panchal et al. [50] whereas most of the costs of the offshore wind farm and ammonia plant sections were based on Morgan [51].

In a Master's Thesis by Maia [57], different scenarios of offshore wind powered green ammonia production in the North Sea were investigated. The four scenarios were: offshore ammonia production with transport of ammonia to shore by pipeline and secondly by shipping, then offshore hydrogen production - transported to shore via pipeline for onshore ammonia production using grid electricity and finally transmission of electricity from an offshore wind farm to an onshore ammonia plant. In each scenario, the costs of implementation of alkaline and solid oxide electrolysers were considered. Offshore in this context means production of hydrogen/ammonia on a sand island, 380 km from the coast of Denmark. Moreover, the use of a floating structure for the ammonia plant and the wind turbines was not considered. The LCOA in each case was determined – the lowest of which was ammonia produced offshore with transport to shore via ship and using a solid oxide electrolyser (the resulting LCOA was 387-

574 EUR/ton in 2030). Moreover, ammonia produced entirely offshore permits a higher overall production efficiency (~65%) and higher total production of ammonia (after 20 years) compared to onshore production.

It should be noted that Salmon and Bañares-Alcántara [53] are the only authors that consider both offshore wind and offshore solar as the offshore energy source. All other studies discussed in section 2.2.3. only consider offshore wind.

2.2.4. Ammonia production on a marine platform and onboard a vessel

There are proposed commercial projects for green ammonia and green hydrogen production offshore using offshore wind as an energy source. For example, in Shetland, Scotland, Aker Offshore Wind are planning a 10 GW floating offshore wind project for 2030, with green hydrogen production on a floating offshore platform, which is transferred to shore via pipeline for green ammonia production onshore [58]. Enterprize Energy propose a 3.4 GW offshore wind project, producing 1.5 million tonnes of green ammonia per year on an offshore platform in Vietnam [59].

The P2XFloater™, designed by H2Carrier, would be able to produce green ammonia onboard a vessel (by converting Very Large Gas Carriers) at an industrial scale, which is a global first. 334 ton/day of ammonia can be produced, with 140 MW electrolyser capacity. The P2XFloater™ exploits renewable energy (wind, solar or hydro energy) when it is inexpensive, depending on the location and the time of year [60].

2.2.5. Green ammonia production from tidal stream energy

To the best of the author's knowledge, there is no publicly available research nor commercial or small-scale testing plants for ammonia production offshore or onshore using tidal stream turbines as an energy source. However, the broad concept of green ammonia production from a tidal lagoon is reported in the literature [61], [62].

The main advantage of tidal stream power is that it is a predictable renewable energy source, which is ideal for green ammonia production as the green ammonia plant can operate with perfect forecasting of input power. Thus, additional CAPEX costs from equipment oversizing and additional OPEX costs from model predictive control (MPC) can be avoided. Equipment oversizing and MPC are necessary for green ammonia production from unpredictable energy sources such as wind [63].

The novelty, predictability and phasing potential (discussed in the next section) of tidal stream energy are the reasons why it is the energy resource focussed on in this thesis for green ammonia production.

2.2.5.1. Grid limitations for tidal stream power hotspots

Some tidal stream power hotspots in the UK are far from the grid (so require new transmission cables to the grid onshore) or are in locations where the grid is constrained (which limits their exploitability). For example, the nearest grid connection to tidal sites in the North Channel of the Irish Sea is via the 132 kV transmission cable in Carradale [64][65] (around 40 km away), on the Kintyre peninsula, Scotland. Moreover, Orkney has significant grid capacity constraints, with only two 20 MW 33 kV cables to mainland Scotland [25]. Even with the new 220 MW transmission link from Orkney to mainland Scotland (Caithness) [66], Orkney is grid-constrained. Orkney has a large surplus of tidal stream energy (and wind energy) that cannot be used within the archipelago as it is sparsely populated [19][25].

Producing green ammonia, an energy vector and hydrogen carrier, from tidal stream sites locally has the potential to improve or enable their exploitation. The green ammonia produced can then be combusted for energy at peak demand, used as the basis for fertilizer production, used as a maritime fuel, and/or transported to where it is needed.

2.2.5.2. Green hydrogen production from tidal stream energy

Green hydrogen has been produced onshore using tidal stream energy. The world's first [67] green hydrogen project utilising tidal stream energy (as well as a 0.9 MW onshore wind turbine and a 1.8MWh vanadium flow battery module [68]) was deployed at the European Marine Energy Centre's tidal test site in Eday, Orkney. A new Orbital O2 tidal turbine and another storage device will be added to the site in the FORWARD2030 (Fast-tracking Offshore Renewable energy With Advanced Research to Deploy 2030MW of tidal energy before 2030) project [69]. A separate tidal stream energy-green hydrogen project has been proposed in Shetland (without wind/batteries) - the Green Hydrogen and Oxygen Supply from Tidal Energy (GHOST) project [70].

Green ammonia production in the Orkney Islands has also been proposed - Eneus Energy have planning permission for the first commercial green ammonia/hydrogen plant in Britain, powered by onshore wind [71].

Tidal stream-produced green hydrogen was suggested as an attractive opportunity over two decades ago [72]. There are a small number of academic studies on hydrogen production from tidal stream energy coupled with other energy sources (such as wind) and grid back-up [73][74][75] and one study on hydrogen production from just tidal stream energy with grid back-up [76]. Ewan and Allen [77] determined hydrogen production costs from fourteen routes (renewable and non-renewable), including tidal stream energy. However, the costs are outdated, generic, and do not incorporate input hourly power profiles. Additionally, Rinaldi et al. [78] presented a brief conference paper on producing hydrogen from a floating tidal farm. Thus, there are no detailed tidal stream-only green hydrogen analyses to date.

2.3. Tidal Phasing

To understand why and how tidal phasing could be useful for green ammonia production, the concept of tidal phasing is explained, and tidal phasing literature is discussed.

2.3.1. Tidal phasing literature

The waters around the UK abide by a semi-diurnal system due to the prominent tidal constituents: M2[1], the lunar constituent (360° period of 12 h 25 min) and S2[2], the solar constituent (360° period of 12 h) [79]. Tidal stream currents are subject to a flood-ebb cycle[3], a spring-neap cycle[4] and an 18.6-year lunar cycle[5] [19]. There is a significant tidal power phase difference along the UK coastline – near firm power could be achieved if three tidal sites with a phase difference of 120° (~4h) are exploited together [80] or if two tidal sites with a phase difference of 90° (~3h) are exploited together [81]. Determining appropriate sites for firm power is challenging as the bathymetry and the British Isles topology significantly impact the tidal stream power phase difference [81].

The most established and most powerful tidal stream devices, first-generation devices, are restricted to water depths of 25-50 m and mean peak spring velocities of >2.5 m/s [81]. Firm power production from sites with first-generation tidal devices around the UK is not possible, as these sites happen to be mostly in-phase [81]. However, less powerful tidal stream sites around the UK have significant phase diversity [82]. For example, the co-tidal lines vary

[1] Semi-diurnal lunar tidal constituent [121]. M is for moon, 2 is for 2 peaks per day.
[2] Semi-diurnal solar tidal constituent [121]. S is for sun, 2 is for 2 peaks per day.
[3] ~12-hour cycle in the UK - this means one flood tide and one ebb tide every ~12 hours [19]. The ebb direction is seaward, and the flood direction is inland [122].
[4] Fortnightly cycle – this means one spring tide and one neap tide every 14 days. The spring tide (the largest tidal range and fastest tidal stream velocities) occurs when the Sun, Earth and Moon are aligned. The neap tide (the lowest tidal range and slowest tidal stream velocities) occurs when the Sun, Earth and Moon are perpendicular [19], [121].
[5] Due to variation in the "inclination of the Moon's orbital path relative to the plane of the Earth's equator" [121]

considerably (6-11h) in the relatively small body of water between the north of Northern Ireland and Scotland (North Channel of the Irish Sea) [81][79]. Co-tidal lines are lines on a map that display the time of high water, which is indicative of the phasing of tidal velocities.

Academic studies on tidal phasing have modelled tidal sites around the UK [83][84][81][82][85][86][87], around Ireland [88], around West Japan [89] and around the states of Washington and Alaska in the US [90]. For example, Neill et al. [84] used the greedy algorithm to find the optimal phasing of combined tidal stream sites in the Pentland Firth, the English Channel (around the Channel Islands), the North Sea (around Flamborough Head), the North Channel and around the Faroe Islands. The sites that optimise the average power and avoid near-zero power periods are determined as the Pentland Firth, the Channel Islands and Anglesey (locations shown in Figure 2.7).

Iyer et al. [81] modelled first-generation tidal sites in the Isle of Wight, the Race of Alderney, Ramsey Island, Anglesey, Islay, Orkney and the Pentland Firth and determined that the combined maximum environmentally acceptable power is around 2 GW. Interestingly, all of these sites are mainly in phase, apart from the Race of Alderney, which has a phase difference of around 1 h.

Lewis et al. [87] reported that utilising peak spring tide velocities >1.5 m/s with no water depth restrictions could enable firm tidal power production in the Irish Sea. The Irish Sea has many areas of substantial tidal potential, including Anglesey, Isle of Man and the Bristol Channel [87]. For example, in the Irish Sea, over seven times less practical power is exploitable for 1st generation turbines, compared to 3rd generation turbines (i.e. utilising mean peak spring velocities > 1.5 m/s and water depths > 25 m). Lewis et al. [87] also highlight that misalignment of flood and ebb currents can introduce significant uncertainty in tidal power quantification for turbines that are not able to yaw (i.e. are fixed).

Commin et al. [91] analysed leased tidal sites in the Pentland Firth and Orkney Waters at 10-minute resolution and determined that exploiting tidal phasing for firm capacity is not feasible in this region. However, they also determined that tidal phasing is useful as zero power is produced between 4.2% and 14.5% of the year for individual sites, but is reduced to 1.4% of the year for combined sites.

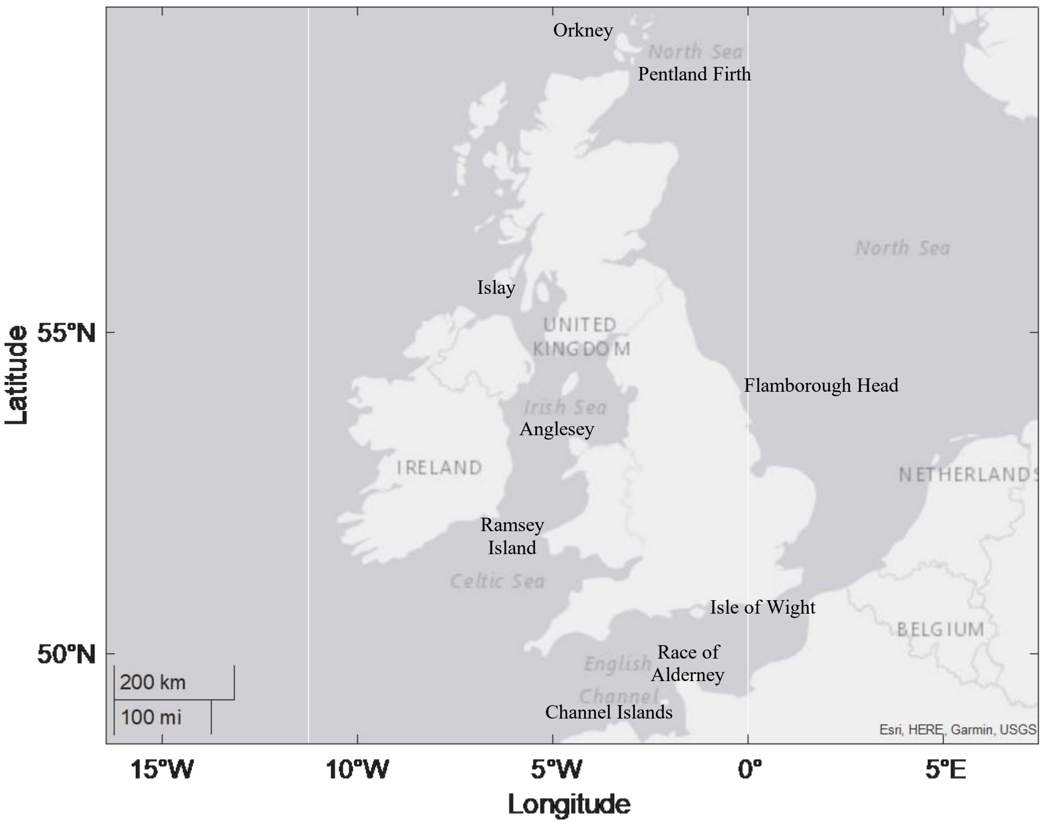

Figure 2.7: Locations of the main tidal sites referred to in section 2.3.1. (around the UK)

The first tidal phasing study in the US [90] analyses the Salish Sea around Washington and Inside Passage, Bristol Bay and Kodiak and Cook Inlet around Alaska. Specific turbine characteristics are not considered (such as cut-in/cut-out speed), but theoretical power is evaluated. The region of Kodiak Island and Cook Inlet is determined as the best region for anticorrelation (complementarity) between turbine sites.

Combining ebb-dominant tidal stream sites with flood-dominant tidal stream sites can facilitate a more consistent power output compared to utilising either site individually, as demonstrated in Orkney between Westray Firth and Stronsay Firth [92]. As well as location, the tidal stream turbine's power curve can affect the smoothness of the power profile. Generally, the rate of increase of tidal stream power with time is lower than the corresponding rate of decrease [81]. Secondly, the cut-in velocity value affects how often the power profile is zero. Therefore, the phase difference between tidal sites can be, effectively, altered. A low cut-in velocity value enables power production at low velocities which is ideal.

The time lag between relevant tidal stream sites around the UK is quantified in Table 1 of Neill et al. [82]. The tidal current phase difference around the UK is also shown visibly in Figure 4 of [82] (and displayed in Figure 2.8 below), in Figure 2 of [84] and in Figure 7 of [79].

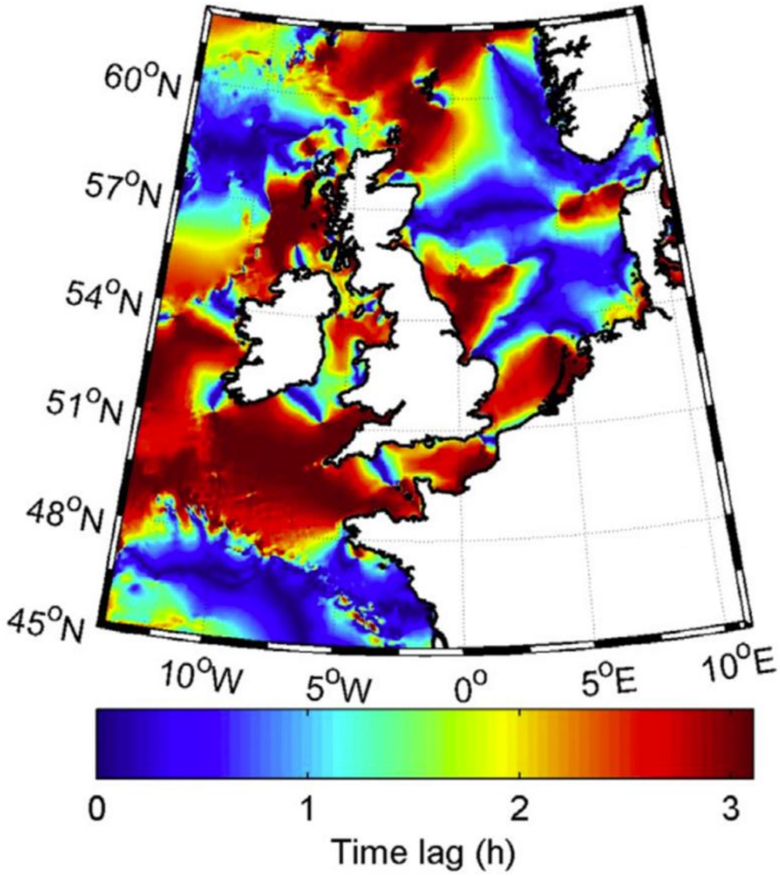

Figure 2.8: Tidal current time lag around the UK (M2 tidal constituent), adapted from [82].

Beyond academic interest, there is no reported practical utilisation of tidal phasing for tidal stream power production globally. This lack of utilisation of tidal phasing at a local and national level is likely due to the prohibitively high tidal stream levelized cost of energy (LCOE) [19].

The literature described in this section demonstrates that tidal phasing can facilitate a smoother power profile, ensuring zero power occurs less frequently than if tidal phasing were not utilised. Most of these studies use tidal sites which are far apart (such as around the UK), and none of the studies illustrate the utilisation of phased tidal power for green fuel production, such as green ammonia or hydrogen. Moreover, to the best of the author's knowledge, there is no academic or commercial work on tidal stream power phasing for the production of green fuels.

2.3.2. Introduction to tidal phasing

A flat power profile is the most ideal profile for green ammonia production as oversizing of equipment can be avoided, and no energy storage or hydrogen storage would be required (unless the capacity factor, CF, is exceptionally low). Moreover, the Haber-Bosch (HB) process is not completely flexible [93], so the less variable the power profile, the more efficiently the HB can operate and the lower the chance of catalyst damage [94][95]. A flat power profile is not possible to achieve with renewable energy, with some exceptions (such as hydropower), unless an external storage component is incorporated. For example, utilising (unphased) tidal stream energy with storage such as flywheels or vanadium flow batteries [96][97][98] or utilising the grid to back-up renewable energy sources [99]. The issue with using tidal energy with external storage or the grid is the added costs of the, albeit predictable [96], storage capacities and grid connection. Moreover, if the grid is not powered by renewables, the emissions associated with utilising the grid could be substantial. Furthermore, grid emission intensities are highly spatio-temporally variable [100].

A smooth (consistent) power profile with a degree of baseload power is a more realistic profile which could be achieved with renewable energy (without external storage) and would still be useful for green ammonia production. This can be achieved, for example, by exploiting the difference in phase of tidal stream currents in different locations [89] or utilising tidal stream energy and tidal range energy together (as they can have a relative phase difference) [101][84]. Combining other renewables, such as solar and wind can increase the capacity factor compared to either resource alone [101], but baseload power is not guaranteed, given the inherent variability and unpredictability of these resources. However, the power profile from tidal stream and tidal range energy can be predicted, and thus, baseload power can be guaranteed. Moreover, although tidal stream and tidal range energy are green solutions to providing baseload power, tidal range energy has notable environmental issues such as those affecting fish migration [102][103]. Thus, exploiting the difference in phase (time) of tidal stream currents in different locations, i.e. tidal phasing, is an attractive option to provide power for green ammonia production.

It is known that tidal phasing increases the minimum power and decreases the maximum power [89], making the power profile less variable. It could be argued that, with infinite phasing, the power profile would be flat with respect to time. Figure 2.9 shows four theoretical power profiles with the same capacity factor – from a single turbine, from two turbines, from 10 turbines and the ideal flat profile (from an infinite number of turbines). The phased profiles are less variable than the unphased (single-turbine) profile. Moreover, more phasing ensures that the power profile is closer to the ideal flat profile. Using these four power profiles as input power to a green ammonia plant will result in very different LCOAs with the flat profile being the lowest and the single-turbine profile being the highest.

It should be noted that in Figure 2.9, the individual turbine power profiles represent an M2 tidal power profile with a period of 12.42 hours and incorporate arbitrary cut-in and rated speeds (0.2 m/s and 0.9 m/s). The free stream velocity is $\sin\left(\frac{2\pi}{12.42}(t+p)\right)$ where t is time in hours and p is phase difference in hours. M2 is the semi-diurnal lunar tidal constituent, which is the most important tidal constituent for the British Isles [84].

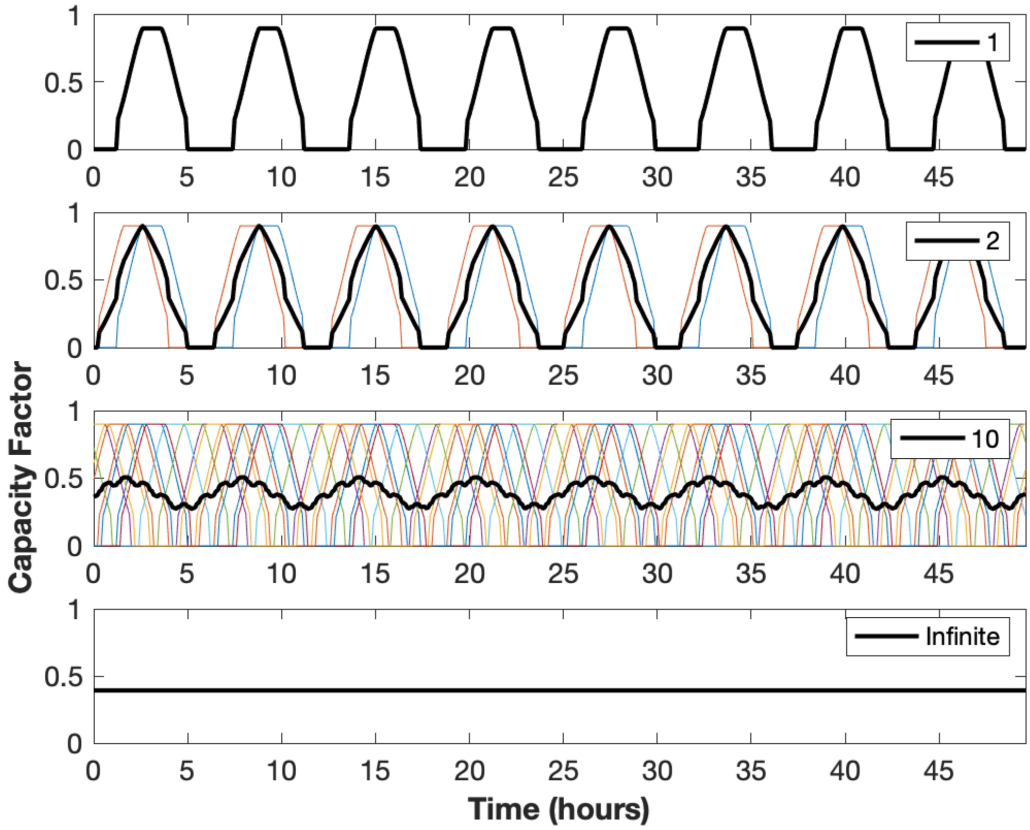

Figure 2.9: Theoretical power profile (hourly capacity factor) from a single turbine, two turbines with a phase difference of one hour, 10 turbines with a phase difference of one hour each and an ideal power profile representative of an infinite (very large) number of turbines. The four power profiles in black have the same annual capacity factor (39%). The non-black power profiles are the individual turbine power profiles.

The HB process power requirement is a small fraction of the total power of the green ammonia plant (< ~5%), and the minimum power of the HB is about 20% of its rated power [93] (i.e. < 1% of the total power of the ammonia plant). One also has to consider that to keep the HB at a minimum load, there is an associated minimum hydrogen supply requirement. Depending on the power profile at any given time, this hydrogen supply requirement may be sourced directly from the electrolyser or from hydrogen storage. Thus, the power requirement associated with the minimum hydrogen supply as a reactant to the HB varies with time. Phasing could ensure that the power profile always meets the minimum power of the HB (from input power directly, avoiding extra battery or fuel cell capacity) as well as the minimum hydrogen supply requirement, providing confidence to manufacturers and investors.

It is acknowledged that tidal phasing is not a unique phenomenon. Regen (an independent centre of energy expertise) demonstrated the benefits of utilizing offshore wind on both the east and west coast of the UK [104]. Similar to tidal phasing, strategically placing wind turbines apart to utilise power profile anti-correlation (in different weather windows) can facilitate less variable and more consistent power generation.

2.3.3. Smooth power profile

In order to achieve a smoother power profile for ammonia production from phased tidal turbine locations compared to unphased tidal turbine locations, various metrics can be compared (Table 2.2). A lower proportion of time in a year with zero power for a combined site compared to an individual site is indicative of tidal phasing [91]. Giorgi and Ringwood [88] used a genetic algorithm to solve a multi-objective optimisation problem to find the best combination of turbines to (i) maximise the average power (i.e. the capacity factor) (ii) maximise the minimum, baseload, power and (iii) minimise the variance of the power profile. Unlike the electrolyser, the HB reactor cannot ramp up and down instantaneously [105] – ramping limits of 2-20% per hour have been suggested [106]. These HB ramping constraints inhibit constant ammonia production with an intermittent power profile, so the rate of change of power is also an important metric to consider.

Table 2.2: Ideal smooth power profile characteristics for green ammonia production

Metric	**Ideal value**	**Main impact on ammonia production**
Frequency of zero power	Low	Size of storage capacity
Minimum power	High	Ability to run HB constantly and size of storage capacity
Average power	High	Amount of ammonia produced
Power variance	Low	Size of equipment capacity
Rate of change of power	Low	Ability to meet HB ramping constraint

In order to achieve a smoother aggregate power profile, various parameters can be changed in the modelling of turbines, as shown in Table 2.3. The turbine type determines the turbine diameter which in turn affects the location of the turbine in the water column, the tidal current velocity at the position of the turbine, and the power output of the turbine. The number of turbine locations (with a net phase difference) will significantly impact the power profile and should be decided based on the ammonia production cost. Almoghayer et al. [25] demonstrated that reducing the rated power of each tidal turbine in a farm by 33% (in Hoy Sound, Orkney) can provide power with less variability to Orkney's grid and improve the capacity factor of the farm by 42.5%. While the aggregate energy produced by the farm is lowered (by 4.29%), decreasing revenue, this is counterbalanced by the lower CAPEX and OPEX costs. However, when tidal energy is used directly for green ammonia production (i.e. not for the grid), limiting the maximum power is unlikely to be justified as there are already internal storage mechanisms in place within the green ammonia production process to provide constant power to the Haber-Bosch process (battery storage, hydrogen storage and fuel cell capacity), see Figure 3.4.

Table 2.3: Modelling parameters and their impact on the aggregate power profile

Parameters impacting smoothness of power profile	**Main impact on aggregate power profile**
Turbine type (cut-in and rated speeds)	Rate of change of power, power variance, frequency of zero power, average power
Velocity averaged over specific water depths	Average power (velocities are generally larger near the ocean-air boundary than near the seabed)
Number of turbine locations (with a net phase difference)	Frequency of zero power, minimum power, power variance, average power
Limiting turbine capacity	Lower power variance

There are restrictions in the placement of turbine locations. The water depth has a major impact on which turbine sites and which types of turbines can be utilised. More powerful turbines have a larger diameter, so shallow water restricts the power production in a given region. Ideally, sites in close proximity should be used to reduce the magnitude of the underwater cable cost between sites. Moreover, shipping routes and fishing areas should be avoided to reduce the impact on the local economy.

2.4. Wake effects and blockage effects

This section outlines why wake and blockage effects are significant for tidal stream energy production.

2.4.1. Tidal turbine layout

Tidal turbine arrays must be designed carefully – the array design changes the overall array power output with a fixed overall installed capacity. As demonstrated by Zazzini et al. [107], the layout (location, quantity and positioning) of the tidal turbines can affect the extractable power of each turbine. Methods of turbine micro-arrangement optimisation include varying inter-row spacing, row staggering and varying turbine arrangement within a row as demonstrated by Vennell et al. [108]. A staggered layout is generally preferred to an aligned layout to optimise power output and reduce array interaction [25], [109], [110], [111]. Good tidal power locations are often area restricted with bi-directional flow, requiring array layout optimisation [109].

2.4.2. Wake effects

Figure 2.10 shows that the flow velocity exiting the turbine (u_3) is lower than the flow velocity entering the turbine (u_1). This is the wake effect. If the downstream distance between turbines is sufficient, the fast bypass flow (u_4) can mix with the flow exiting the turbine (u_3) to return to the free-stream flow (u) [112].

There is scarce information available on real tidal turbine wake recovery rates [113]. Generally, the downstream spacing of turbines should be >10-20D to allow for wake recovery [25], [114]. Since tidal turbines generally occupy significantly more of the free flow compared to wind turbines, a larger distance (in multiples of blade diameters) is needed for kinetic flux recovery downstream of a tidal turbine compared to a wind turbine [21], [108]. Thus, the power extracted by a fixed number of tidal turbines is limited by the occurrence of wake effects.

Stansby and Stallard [115] optimised the power of various small array layouts. They demonstrate that downstream turbines are significantly affected by wakes from upstream turbines which decreases the power output of downstream turbines.

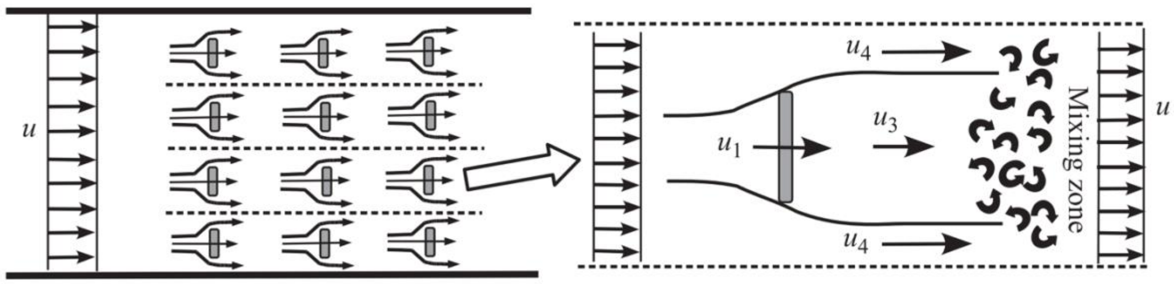

Figure 2.10: Flows around tidal stream turbines in a channel. The velocity sizes are as follows: $u_4 \geq u > u_1 > u_3$ [112].

2.4.3. Blockage effects

In a constrained flow, the fluid flow is affected by neighbouring boundaries [116]. When the fraction of the channel cross-sectional area occupied by the turbine swept area is more than around 10%, turbine blockage corrections are required [110], [117]. Turbine blockage corrections can increase the power output of turbines [117] due to the fast bypass flow [116][118] (u_4 in Figure 2.10). Incorporating turbine blockage correction factors (increasing power), such as those detailed by Zilic de Arcos et al. [116], is complex and beyond the scope of this thesis.

Channel blockage effects refer to the reduction in tidal stream velocity in a channel due to the presence of turbines [119] - the tidal stream turbines act as a momentum sink [120]. Channel blockage effects are discussed further in section 5.1.1.

2.5. Conclusion

The literature review has explained how green ammonia is produced at present (with onshore wind/solar and ammonia production onshore), discussed offshore ammonia production literature, and explained why tidal stream energy is a promising offshore energy resource for green ammonia production (novelty, predictability and phasing ability).

References:

[1] The Royal Society, “Ammonia: zero-carbon fertiliser, fuel and energy store,” London, UK, 2020. [Online]. Available: https://royalsociety.org/-/media/policy/projects/green-ammonia/green-ammonia-policy-briefing.pdf

[2] E. R. Morgan, J. F. Manwell, and J. G. McGowan, “Sustainable Ammonia Production from U.S. Offshore Wind Farms: A Techno-Economic Review,” *ACS Sustain. Chem. Eng.*, vol. 5, no. 11, pp. 9554–9567, 2017.

[3] V. Parmar, J. Manwell, and J. McGowan, “Ammonia Production from a Non-Grid Connected Floating Offshore Windfarm,” *J. Phys. Conf. Ser.*, vol. 1452, no. 1, p. 012015, 2020.

[4] “Green ammonia – Save costs and CO2 by using renewable energy,” Thyssenkrupp. Accessed: Dec. 10, 2021. [Online]. Available: https://www.thyssenkrupp-industrial-solutions.com/power-to-x/en/green-ammonia

[5] K. A. Prasad, A. A. Chand, N. M. Kumar, S. Narayan, and K. A. Mamun, “A Critical Review of Power Take-Off Wave Energy Technology Leading to the Conceptual Design of a Novel Wave-Plus-Photon Energy Harvester for Island/Coastal Communities’ Energy Needs,” *Sustainability*, vol. 14, no. 4, p. 2354, 2022.

[6] International Energy Agency, “Energy Technologies at the Cutting Edge,” Paris, France, 2007. [Online]. Available: https://www.iea.org/reports/energy-technologies-at-the-cutting-edge

[7] International Energy Agency, “Offshore Wind Outlook 2019,” Paris, France, 2019. [Online]. Available: https://www.iea.org/reports/offshore-wind-outlook-2019

[8] World Bank Group, ESMAP, and SERIS, “Where Sun Meets Water: Floating Solar Market Report—Executive Summary,” Washington DC, USA, 2018. [Online]. Available:

https://documents1.worldbank.org/curated/en/579941540407455831/pdf/Floating-Solar-Market-Report-Executive-Summary.pdf

[9] S. Lindroth and M. Leijon, "Offshore wave power measurements - A review," *Renew. Sustain. Energy Rev.*, vol. 15, no. 9, pp. 4274–4285, 2011.

[10] A. Poullikkas, "Technology Prospects of Wave Power Systems," *Electron. J. Energy Environ.*, vol. 2, no. 1, pp. 47–69, 2014.

[11] O. Farrok, K. Ahmed, A. D. Tahlil, M. M. Farah, M. R. Kiran, and M. R. Islam, "Electrical Power Generation from the Oceanic Wave for Sustainable Advancement in Renewable Energy Technologies," *Sustainability*, vol. 12, no. 6, p. 2178, 2020.

[12] O. Farrok, M. R. Islam, M. R. I. Sheikh, Y. G. Guo, and J. G. Zhu, "Design and Analysis of a Novel Lightweight Translator Permanent Magnet Linear Generator for Oceanic Wave Energy Conversion," *IEEE Trans. Magn.*, vol. 53, no. 11, pp. 1–4, 2017.

[13] N. El Bassam, "Technologies at the experimental stages," in *Distributed Renewable Energies for Off-Grid Communities*, 2nd ed., N. El Bassam, Ed., Elsevier Inc., 2021, pp. 435–442.

[14] R. J. Aaberg, "Osmotic power: A new and powerful renewable energy source?," *Refocus*, vol. 4, no. 6, pp. 48–50, 2003.

[15] G. L. Dugger and E. J. Francis, "Design of an ocean thermal energy plant ship to produce ammonia via hydrogen," *Int. J. Hydrogen Energy*, vol. 2, no. 3, pp. 231–249, 1977.

[16] J. Herrera, S. Sierra, and A. Ibeas, "Ocean Thermal Energy Conversion and Other Uses of Deep Sea Water: A Review," *J. Mar. Sci. Eng.*, vol. 9, no. 4, p. 356, 2021.

[17] I. Fairley, P. Evans, C. Wooldridge, M. Willis, and I. Masters, "Evaluation of tidal stream resource in a potential array area via direct measurements," *Renew. Energy*,

vol. 57, pp. 70–78, 2013.

[18] A. Roberts, B. Thomas, P. Sewell, Z. Khan, S. Balmain, and J. Gillman, “Current tidal power technologies and their suitability for applications in coastal and marine areas,” *J. Ocean Eng. Mar. Energy*, vol. 2, no. 2, pp. 227–245, 2016.

[19] D. Coles, A. Angeloudis, D. Greaves, G. Hastie, M. Lewis, L. Mackie, J. McNaughton, J. Miles, S. Neill, M. Piggott, D. Risch, B. Scott, C. Sparling, T. Stallard, P. Thies, S. Walker, D. White, R. Willden, and B. Williamson, “A review of the UK and British Channel Islands practical tidal stream energy resource,” *Proc. R. Soc. A*, vol. 477, no. 2255, p. 20210469, 2021.

[20] G. Smart and M. Noonan, “Tidal Stream and Wave Energy Cost Reduction and Industrial Benefit Summary Analysis,” Glasgow, UK, 2018. [Online]. Available: https://www.marineenergywales.co.uk/wp-content/uploads/2018/05/ORE-Catapult-Tidal-Stream-and-Wave-Energy-Cost-Reduction-and-Ind-Benefit-FINAL-v03.02.pdf

[21] I. G. Bryden, T. Grinsted, and G. T. Melville, “Assessing the potential of a simple tidal channel to deliver useful energy,” *Appl. Ocean Res.*, vol. 26, no. 5, pp. 198–204, 2004.

[22] A. S. Bahaj and L. E. Myers, “Fundamentals applicable to the utilisation of marine current turbines for energy production,” *Renew. Energy*, vol. 28, no. 14, pp. 2205–2211, 2003.

[23] T. R. Munaweera Thanthirige, J. Goggins, M. Flanagan, and W. Finnegan, “A State-of-the-Art Review of Structural Testing of Tidal Turbine Blades,” *Energies*, vol. 16, no. 10, p. 4061, 2023.

[24] A. J. Goward Brown, S. P. Neill, and M. J. Lewis, “Tidal energy extraction in three-dimensional ocean models,” *Renew. Energy*, vol. 114, pp. 244–257, 2017.

[25] M. A. Almoghayer, D. K. Woolf, S. Kerr, and G. Davies, “Integration of tidal energy into an island energy system - A case study of Orkney islands,” *Energy*, vol. 242, p.

122547, 2022.

[26] M. Lewis, R. O'Hara Murray, S. Fredriksson, J. Maskell, A. de Fockert, S. P. Neill, and P. E. Robins, "A standardised tidal-stream power curve, optimised for the global resource," *Renew. Energy*, vol. 170, pp. 1308–1323, 2021.

[27] E. Serin, P. Andres, R. Martin, A. Shah, and A. Valero, "Seizing sustainable growth opportunities from tidal stream energy in the UK," London School of Economics and Political Science, London, 2023. [Online]. Available: https://www.lse.ac.uk/granthaminstitute/publication/seizing-sustainable-growth-opportunities-from-tidal-stream-energy-in-the-uk/

[28] "Contracts for Difference (CfD) Allocation Round 5: results," Department for Energy Security and Net Zero. Accessed: Nov. 01, 2022. [Online]. Available: https://www.gov.uk/government/publications/contracts-for-difference-cfd-allocation-round-5-results

[29] "Contracts for Difference (CfD) Allocation Round 6: results," Department for Energy Security and Net Zero. Accessed: Jan. 10, 2025. [Online]. Available: https://www.gov.uk/government/publications/contracts-for-difference-cfd-allocation-round-6-results

[30] Z. Yang, T. Wang, R. Branch, Z. Xiao, and M. Deb, "Tidal stream energy resource characterization in the Salish Sea," *Renew. Energy*, vol. 172, pp. 188–208, 2021.

[31] T. Wang and Z. Yang, "A Tidal Hydrodynamic Model for Cook Inlet, Alaska, to Support Tidal Energy Resource Characterization," *J. Mar. Sci. Eng.*, vol. 8, no. 4, p. 254, 2020.

[32] Z. Yang, T. Wang, Z. Xiao, L. Kilcher, K. Haas, H. Xue, and X. Feng, "Modeling Assessment of Tidal Energy Extraction in the Western Passage," *J. Mar. Sci. Eng.*, vol. 8, no. 6, p. 411, Jun. 2020.

[33] M. De Dominicis, J. Wolf, and R. O’Hara Murray, “Comparative Effects of Climate Change and Tidal Stream Energy Extraction in a Shelf Sea,” *J. Geophys. Res. Ocean.*, vol. 123, no. 7, pp. 5041–5067, 2018.

[34] L. Hatton, R. Bañares-Alcántara, S. Sparrow, F. Lott, and N. Salmon, “Assessing the impact of climate change on the cost of production of green ammonia from offshore wind,” *Int. J. Hydrogen Energy*, vol. 49, pp. 635–643, 2024.

[35] R. J. Barthelmie and S. C. Pryor, “Climate Change Mitigation Potential of Wind Energy,” *Climate*, vol. 9, no. 9, p. 136, 2021.

[36] G. Gulabani, B. S. A. Karim, J. Radhakrishnan, S. Shenoy B, and M. Zuber, “Review on Unconventional Wind Energy,” *J. Eng. Technol. Sci.*, vol. 52, no. 4, pp. 565–583, 2020.

[37] H. Junqueira, M. Robaina, S. Garrido, R. Godina, and J. C. O. Matias, “Viability of Creating an Offshore Wind Energy Cluster: A Case Study,” *Appl. Sci.*, vol. 11, no. 1, p. 308, 2020.

[38] F. Manzano-Agugliaro, M. Sánchez-Calero, A. Alcayde, C. San-Antonio-Gómez, A.-J. Perea-Moreno, and E. Salmeron-Manzano, “Wind Turbines Offshore Foundations and Connections to Grid,” *Inventions*, vol. 5, no. 1, p. 8, 2020.

[39] R. Wiser, J. Rand, J. Seel, P. Beiter, E. Baker, E. Lantz, and P. Gilman, “Expert elicitation survey predicts 37% to 49% declines in wind energy costs by 2050,” *Nat. Energy*, vol. 6, no. 5, pp. 555–565, 2021.

[40] Y. Qu, T. Hooper, J. K. Swales, E. Papathanasopoulou, M. C. Austen, and X. Yan, “Energy-food nexus in the marine environment: A macroeconomic analysis on offshore wind energy and seafood production in Scotland,” *Energy Policy*, vol. 149, p. 112027, 2021.

[41] IRENA (International Renewable Energy Agency), “Future of wind: Deployment,

investment, technology, grid integration and socio-economic aspects (A Global Energy Transformation paper)," Abu Dhabi, United Arab Emirates, 2019. [Online]. Available: https://www.irena.org/-/media/Files/IRENA/Agency/Publication/2019/Oct/IRENA_Future_of_wind_2019.pdf

[42] A. Bonou, A. Laurent, and S. I. Olsen, "Life cycle assessment of onshore and offshore wind energy-from theory to application," *Appl. Energy*, vol. 180, pp. 327–337, 2016.

[43] P. Potisomporn and C. R. Vogel, "Spatial and temporal variability characteristics of offshore wind energy in the United Kingdom," *Wind Energy*, vol. 25, no. 3, pp. 537–552, 2022.

[44] C. Neubacher, D. Witthaut, and J. Wohland, "Multi-decadal offshore wind power variability can be mitigated through optimized European allocation," *Adv. Geosci.*, vol. 54, pp. 205–215, 2021.

[45] E. G. A. Antonini, E. Virgüez, S. Ashfaq, L. Duan, T. H. Ruggles, and K. Caldeira, "Identification of reliable locations for wind power generation through a global analysis of wind droughts," *Commun. Earth Environ.*, vol. 5, no. 1, p. 103, 2024.

[46] E. Solomin, E. Sirotkin, E. Cuce, S. P. Selvanathan, and S. Kumarasamy, "Hybrid Floating Solar Plant Designs: A Review," *Energies*, vol. 14, no. 10, p. 2751, 2021.

[47] S. Oliveira-Pinto and J. Stokkermans, "Assessment of the potential of different floating solar technologies – Overview and analysis of different case studies," *Energy Convers. Manag.*, vol. 211, p. 112747, 2020.

[48] J. Langer, J. Quist, and K. Blok, "Recent progress in the economics of ocean thermal energy conversion: Critical review and research agenda," *Renew. Sustain. Energy Rev.*, vol. 130, p. 109960, 2020.

[49] J. F. George and D. Richards, "Baseline designs of moored and grazing 40-MW OTEC pilot plants. Volumes A and B.," Laurel, USA, 1980. [Online]. Available:

https://www.osti.gov/servlets/purl/6564705/

[50] C. B. Panchal, P. P. Pandolfini, and W. H. Kumm, “Ocean Thermal Plantships for Production of Ammonia as the Hydrogen Carrier,” Oak Ridge, USA, 2009. [Online]. Available: https://publications.anl.gov/anlpubs/2009/12/65627.pdf

[51] E. R. Morgan, “Techno-economic feasibility study of ammonia plants powered by offshore wind (Ph.D. Thesis),” University of Massachusetts Amherst, 2013.

[52] E. Morgan, J. Manwell, and J. McGowan, “Wind-powered ammonia fuel production for remote islands: A case study,” *Renew. Energy*, vol. 72, pp. 51–61, 2014.

[53] N. Salmon and R. Bañares-Alcántara, “A global, spatially granular techno-economic analysis of offshore green ammonia production,” *J. Clean. Prod.*, vol. 367, p. 133045, 2022.

[54] H. Wang, P. Daoutidis, and Q. Zhang, “Harnessing the Wind Power of the Ocean with Green Offshore Ammonia,” *ACS Sustain. Chem. Eng.*, vol. 9, no. 43, pp. 14605–14617, 2021.

[55] C. Thommessen, M. Otto, F. Nigbur, J. Roes, and A. Heinzel, “Techno-economic system analysis of an offshore energy hub with an outlook on electrofuel applications,” *Smart Energy*, vol. 3, p. 100027, 2021.

[56] V. V Parmar, “Ammonia Production from a Non-Grid Connected Floating Offshore Wind-Farm: A System-Level Techno-Economic Review (Master’s Thesis),” University of Massachusetts Amherst, 2019.

[57] M. M. Maia, “Techno-Economic Analysis of Green Ammonia Production using Offshore Wind Farms (Master’s Thesis),” Reykjavík University, 2021.

[58] A. Buljan, “Aker Presents Massive Offshore Wind-to-Hydrogen Project in Scotland at COP26,” offshorewind.biz. Accessed: Jul. 19, 2022. [Online]. Available: https://www.offshorewind.biz/2021/11/04/aker-presents-massive-offshore-wind-to-

hydrogen-project-in-scotland-at-cop26/

[59] J. Atchison, “Renewable ammonia in Vietnam,” Ammonia Energy Association. Accessed: Jul. 19, 2022. [Online]. Available: https://www.ammoniaenergy.org/articles/renewable-ammonia-in-vietnam/

[60] “The P2XFloater^{TM},” H2CARRIER. Accessed: Mar. 04, 2022. [Online]. Available: https://www.h2carrier.com/the-p2x-floater

[61] A. Valera-Medina, “Sustainable Energy for Wales: Tidal and Wind with Ammonia Storage,” Ammonia Energy Association. Accessed: Apr. 01, 2022. [Online]. Available: https://www.ammoniaenergy.org/articles/sustainable-energy-for-wales-tidal-and-wind-with-ammonia-storage/

[62] D. Warwick-Brown, H. Berge-Karevoll, M. Al Abdullatif, and A. Valera-Medina, “Assessing the Techno-Economic Feasibility of a Wind-Tidal Lagoon Hybrid System for Green Ammonia Storage in Wales, UK,” in *Congreso Internacional de Desarrollo Sustentable y Energías Renovables (CIDSER 2020)*, 2020, pp. 4–6. [Online]. Available: https://orca.cardiff.ac.uk/id/eprint/136225/

[63] N. Salmon and R. Bañares-Alcántara, “Impact of process flexibility and imperfect forecasting on the operation and design of Haber–Bosch green ammonia,” *RSC Sustain.*, vol. 1, no. 4, pp. 923–937, 2023.

[64] The Scottish Government, “A vision for Scotland’s electricity and gas networks,” Edinburgh, UK, 2019. [Online]. Available: https://www.gov.scot/binaries/content/documents/govscot/publications/strategy-plan/2019/03/vision-scotlands-electricity-gas-networks-2030/documents/vision-scotlands-electricity-gas-networks-detail-2019-2030/vision-scotlands-electricity-gas-networks-detail-2019-2030/govscot%3Adocument/vision-scotlands-electricity-gas-networks-detail-2019-2030.pdf

[65] The Scottish Government, “Electricity Generation Policy Statement – 2013,” Edinburgh, UK, 2013. [Online]. Available: https://www.gov.scot/binaries/content/documents/govscot/publications/speech-statement/2013/06/electricity-generation-policy-statement-2013/documents/00427293-pdf/00427293-pdf/govscot%3Adocument/00427293.pdf

[66] “Ofgem approves Orkney transmission link,” SSEN Transmission. Accessed: Aug. 21, 2022. [Online]. Available: https://www.ssen-transmission.co.uk/news/news--views/2023/7/ofgem-approves-orkney-transmission-link/

[67] “Press release: World’s first tidal-powered hydrogen generated at EMEC,” European Marine Energy Centre. Accessed: Nov. 18, 2021. [Online]. Available: https://www.emec.org.uk/press-release-worlds-first-tidal-powered-hydrogen-generated-at-emec/

[68] “HYDROGEN R&D FACILITIES,” European Marine Energy Centre. Accessed: Oct. 31, 2022. [Online]. Available: https://www.emec.org.uk/facilities/hydrogen/

[69] “Project overview,” FORWARD2030. Accessed: Jul. 19, 2022. [Online]. Available: https://www.forward2030.tech/project-overview

[70] “Green Hydrogen Project Win,” Nova Innovation. Accessed: Oct. 30, 2022. [Online]. Available: https://novainnovation.com/news/green-hydrogen-project-win

[71] J. Atchison, “The Ammonia Wrap: EU ambitions, new tankers, and GW scale green ammonia in Denmark, Norway, and Chile,” Ammonia Energy Association. Accessed: Nov. 30, 2021. [Online]. Available: https://www.ammoniaenergy.org/articles/the-ammonia-wrap-eu-ambitions-new-tankers-and-gw-scale-green-ammonia-in-denmark-norway-and-chile/

[72] R. H. Charlier, “A ‘sleeper’ awakes: tidal current power,” *Renew. Sustain. Energy Rev.*, vol. 7, no. 6, pp. 515–529, 2003.

[73] A. Alex, R. Petrone, B. Tala-Ighil, D. Bozalakov, L. Vandevelde, and H. Gualous, "Optimal techno-enviro-economic analysis of a hybrid grid connected tidal-wind-hydrogen energy system," *Int. J. Hydrogen Energy*, vol. 47, no. 86, pp. 36448–36464, 2022.

[74] A. Kartalidis, K. Atsonios, and N. Nikolopoulos, "Enhancing the self-resilience of high-renewable energy sources, interconnected islanding areas through innovative energy production, storage, and management technologies: Grid simulations and energy assessment," *Int. J. Energy Res.*, vol. 45, no. 9, pp. 13591–13615, 2021.

[75] J. L. B. Ferguson, A. Robinson, S. Crawford, and D. Mignard, "Impact of integration of wind and tidal power on hydrogen production costs (March 2021)," in *Proceedings of the European Wave and Tidal Energy Conference*, 2021, pp. 1–7.

[76] M. Barakat, B. Tala-Ighil, H. Chaoui, H. Gualous, and D. Hissel, "Energy Management of a Hybrid Tidal Turbine-Hydrogen Micro-Grid: Losses Minimization Strategy," *Fuel Cells*, vol. 20, no. 3, pp. 342–350, 2020.

[77] B. C. R. Ewan and R. W. K. Allen, "A figure of merit assessment of the routes to hydrogen," *Int. J. Hydrogen Energy*, vol. 30, no. 8, pp. 809–819, 2005.

[78] G. Rinaldi, B. Wray, R. Parkinson, and L. Johanning, "The operational assessment of a floating tidal farm with hydrogen production capabilities," in *14th European wave and tidal energy conference 5-9th sept 2021*, 2021, pp. 1–8.

[79] S. P. Neill, A. Vögler, A. J. Goward-Brown, S. Baston, M. J. Lewis, P. A. Gillibrand, S. Waldman, and D. K. Woolf, "The wave and tidal resource of Scotland," *Renew. Energy*, vol. 114, pp. 3–17, 2017.

[80] M. Lewis, J. McNaughton, C. Márquez-Dominguez, G. Todeschini, M. Togneri, I. Masters, M. Allmark, T. Stallard, S. Neill, A. Goward-Brown, and P. Robins, "Power variability of tidal-stream energy and implications for electricity supply," *Energy*, vol.

183, pp. 1061–1074, 2019.

[81] A. S. Iyer, S. J. Couch, G. P. Harrison, and A. R. Wallace, "Variability and phasing of tidal current energy around the United Kingdom," *Renew. Energy*, vol. 51, pp. 343–357, 2013.

[82] S. P. Neill, M. R. Hashemi, and M. J. Lewis, "Tidal energy leasing and tidal phasing," *Renew. Energy*, vol. 85, pp. 580–587, 2016.

[83] J. Hardisty, "Power intermittency, redundancy and tidal phasing around the United Kingdom," *Geogr. J.*, vol. 174, no. 1, pp. 76–84, 2008.

[84] S. P. Neill, M. R. Hashemi, and M. J. Lewis, "Optimal phasing of the European tidal stream resource using the greedy algorithm with penalty function," *Energy*, vol. 73, pp. 997–1006, 2014.

[85] J. A. Clarke, G. Connor, A. D. Grant, and C. M. Johnstone, "Regulating the output characteristics of tidal current power stations to facilitate better base load matching over the lunar cycle," *Renew. Energy*, vol. 31, no. 2, pp. 173–180, 2006.

[86] P. E. Robins, S. P. Neill, M. J. Lewis, and S. L. Ward, "Characterising the spatial and temporal variability of the tidal-stream energy resource over the northwest European shelf seas," *Appl. Energy*, vol. 147, pp. 510–522, 2015.

[87] M. Lewis, S. P. Neill, P. E. Robins, and M. R. Hashemi, "Resource assessment for future generations of tidal-stream energy arrays," *Energy*, vol. 83, pp. 403–415, 2015.

[88] S. Giorgi and J. Ringwood, "Can Tidal Current Energy Provide Base Load?," *Energies*, vol. 6, no. 6, pp. 2840–2858, 2013.

[89] P. G. Novo and Y. Kyozuka, "Tidal stream energy as a potential continuous power producer: A case study for West Japan," *Energy Convers. Manag.*, vol. 245, p. 114533, 2021.

[90] D. Preziuso, G. García-Medina, R. O'Neil, Z. Yang, and T. Wang, "Evaluating the

Potential for Tidal Phase Diversity to Produce Smoother Power Profiles," *J. Mar. Sci. Eng.*, vol. 8, no. 4, p. 246, 2020.

[91] A. N. Commin, J. McClatchey, M. W. H. Davidson, and S. W. Gibb, "Close-proximity tidal phasing for 'firm' electricity supply," *Renew. Energy*, vol. 102, pp. 380–389, 2017.

[92] S. P. Neill, M. R. Hashemi, and M. J. Lewis, "The role of tidal asymmetry in characterizing the tidal energy resource of Orkney," *Renew. Energy*, vol. 68, pp. 337–350, 2014.

[93] N. Salmon and R. Bañares-Alcántara, "Green ammonia as a spatial energy vector: a review," *Sustain. Energy Fuels*, vol. 5, no. 11, pp. 2814–2839, 2021.

[94] O. Osman, S. Sgouridis, and A. Sleptchenko, "Scaling the production of renewable ammonia: A techno-economic optimization applied in regions with high insolation," *J. Clean. Prod.*, vol. 271, p. 121627, 2020.

[95] N. Campion, H. Nami, P. R. Swisher, P. Vang Hendriksen, and M. Münster, "Techno-economic assessment of green ammonia production with different wind and solar potentials," *Renew. Sustain. Energy Rev.*, vol. 173, p. 113057, 2023.

[96] I. G. Bryden and D. M. Macfarlane, "The utilisation of short term energy storage with tidal current generation systems," *Energy*, vol. 25, no. 9, pp. 893–907, 2000.

[97] "A world first for Nova Innovation - the 'Holy Grail' of baseload tidal power," Nova Innovation. Accessed: Aug. 20, 2022. [Online]. Available: https://www.novainnovation.com/news/news_/i/a-world-first-for-nova-innovation-the-holy-grail-of-baseload-tidal-power/

[98] "Eday Flow Battery Project," The European Marine Energy Centre. Accessed: Aug. 21, 2022. [Online]. Available: https://www.emec.org.uk/projects/hydrogen-projects/eday-flow-battery-project/

[99] N. Salmon and R. Bañares-Alcántara, “Impact of grid connectivity on cost and location of green ammonia production: Australia as a case study,” *Energy Environ. Sci.*, vol. 14, no. 12, pp. 6655–6671, 2021.

[100] H. Stevens, “America needs clean electricity. These states show how to do it.,” The Washington Post. Accessed: Aug. 21, 2022. [Online]. Available: https://www.washingtonpost.com/climate-environment/interactive/2023/clean-energy-electricity-sources/

[101] G. Todeschini, D. Coles, M. Lewis, I. Popov, A. Angeloudis, I. Fairley, F. Johnson, A. J. Williams, P. Robins, and I. Masters, “Medium-term variability of the UK’s combined tidal energy resource for a net-zero carbon grid,” *Energy*, vol. 238, p. 121990, 2022.

[102] S. P. Neill, A. Angeloudis, P. E. Robins, I. Walkington, S. L. Ward, I. Masters, M. J. Lewis, M. Piano, A. Avdis, M. D. Piggott, G. Aggidis, P. Evans, T. A. A. Adcock, A. Židonis, R. Ahmadian, and R. Falconer, “Tidal range energy resource and optimization – Past perspectives and future challenges,” *Renew. Energy*, vol. 127, pp. 763–778, 2018.

[103] A. Cornett, J. Cousineau, and I. Nistor, “Assessment of hydrodynamic impacts from tidal power lagoons in the Bay of Fundy,” *Int. J. Mar. Energy*, vol. 1, pp. 33–54, 2013.

[104] “Go West! An analysis of the energy system benefits and policy implications of a more geographically diverse offshore wind portfolio,” Regen. Accessed: Sep. 18, 2022. [Online]. Available: https://www.regen.co.uk/publications/go-west/

[105] R. Nayak-Luke, R. Bañares-Alcántara, and I. Wilkinson, “‘Green’ Ammonia: Impact of Renewable Energy Intermittency on Plant Sizing and Levelized Cost of Ammonia,” *Ind. Eng. Chem. Res.*, vol. 57, no. 43, pp. 14607–14616, 2018.

[106] M. Fasihi, R. Weiss, J. Savolainen, and C. Breyer, “Global potential of green ammonia

based on hybrid PV-wind power plants," *Appl. Energy*, vol. 294, p. 116170, 2021.

[107] S. Zazzini, M. de Dominicis, A. Pini, G. Leuzzi, P. Monti, R. O'Hara Murray, and X. Li, "Turbulence changes due to a tidal stream turbine operation in the Pentland Firth (Scotland, UK)," in *2019 IMEKO TC-19 International Workshop on Metrology for the Sea*, 2019, pp. 309–314.

[108] R. Vennell, S. W. Funke, S. Draper, C. Stevens, and T. Divett, "Designing large arrays of tidal turbines: A synthesis and review," *Renew. Sustain. Energy Rev.*, vol. 41, pp. 454–472, 2015.

[109] L. E. Myers and A. S. Bahaj, "An experimental investigation simulating flow effects in first generation marine current energy converter arrays," *Renew. Energy*, vol. 37, no. 1, pp. 28–36, 2012.

[110] J. Thiébot, N. Guillou, S. Guillou, A. Good, and M. Lewis, "Wake field study of tidal turbines under realistic flow conditions," *Renew. Energy*, vol. 151, pp. 1196–1208, 2020.

[111] M. A. Almoghayer and D. K. Woolf, "An assessment of efficient tidal stream energy extraction using 3D numerical modelling techniques," in *Proceedings of the 13th EWTEC*, 2019, pp. 1–10.

[112] R. Vennell, "Tuning turbines in a tidal channel," *J. Fluid Mech.*, vol. 663, pp. 253–267, 2010.

[113] P. K. Stansby and P. Ouro, "Modelling marine turbine arrays in tidal flows," *J. Hydraul. Res.*, vol. 60, no. 2, pp. 187–204, 2022.

[114] T. Stallard, R. Collings, T. Feng, and J. Whelan, "Interactions between tidal turbine wakes: experimental study of a group of three-bladed rotors," *Philos. Trans. R. Soc. A*, vol. 371, no. 1985, p. 20120159, 2013.

[115] P. Stansby and T. Stallard, "Fast optimisation of tidal stream turbine positions for

power generation in small arrays with low blockage based on superposition of self-similar far-wake velocity deficit profiles," *Renew. Energy*, vol. 92, pp. 366–375, 2016.

[116] F. Zilic de Arcos, G. Tampier, and C. R. Vogel, "Numerical analysis of blockage correction methods for tidal turbines," *J. Ocean Eng. Mar. Energy*, vol. 6, no. 2, pp. 183–197, 2020.

[117] N. Djama Dirieh, J. Thiébot, S. Guillou, and N. Guillou, "Blockage Corrections for Tidal Turbines—Application to an Array of Turbines in the Alderney Race," *Energies*, vol. 15, no. 10, p. 3475, 2022.

[118] J. Schluntz and R. H. J. Willden, "The effect of blockage on tidal turbine rotor design and performance," *Renew. Energy*, vol. 81, pp. 432–441, 2015.

[119] C. Garrett and P. Cummins, "The power potential of tidal currents in channels," *Proc. R. Soc. A Math. Phys. Eng. Sci.*, vol. 461, no. 2060, pp. 2563–2572, 2005.

[120] R. O'Hara Murray and A. Gallego, "A modelling study of the tidal stream resource of the Pentland Firth, Scotland," *Renew. Energy*, vol. 102, no. B, pp. 326–340, 2017.

[121] S. P. Neill, K. A. Haas, J. Thiébot, and Z. Yang, "A review of tidal energy—Resource, feedbacks, and environmental interactions," *J. Renew. Sustain. Energy*, vol. 13, no. 6, p. 062702, 2021.

[122] Z. L. Goss, "Design tools for the optimal exploitation of tidal-stream renewable energy (Ph.D. Thesis)," Imperial College London, 2021.

Chapter 3: Technoeconomic Evaluation of Offshore Green Ammonia Production using Tidal and Wind Energy: A case study

The objective of this chapter is to determine if tidal stream energy is a useful energy resource (technically and economically) for offshore green ammonia production. This idea is presented through a case study on the Pentland Firth, a globally excellent tidal stream location. Using 30 years of hourly wind and tidal data, the addition of tidal stream capacity to wind capacity is incorporated to see the effect on storage requirements and the levelized cost of ammonia (LCOA).

As mentioned in the Introduction (page 1), 2020 USD is used with a 2020 GBP to USD exchange rate.

3.1. Introduction

3.1.1. Tidal stream power location

The maximum tidal stream current speeds are above 4 m/s in the Pentland Firth, above 3.5 m/s in the Inner Sound of Stroma (next to the Isle of Stroma) [1], and almost 4 m/s at Fall of Warness [2]. These fast current speeds ensure this region of Scottish waters is a globally prominent tidal energy hotspot [3]. SIMEC Atlantis is leading the deployment of tidal turbines globally [4], specifically with their MEYGEN project (between mainland Scotland and the island of Stroma) which has a lease for the installation of 398 MW power [5]. Figure 3.1 displays the location of the Pentland Firth in relation to the United Kingdom and Figure 3.2 displays a close-up map of the Pentland Firth.

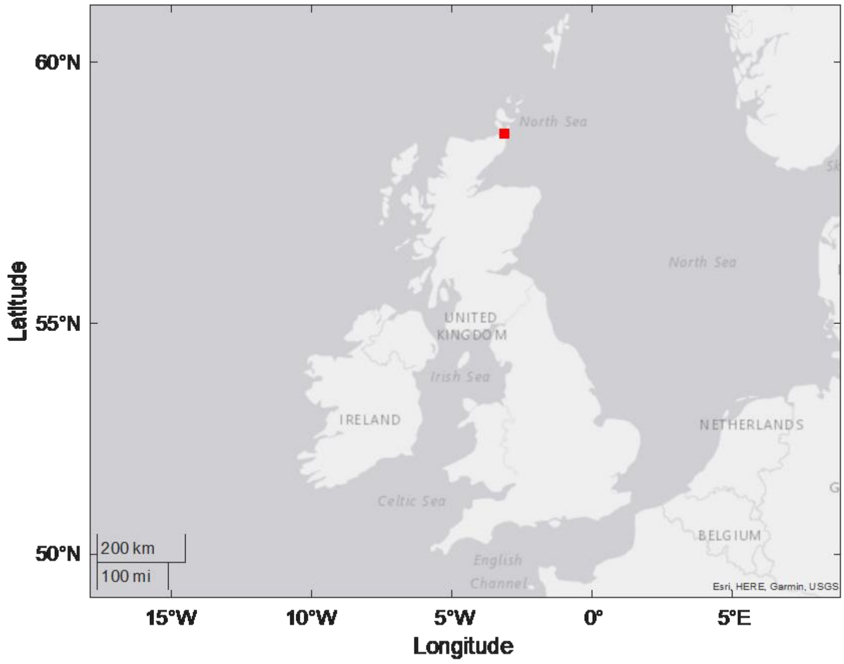

Figure 3.1: Location of the Pentland Firth (red square)

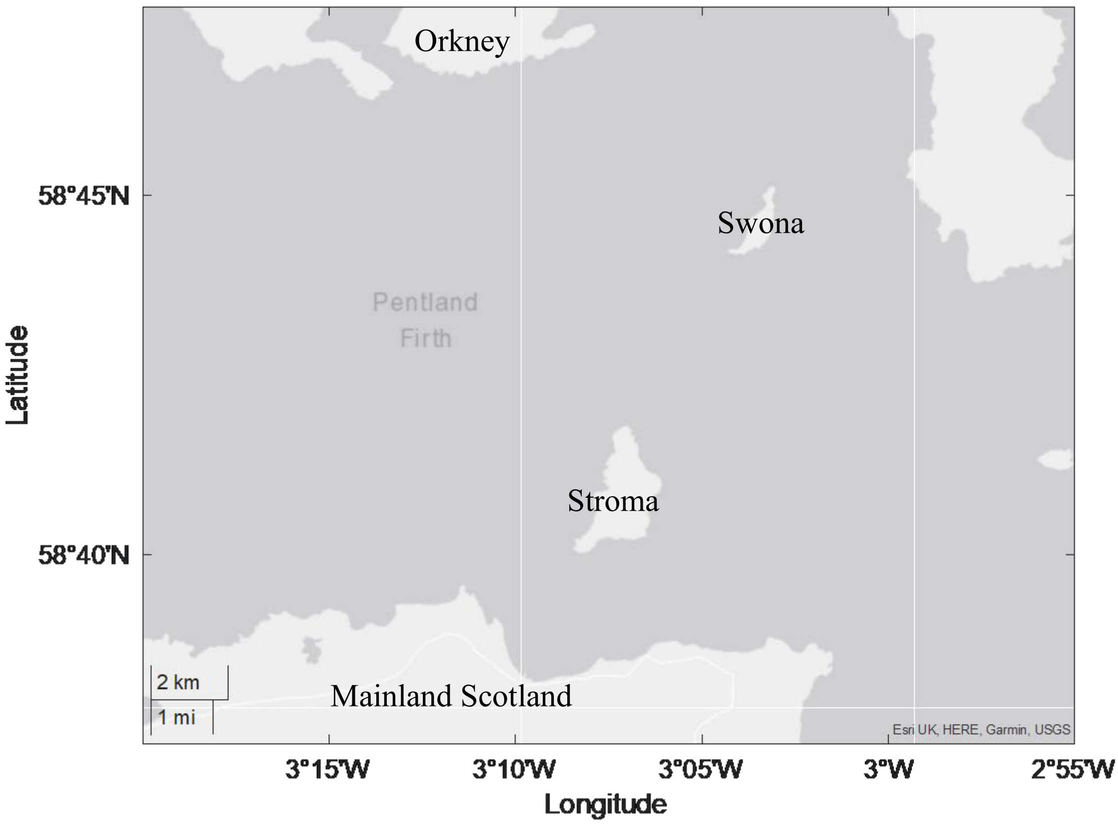

Figure 3.2: Notable land around the Pentland Firth

The extractable tidal stream power limit without significant flow disruption in the Pentland Firth is 1.4 GW, according to a 3-D hydrodynamic model by O'Hara Murray and Gallego [3]. The study presented in this chapter focuses on tidal stream power extraction from the Pentland Firth of an order of magnitude lower than 1.4 GW. However, it should be noted that the total operational tidal stream capacity for the UK was only around 10 MW in 2021 [6].

3.1.2. Tidal stream velocity models

The Pentland Firth and Orkney Waters (PFOW) 1.02 model [3], [7] displays 3-D tidal current flow velocity data (north and east components) on an unstructured grid over 0° - 5° W and 57° - 61° N (horizontal resolution in the Pentland Firth of ~100-150 m). The water column is divided into 10 terrain-following sigma layers. The PFOW 1.02 model data is over one climatological year (averaging 1990-2014), using the Finite Volume Community Ocean Model (FVCOM). The PFOW model is easily accessible - a copy of the model output is available publicly.

3.2. Methodology

3.2.1. Technoeconomic modelling

A green ammonia plant optimisation model minimises the LCOA (USD/t). This model is adapted from the mixed-integer linear program (MILP) optimisation model developed in [8], which uses Python's pyomo package and is solved using Gurobi. The capacity constraints and balance equations are modified to account for three major differences: adding tidal stream energy instead of solar PV, removing grid connection, and incorporating an offshore platform for offshore ammonia production. A summary of the ammonia model's inputs and outputs is shown in Figure 3.3. Further details on the model are in Appendix E. MATLAB is used to process the input wind and tidal velocities (which have a temporal resolution of 1 hour) to power profiles.

Wind and tidal energy are used to supply power to three components: the electrolyser to produce hydrogen, a battery, and the air separation unit (ASU) to produce nitrogen in addition to the Haber-Bosch (HB) unit to produce ammonia from nitrogen and hydrogen (Figure 3.4). To account for variable wind and tidal energy inputs and thus variable hydrogen production in the electrolyser, hydrogen storage between the electrolyser and the HB unit is included. A fuel cell is also included to supply back-up electricity to the HB and ASU from stored hydrogen. Battery storage, charged by wind and tidal energy, is used to supply back-up electricity to the electrolyser, HB and ASU. Electricity can also be curtailed if necessary.

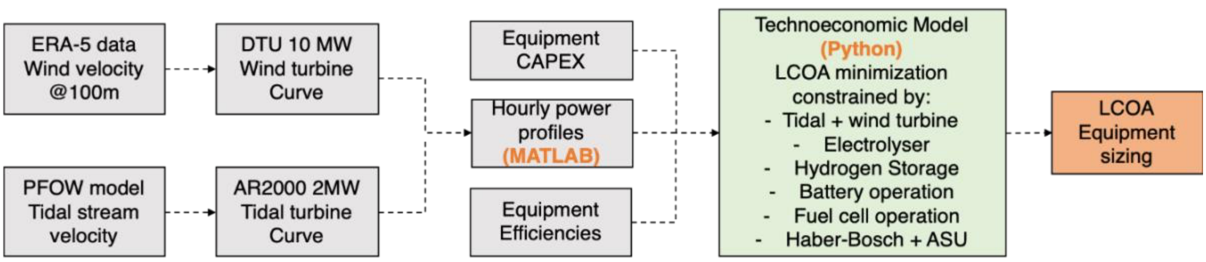

Figure 3.3: Overview of the offshore green ammonia production model

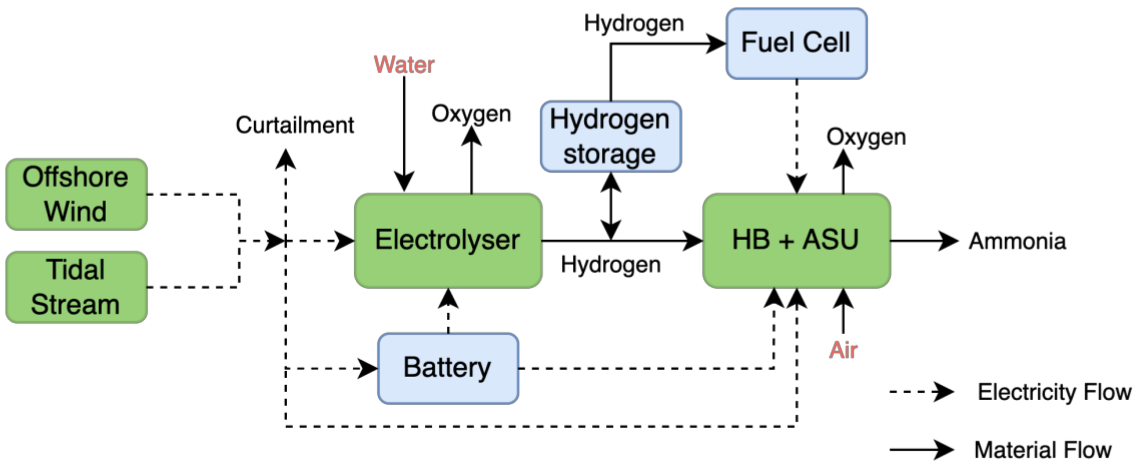

Figure 3.4: Flow diagram displaying the units involved in ammonia production, electricity flow between them and material inputs and outputs. Internal energy storage units are in blue

The ammonia plant optimisation model minimises the levelized cost of ammonia, $LCOA$ (USD/t) - Eqn. 1.

$$LCOA = \frac{\left(\frac{i(1+i)^{PL}}{(1+i)^{PL-1}}\right) \times CAPEX + OPEX}{F} \qquad \text{(Eqn. 1)}$$

where F is the yearly ammonia production in tons (set to 100,000 tons/year), i is the discount rate of 7% [9] and PL is plant lifetime, assumed to be 30 years.

The total $CAPEX$ (USD) calculation is presented in Eqn. 2, and individual equipment CAPEX values are listed in Table A.1.

$$CAPEX = \sum \sigma_R \, Cost_R + \sum \sigma_C \, Cost_C + \sum \sigma_{SC} \, Cost_{SC} + \sigma_{FC} Cost_{FC} + Cost_P \qquad \text{(Eqn. 2)}$$

where σ_R is the installed capacity of the renewable energy source (MW), $Cost_R$ is the cost of renewable power (USD/MW), σ_C is the installed capacity of the component (MW), $Cost_C$ is the cost of the component (USD/MW), σ_{SC} is the installed capacity of the storage component (MWh for battery, t for hydrogen), $Cost_{SC}$ is the cost of the storage component (USD/MWh for battery, USD/t for hydrogen), σ_{FC} is the installed capacity of the fuel cell (MW), $Cost_{FC}$ is the cost of fuel cell (USD/MW), and $Cost_P$ is the cost of offshore platform (USD). Renewable energy sources considered are tidal stream and wind. Components considered are the electrolyser, HB+ASU, and battery interface (for power sizing). As described in Appendix A, the tidal turbine CAPEX is appropriate for 100-200 MW of tidal capacity. There is a large uncertainty in the tidal turbine CAPEX, thus an upper (2,900 USD kW^{-1}) and lower (2,200 USD kW^{-1}) bound will be applied in the model (Table A.1).

Storage components considered are battery and hydrogen storage. The battery self-discharge is 5% per month [8]. The HB ramp up and down limits are 2% per hour and 20% per hour respectively [10]. The minimum load of the HB is 20% of rated capacity [11]. The electrolyser is assumed to ramp up and down instantaneously and is modelled with a constant conversion efficiency of $50\ kW\ h\ kg^{-1}$ [8], [12]. The last 14 days of every year modelled are allocated to maintenance time [8], whereby no ammonia is produced. Hence, an operational year is 8,424 hours (365 days minus 14 days). However, ideally, maintenance could be done during the least productive power periods.

The total $OPEX$ (USD/y) is presented in Eqn. 3:

$$OPEX = \frac{CF(H_2O,H_2)}{CF(NH_3,H_2)} Cost_W F + Cost_{OM} CAPEX \qquad \textit{(Eqn. 3)}$$

where $Cost_W$ is the cost of desalinated water (2 USD/t [8]) and $Cost_{OM}$ are the operating and maintenance costs (2% of CAPEX [8]). The conversion factors are $CF(H_2O, H_2)$, water to hydrogen mass ratio, and $CF(NH_3, H_2)$, ammonia to hydrogen mass ratio. From stoichiometry: $CF(H_2O, H_2) = 9\ kg_{H_2O}/kg_{H_2}$ and $CF(NH_3, H_2) = 17/3\ kg_{NH_3}/kg_{H_2}$.

To account for different energy sources and variability of wind, two studies are simulated:

Study 1:

Low, baseline, and high wind years for both tidal and wind vs wind only, i.e. 6 scenarios.

Study 2:

30 consecutive years, representing the plant's lifetime, for both tidal and wind vs wind only, i.e. 2 scenarios.

A sensitivity analysis is performed on the tidal CAPEX value relative to the wind CAPEX value to determine the cut-off CAPEX values at which no tidal and all wind is utilised by the techno-economic model and vice versa.

3.2.2. Tidal stream resource

3.2.2.1. Tidal stream turbine power

The tidal current flow velocity data from the PFOW model [3], [7] is used in this research to determine the power variation of an Atlantis AR2000 tidal turbine in the Pentland Firth (the AR2000 will be utilised in the MeyGen Project [13]). The AR2000 has a rated capacity of 2 MW, a cut-in velocity of <1 m/s, rated velocity of 3.05 m/s and rotor diameter of 20 m [14], [15].

The tidal turbine power P (MW) is determined (as shown in Appendix B) using Eqn. 4:

$$P = \frac{1}{2}\rho A C_p u^3 \qquad \textit{(Eqn. 4)}$$

where ρ is the density of fluid, A is the swept area of turbine, C_p is the power coefficient and u is the fluid velocity.

The velocities at each location are taken as the average of the middle 3 sigma layers. This is to account for the location of the turbine in the water. Yang et al. [16] demonstrate that the location of the largest power output of a tidal turbine is at the middle of the water column.

3.2.2.2. Tidal stream turbine location and layout

The ideal tidal turbine location is where the tidal stream currents are reliably and consistently fast. This results in a large power output from the turbines over a period of time, requiring fewer turbines to produce a fixed amount of ammonia, which will enable a lower LCOA. Thus, a region in the Pentland Firth with high annual energy production from tidal turbines is chosen for analysis.

Due to local tidal current velocity variation, each tidal turbine will have a different annual energy production capacity.

To determine which tidal turbine power profiles are used as an input to the technoeconomic model, the locations (nodes in the PFOW model) with the largest annual energy production in the region considered are selected, which constrains the layout of tidal turbines. The average power profiles from 100 MW (i.e. 50 nodes with one turbine per node) of tidal power capacity were input to the technoeconomic model (Figure 3.3). The calculated total tidal power capacity output by the technoeconomic model may be more or less than 100 MW. This is justified since only a small region of the Pentland Firth is exploited for tidal stream power in this chapter. Moreover, each node (and thus power profile) could potentially represent more than one turbine, so a capacity output by the technoeconomic model of more than 100 MW is justified. If the capacity output by the technoeconomic model is less than 100 MW, this would be a conservative approximation as fewer, better power profiles (and thus a lower tidal capacity) could represent the required tidal stream power input. The LCOA could be lowered (by a couple percentage points) if the required and calculated tidal turbine power capacities in the ammonia model (Figure 3.3) are matched. However, using a fixed number of tidal turbine power profiles is a justified engineering approximation for this chapter.

3.2.3. Wind resource

The wind profile is from ECMWF (European Centre for Medium-Range Weather Forecasts) Reanalysis v5 (ERA5) [17]. ERA5 data is reported every hour since 1979 and has a high resolution of 0.25° for latitude and longitude. The north and east velocity components are converted to the resultant velocity for 1991-2020. The reference height, h_{ref}, at which the velocities, u_{ref}, are reported at in ERA5 is $100\ m$. In Eqn. 5, the Hellmann exponent, α, is about 0.1 for wind turbines above the ocean [18], [19] which allows the wind velocities, u, at $h = 119\ m$ (the hub height) to be calculated.

$$u = u_{ref}\left(\frac{h}{h_{ref}}\right)^{\alpha} \qquad \textit{(Eqn. 5)}$$

The power curve used is that of the DTU 10 MW wind turbine [20] – the cut-in, rated and cut-out wind speeds are 4, 11.4, and 25 m/s respectively, the blade diameter is 178.3 m and the hub height is 119 m. Several recent, relevant papers utilising offshore wind also use the DTU 10 MW turbine including Baldi et al. [21], Martinez and Iglesias [22] and Wang et al. [23]. The wind turbine power is determined using Eqn. 4 (as shown in Appendix B).

3.2.3.1. Wind turbine location and layout

The wind location is constrained to the same region of the Pentland Firth with high tidal turbine annual energy production. The wind turbine layout is less constrained compared to the tidal stream turbine layout (in terms of wake recovery distance [24]). The specific layout of wind turbines will not be considered but rather the maximum limit on wind power in an area will be factored in. The maximum wind turbine power density that avoids hindrance due to wake effects is 5 MW km^{-2} [25].

3.3. Results and Discussion

3.3.1. Tidal stream energy in the Pentland Firth

A heat map of the annual energy produced from an isolated, 2 MW tidal turbine within the Pentland Firth is shown in Figure 3.5. A smaller region within the Pentland Firth with the highest annual energy production is focused upon in the inset of Figure 3.5. The highest capacity factor in this smaller region is 0.631 with 10,634 MWh of energy produced per year. Figure C.1 (in Appendix C) shows the proposed layout of tidal turbines in that region. The turbine downstream spacing is approximately 200 m (10 diameters).

3.3.2. Wind energy in the Pentland Firth

Wind velocities are determined at [-3.24, 58.65], as this is the closest location to the inset of Figure 3.5. At this wind location, the annual capacity factor is relatively high but variable over 1991-2020 (Figure 3.6). For Study 1 of the technoeconomic analysis, 2010 is the low wind year (capacity factor 0.488), 2020 is the baseline wind year (capacity factor 0.536) and 2015 is the high wind year (capacity factor 0.589).

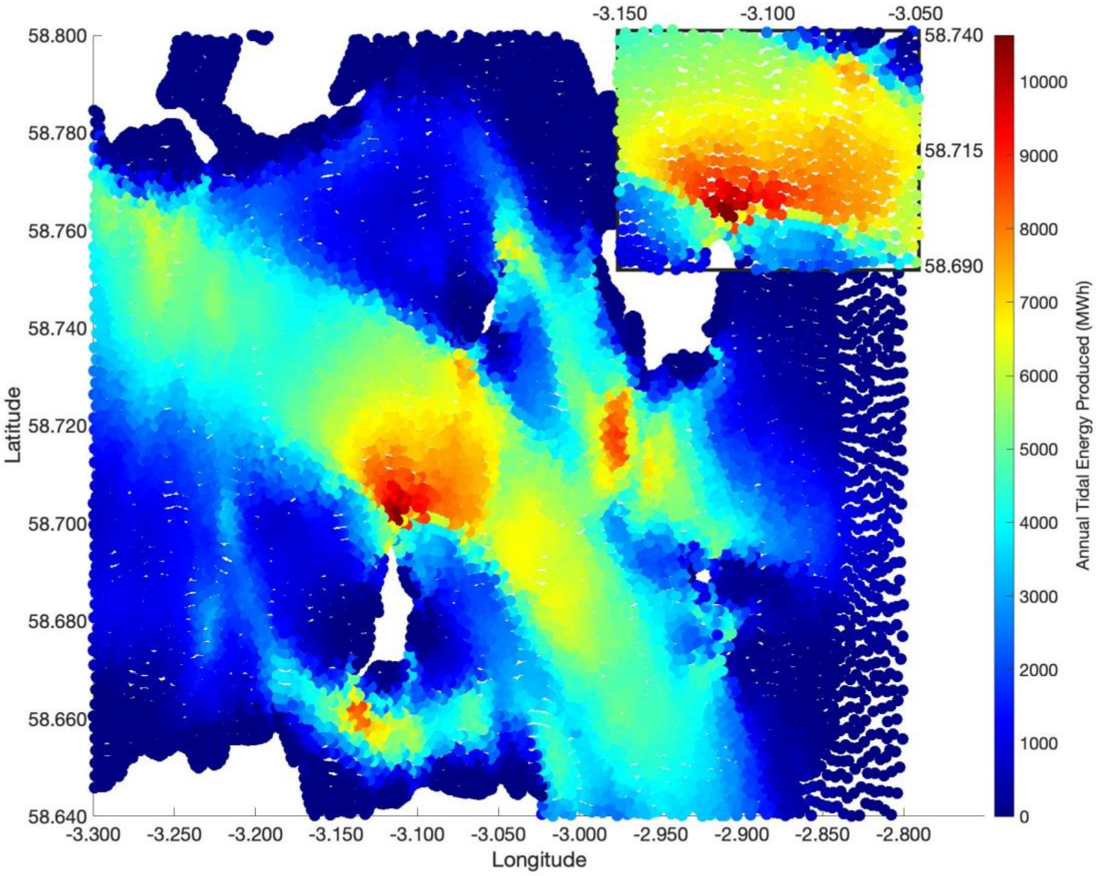

Figure 3.5: Heat map of the Annual Energy Produced from an AR2000 2 MW turbine in the Pentland Firth. The longitude range is (-3.300)-(-2.800) and the latitude range is 58.640-58.800. For the inset, the longitude range is (-3.150)-(-3.050) and the latitude range is 58.690-58.740

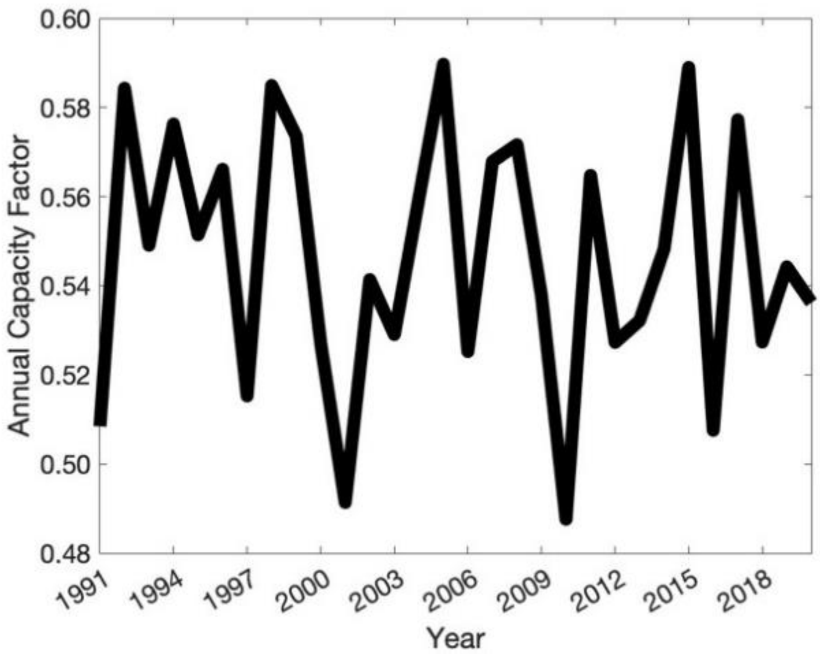

Figure 3.6: Annual Capacity Factor of a 10 MW DTU Offshore Wind Turbine at [-3.24, 58.65] over the years 1991-2020

3.3.3. Study 1: Low, baseline, and high wind years

Using a basis of 100,000 tons NH_3 produced per year, the model is run for 2010 (low wind year), 2020 (baseline wind year) and 2015 (high wind year).

In the wind-only case and compared to a baseline wind year, on a low wind year 10% more wind capacity is required, and on a high wind year 9% less wind capacity is required (Figure 3.7). This is expected as more wind capacity is necessary to produce 100,000 tons/y of NH_3 on a low wind year and vice versa.

In the wind+tidal case and compared to a baseline wind year, on a low wind year, 86% less wind and 6% more tidal capacity are required, and on a high wind year, 362% more wind and 32% less tidal capacity are required (Figure 3.8). This makes sense as wind capacity is favoured over tidal capacity in a high wind year and vice versa.

The LCOA is 18%, 12%, and 5% lower when tidal capacity is added to wind capacity in 2010, 2020 and 2015 respectively (Figure 3.9), quantifying the benefit of utilising tidal stream energy for ammonia production.

When the higher value of the tidal turbine CAPEX is used (2,900 USD kW^{-1}), significantly more wind and less tidal is utilised, which is expected, as the ammonia model operates to minimize the LCOA. The LCOA is still lower when tidal capacity is added to wind capacity, but by a smaller margin (by 5%, 3%, and 1% in 2010, 2020 and 2015 respectively).

Comparing the wind+tidal case (Figure 3.8) to the wind-only case (Figure 3.7), significantly less fuel cell capacity and hydrogen storage are required for the former. Figure 3.10 helps to explain this behaviour: tidal stream power displays a different, more consistent power profile compared to wind power, demonstrating the practical benefit of utilising tidal stream energy.

In each case (Figure 3.9), the LCOA is above the historical (2000-2020) brown ammonia price range (100-600 USD/t [26]).

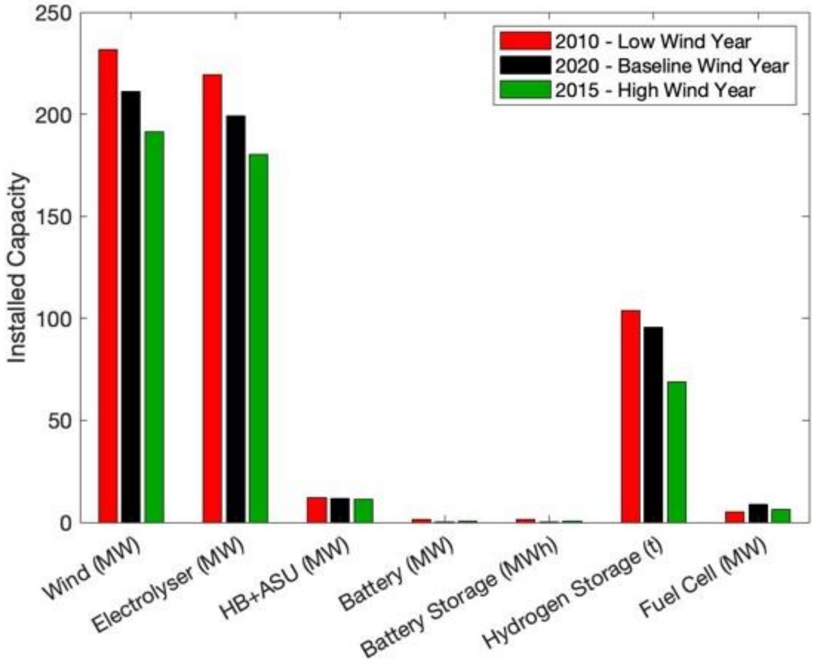

Figure 3.7: Wind only - Comparison of Equipment Capacities for wind years 2010, 2020 and 2015 (Study 1). The ammonia production is fixed at 100,000 tons/year

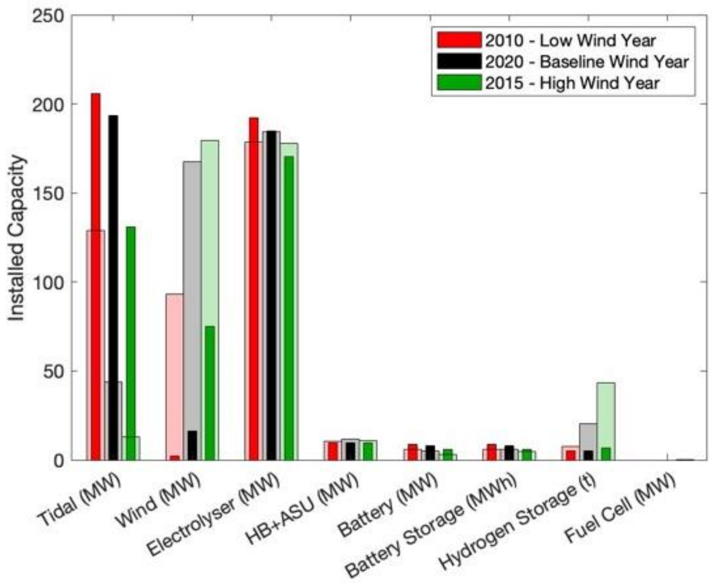

Figure 3.8: Wind+tidal - Comparison of Equipment Capacities for wind years 2010, 2020 and 2015 (Study 1). The ammonia production is fixed at 100,000 tons/year. The wider bars represent the higher value of tidal turbine CAPEX

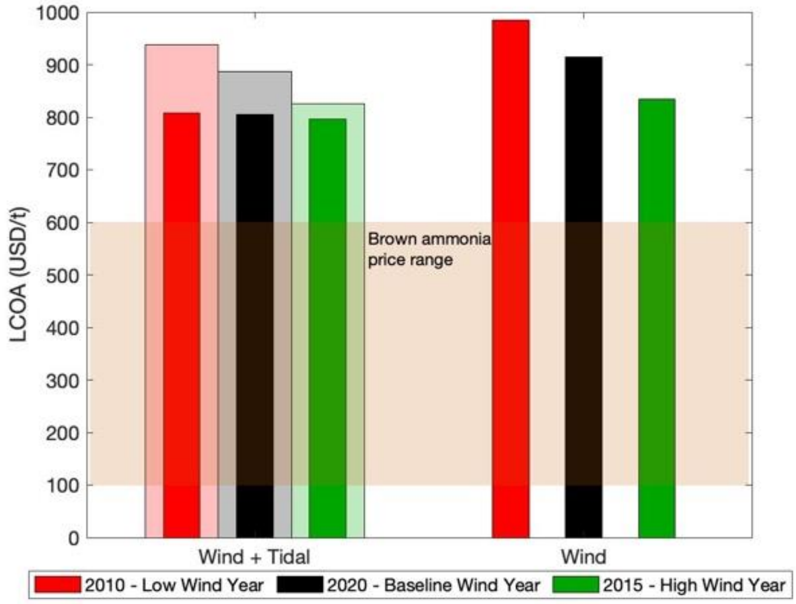

Figure 3.9: Comparison of LCOA for wind+tidal vs. wind only for wind years 2010, 2020 and 2015 (Study 1). The ammonia production is fixed at 100,000 tons/year. The historical brown ammonia price range is 100-600 USD/t [26]. The wider bars represent the higher value of tidal turbine CAPEX

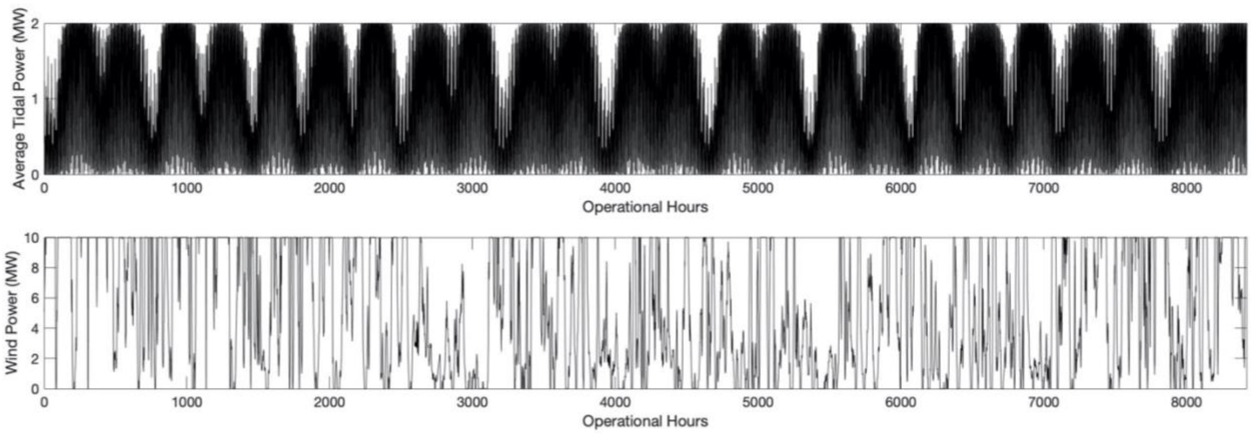

Figure 3.10: Power profile for an average tidal turbine and wind turbine over the 2020 operational year

3.3.4. Study 2: Consecutive wind years

The results for three separate wind years are useful to show how wind variability must be incorporated to plant design, but it is unrealistic to run the plant with a different number of tidal turbines and wind turbines each year. Running 30 years of consecutive wind and tidal data gives a robust plant design and a single installed capacity value for each piece of equipment. Using the same basis of 100,000 tons NH_3 per year, the model is run for 30 consecutive years, 1991-2020.

In the wind-only case, 209 MW of wind is required (Figure 3.11). In the wind+tidal case, 17 MW of wind and 192 MW of tidal are required. When the higher value of the tidal turbine CAPEX is used, in the wind+tidal case, 176 MW of wind and 32 MW of tidal are required. Similar to Study 1, when the higher value of the tidal turbine CAPEX is used, significantly more wind and less tidal is utilised, which makes sense. Moreover, if adding tidal capacity to wind capacity were not economically beneficial, the technoeconomic model would not utilise tidal capacity. Since the tidal capacity utilised is large relative to the wind capacity utilised (in the wind+tidal case with the lower tidal CAPEX case), utilising tidal can be remarkably beneficial.

The LCOA for green ammonia utilising wind+tidal (806 USD/t or 885 USD/t when the higher value of the tidal turbine CAPEX is used), and wind only (918 USD/t) is not competitive with the historical (2000-2020) brown ammonia price range (Figure 3.12). However, 2021 grey ammonia prices were >1,000 USD/t due to natural gas shortages [26]. Moreover, according to IRENA and AEA, the general LCOA for green ammonia is 720-1,400 USD per tonne today (and is predicted to drop to 310-610 USD per tonne in 2050) [26]. Thus, the LCOA for both wind+tidal and wind only in this chapter are economically attractive compared to the IRENA and AEA estimations of green ammonia today. This could enhance the capacity of the UK to produce ammonia locally, which is important in the context of energy security.

Similar to Study 1, the LCOA is lower (by 12% or 4% when the lower/higher value of the tidal turbine CAPEX is used) when tidal capacity is added to wind capacity. This is primarily due to the significantly reduced storage requirements: the wind+tidal case requires no fuel cell capacity and up to 96% less hydrogen storage (corresponding to a 63 M USD CAPEX reduction – Figure 3.13) compared to the wind-only case. However, the wind+tidal case requires up to 7.3 MWh more battery storage (with a minimal CAPEX increase of around 3 M USD) compared to the wind-only case, due to the (predictable) short-term tidal power variation. The total renewables CAPEX is 464-510 M USD for the wind+tidal case and 495 M USD for the wind-only case. The electrolyser requires the largest capacity in the ammonia plant and a 6-7% lower electrolyser capacity is required for the wind+tidal case compared to the wind-only case (corresponding to a 9-10 M USD lower CAPEX).

Since the fuel cell is not utilised in the wind+tidal case, the HB and ASU can operate successfully from wind and tidal energy with battery back-up. Moreover, in the wind-only case, all three internal energy storage assets (battery storage, hydrogen storage and fuel cell capacity) are needed thus adding cost and complexity to the overall system.

In both studies, the curtailed energy is <3% which is relatively low.

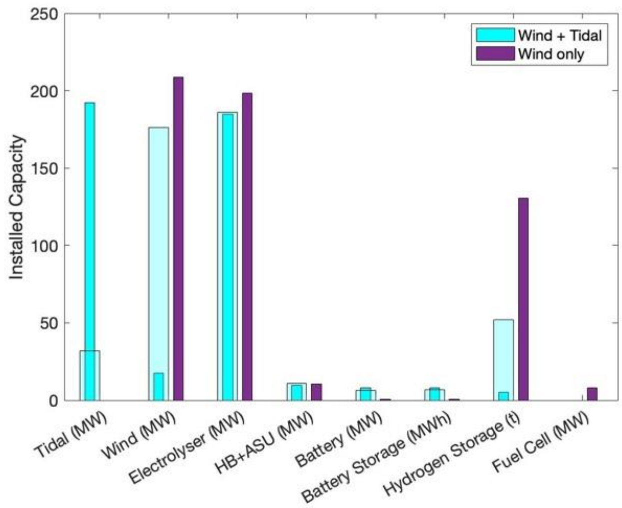

Figure 3.11: Comparison of Equipment Capacities for wind+tidal vs. wind only for consecutive wind years 1991-2020 (Study 2). The ammonia production is fixed at 100,000 tons/year. The wider bars represent the higher value of tidal turbine CAPEX

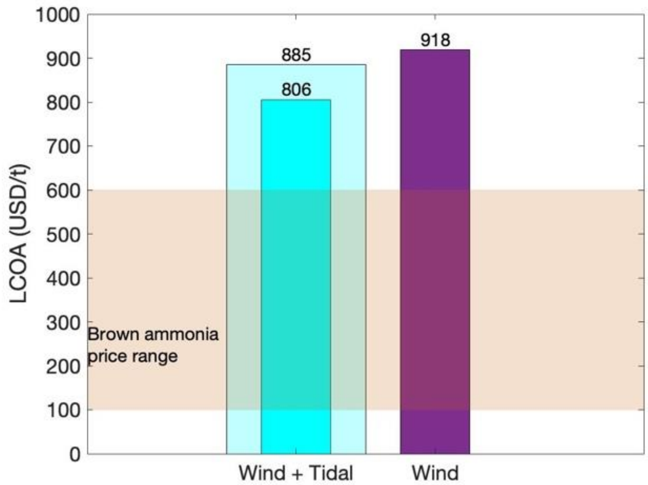

Figure 3.12: Comparison of LCOA for wind+tidal vs. wind only for consecutive wind years 1991-2020 (Study 2). The ammonia production is fixed at 100,000 tons/year. The historical brown ammonia price range is 100-600 USD/t [26]. The wider bars represent the higher tidal turbine CAPEX

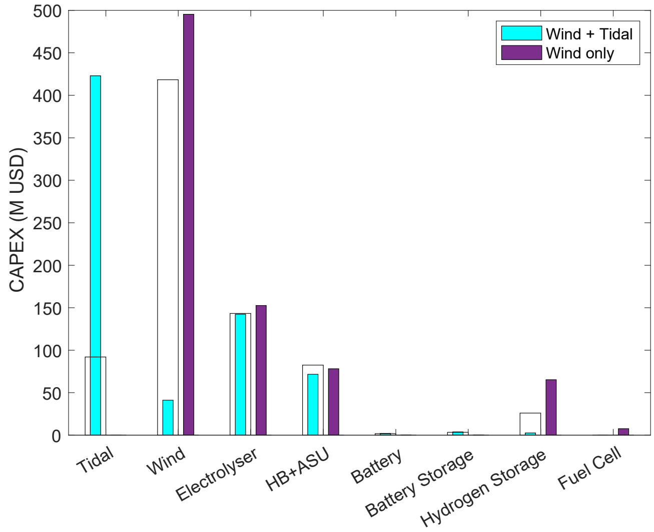

Figure 3.13: Comparison of Equipment CAPEX for wind+tidal vs. wind only for consecutive wind years 1991-2020 (Study 2). The ammonia production is fixed at 100,000 tons/year. The wider bars represent the higher value of tidal turbine CAPEX

3.3.5. Comparison of offshore and onshore cost

The results in this chapter are valid for offshore ammonia production. The offshore platform cost for ammonia production is substantial (see Table A.1). Onshore production of ammonia may be more appropriate since the tidal turbines that are utilised are close to shore (~10 km). Using Eqn. A.2 in Appendix A, the cost of a HVAC offshore cable to shore is around 45 M USD for this case study, which is significantly lower than the cost of an offshore ammonia platform (120 M USD [27]). Moreover, tidal stream energy hotspots tend to be remote for grid connectivity but close to shore [6].

Thus, while offshore production is likely to be more expensive than onshore production, in general land limitations and restrictions may motivate offshore ammonia production, particularly for places such as the UK which have low land availability but good offshore energy resources [28].

3.3.6. Tidal CAPEX sensitivity

The tidal turbine CAPEX has a large uncertainty, so an upper and lower bound was incorporated into the analysis, corresponding to 1.22 and 0.93 times the wind CAPEX. Moreover, in Section 2.1.5., it is acknowledged that in the UK today, tidal stream energy has an LCOE three times larger than offshore wind energy [6]. To see the extent to which the techno-economic model utilises tidal capacity over wind capacity, the tidal CAPEX is varied from 0.5 to 3 times the wind CAPEX (Figure 3.14 - using the baseline wind year, 2020). When the tidal CAPEX is less than around 0.75 times the wind CAPEX, the techno-economic model utilises all tidal capacity and no wind capacity. However, when the tidal CAPEX is more than around 2.4 times the wind CAPEX, the techno-economic model utilises all wind capacity and no tidal capacity. These cut-off values will likely vary with location-dependent wind and tidal power profiles, the time frame (e.g. 1 year or 30 years), as well as the relative energy storage equipment CAPEX costs. Interestingly, when the tidal and wind CAPEX values are equal, around 83% of the renewable capacity is tidal capacity. Thus, tidal stream power is a better renewable resource than offshore wind power for this green ammonia production scenario.

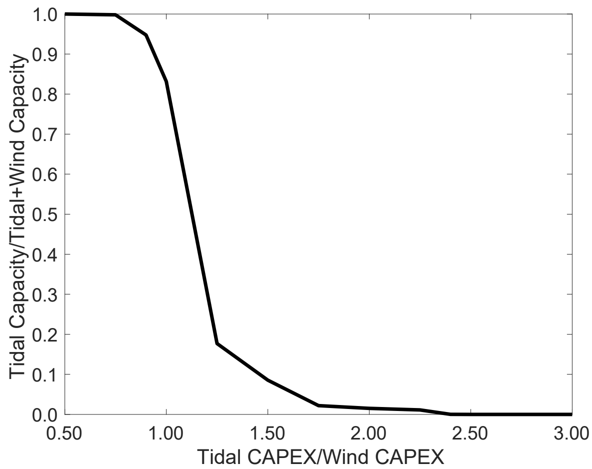

Figure 3.14: Sensitivity of tidal CAPEX relative to wind CAPEX and the impact on the fraction of tidal capacity out of the total renewable capacity (tidal and wind) that the techno-economic model utilises. A single baseline wind year, 2020, is used for the wind power profile

3.4. Limitations

In order to model the green ammonia plant, powered by wind and tidal stream energy, practical modelling decisions were made. There are four modelling decisions which could be further improved.

Firstly, the power coefficient of each tidal turbine and wind turbine is assumed constant, in line with Lewis et al. [15], although the power coefficient may vary with velocity, turbulence and blade design [29].

Secondly, the average of the middle 3 sigma layers is used to find the tidal stream velocity values. This may not be representative of the actual velocity profile that enters the turbine since the turbine may not be located exactly in the middle of the water column at all locations considered. To account for this, O'Hara Murray and Gallego [3] include a factor in the velocity terms to account for the percentage of the area of the turbine (perpendicular to the flow) in each sigma layer. This may be a more accurate way to represent the velocity profile entering the turbine.

Thirdly, the tidal turbine CAPEX was not specific to an AR2000, due to lack of public domain information. More accurate tidal stream turbine CAPEX values should be used in future work, for example, using the Metric Space criterion designed by Garcia-Sanz [30] at the ARPA-E ATLANTIS program (U.S. Department of Energy).

In the wind-only case there are consecutive hours when there is no wind power. However, the Haber-Bosch reactor still operates at 20% capacity, requiring significant hydrogen storage and fuel cell capacity. It could be economically beneficial to shut down the plant when there is an extended period of low wind power input. To achieve this, instead of having maintenance time at the last 14 days of the year, the maintenance time could be optimised to a particularly low wind power period.

3.5. Conclusion

The objective of this chapter was to determine if tidal stream energy is a useful energy resource (technically and economically) for offshore green ammonia production. The case study on the Pentland Firth demonstrated that producing green ammonia from tidal and wind energy resources is technically feasible and economically attractive compared to conventional green ammonia from solar and wind onshore (in 2020). For both wind+tidal vs. wind only, two studies are simulated; firstly, using separate low, baseline, and high wind years to show the impact of variable wind years on LCOA and secondly, using 30 consecutive wind years - representing the plant's lifetime.

For the 30-year study, the LCOA for green ammonia utilising wind+tidal (806 USD/t), and wind only (918 USD/t) is lower than recent extreme grey ammonia prices (>1,000 USD/t given natural gas shortages [26]) but higher than the historical brown ammonia price (100-600 USD/t [26]). Adding tidal stream capacity to wind capacity decreases the hydrogen storage requirement by 96% and eliminates the fuel cell requirement and thus reduces the LCOA (by 12%). In the first study, for low, baseline, and high wind years, the LCOA is 5-18% lower when tidal capacity is added to wind capacity. When the higher tidal turbine CAPEX is used, the LCOA is also lower, but by a smaller margin (1-5%). Thus, utilising tidal stream power is economically beneficial in both cases.

A sensitivity analysis was performed on the tidal CAPEX – the tidal CAPEX was varied from 0.5 to 3 times the wind CAPEX to see the extent to which the techno-economic model utilises tidal capacity over wind capacity. Using the baseline wind year, 2020, it is shown that when the tidal and wind CAPEX values are equal, tidal capacity dominates (83%) the total renewable capacity, demonstrating the adequacy of tidal power as an energy source for green ammonia production.

This chapter did not include tidal-only green ammonia production analysis in the Pentland Firth and in other tidal hotspots. This is explored in Chapter 5.

Given the global transition to green ammonia from conventional high-carbon ammonia, it is valuable to identify all suitable sources of renewable energy. Tidal stream energy is a novel and ideal energy source for offshore green ammonia production given its high resource availability and predictability.

References:

[1] A. J. Goward Brown, S. P. Neill, and M. J. Lewis, "Tidal energy extraction in three-dimensional ocean models," *Renew. Energy*, vol. 114, pp. 244–257, 2017.

[2] S. P. Neill, A. Vögler, A. J. Goward-Brown, S. Baston, M. J. Lewis, P. A. Gillibrand, S. Waldman, and D. K. Woolf, "The wave and tidal resource of Scotland," *Renew. Energy*, vol. 114, pp. 3–17, 2017.

[3] R. O'Hara Murray and A. Gallego, "A modelling study of the tidal stream resource of the Pentland Firth, Scotland," *Renew. Energy*, vol. 102, no. B, pp. 326–340, 2017.

[4] "TIDAL STREAM TECHNOLOGY ROADMAP," SIMEC Atlantis Energy. Accessed: Jun. 15, 2022. [Online]. Available: https://simecatlantis.com/tidal-stream/

[5] "MEYGEN," SIMEC Atlantis Energy. Accessed: Nov. 14, 2021. [Online]. Available: https://simecatlantis.com/projects/meygen/

[6] D. Coles, A. Angeloudis, D. Greaves, G. Hastie, M. Lewis, L. Mackie, J. McNaughton, J. Miles, S. Neill, M. Piggott, D. Risch, B. Scott, C. Sparling, T. Stallard, P. Thies, S. Walker, D. White, R. Willden, and B. Williamson, "A review of the UK and British Channel Islands practical tidal stream energy resource," *Proc. R. Soc. A*, vol. 477, no. 2255, p. 20210469, 2021.

[7] R. O'Hara Murray and L. Campbell, "Pentland Firth and Orkney Waters Climatology 1.02," Marine Scotland. Accessed: Jan. 06, 2022. [Online]. Available: 10.7489/12041-1

[8] N. Salmon and R. Bañares-Alcántara, "Impact of grid connectivity on cost and location of green ammonia production: Australia as a case study," *Energy Environ. Sci.*, vol. 14, no. 12, pp. 6655–6671, 2021.

[9] N. Salmon, R. Bañares-Alcántara, and R. Nayak-Luke, "Optimization of green ammonia distribution systems for intercontinental energy transport," *iScience*, vol. 24,

no. 8, p. 102903, 2021.

[10] M. Fasihi, R. Weiss, J. Savolainen, and C. Breyer, “Global potential of green ammonia based on hybrid PV-wind power plants,” *Appl. Energy*, vol. 294, p. 116170, 2021.

[11] S. S. Beerbühl, M. Fröhling, and F. Schultmann, “Combined scheduling and capacity planning of electricity-based ammonia production to integrate renewable energies,” *Eur. J. Oper. Res.*, vol. 241, no. 3, pp. 851–862, 2015.

[12] R. M. Nayak-Luke and R. Bañares-Alcántara, “Techno-economic viability of islanded green ammonia as a carbon-free energy vector and as a substitute for conventional production,” *Energy Environ. Sci.*, vol. 13, no. 9, pp. 2957–2966, 2020.

[13] Black & Veatch, “Lessons Learnt from MeyGen Phase 1A Final Summary Report,” Surrey, UK, 2020. [Online]. Available: https://webassets.bv.com/2020-06/MeyGen Lessons Learnt Full Report_0.pdf

[14] J. I. Encarnacion, C. Johnstone, and S. Ordonez-Sanchez, “Design of a Horizontal Axis Tidal Turbine for Less Energetic Current Velocity Profiles,” *J. Mar. Sci. Eng.*, vol. 7, no. 7, p. 197, 2019.

[15] M. Lewis, R. O’Hara Murray, S. Fredriksson, J. Maskell, A. de Fockert, S. P. Neill, and P. E. Robins, “A standardised tidal-stream power curve, optimised for the global resource,” *Renew. Energy*, vol. 170, pp. 1308–1323, 2021.

[16] Z. Yang, T. Wang, and A. E. Copping, “Modeling tidal stream energy extraction and its effects on transport processes in a tidal channel and bay system using a three-dimensional coastal ocean model,” *Renew. Energy*, vol. 50, pp. 605–613, 2013.

[17] H. Hersbach, B. Bell, P. Berrisford, G. Biavati, A. Horányi, J. Muñoz Sabater, J. Nicolas, C. Peubey, R. Radu, I. Rozum, D. Schepers, A. Simmons, C. Soci, D. Dee, and J.-N. Thépaut, “ERA5 hourly data on single levels from 1979 to present,” Copernicus Climate Change Service (C3S) Climate Data Store (CDS). Accessed: Mar.

10, 2022. [Online]. Available: 10.24381/cds.adbb2d47

[18] A. Abolude and W. Zhou, “A Comparative Computational Fluid Dynamic Study on the Effects of Terrain Type on Hub-Height Wind Aerodynamic Properties,” *Energies*, vol. 12, no. 1, p. 83, 2019.

[19] Y. Liu, D. Chen, Q. Yi, and S. Li, “Wind Profiles and Wave Spectra for Potential Wind Farms in South China Sea. Part I: Wind Speed Profile Model,” *Energies*, vol. 10, no. 1, p. 125, 2017.

[20] C. Bak, F. Zahle, R. Bitsche, T. Kim, A. Yde, L. C. Henriksen, M. H. Hansen, J. P. A. A. Blasques, M. Gaunaa, and A. Natarajan, “The DTU 10-MW Reference Wind Turbine,” 2013. [Online]. Available: https://backend.orbit.dtu.dk/ws/portalfiles/portal/55645274/The_DTU_10MW_Reference_Turbine_Christian_Bak.pdf

[21] F. Baldi, A. Coraddu, M. Kalikatzarakis, D. Jeleňová, M. Collu, J. Race, and F. Maréchal, “Optimisation-based system designs for deep offshore wind farms including power to gas technologies,” *Appl. Energy*, vol. 310, p. 118540, 2022.

[22] A. Martinez and G. Iglesias, “Mapping of the levelised cost of energy for floating offshore wind in the European Atlantic,” *Renew. Sustain. Energy Rev.*, vol. 154, p. 111889, 2022.

[23] S. Wang, A. R. Nejad, and T. Moan, “On design, modelling, and analysis of a 10-MW medium-speed drivetrain for offshore wind turbines,” *Wind Energy*, vol. 23, no. 4, pp. 1099–1117, 2020.

[24] R. Vennell, S. W. Funke, S. Draper, C. Stevens, and T. Divett, “Designing large arrays of tidal turbines: A synthesis and review,” *Renew. Sustain. Energy Rev.*, vol. 41, pp. 454–472, 2015.

[25] P. Ruiz, W. Nijs, D. Tarvydas, A. Sgobbi, A. Zucker, R. Pilli, R. Jonsson, A. Camia,

C. Thiel, C. Hoyer-Klick, F. Dalla Longa, T. Kober, J. Badger, P. Volker, B. S. Elbersen, A. Brosowski, and D. Thrän, “ENSPRESO - an open, EU-28 wide, transparent and coherent database of wind, solar and biomass energy potentials,” *Energy Strateg. Rev.*, vol. 26, p. 100379, 2019.

[26] IRENA and AEA, “Innovation Outlook: Renewable Ammonia,” International Renewable Energy Agency, Abu Dhabi, Ammonia Energy Association, Brooklyn, 2022. [Online]. Available: https://www.irena.org/publications/2022/May/Innovation-Outlook-Renewable-Ammonia

[27] H. Wang, P. Daoutidis, and Q. Zhang, “Harnessing the Wind Power of the Ocean with Green Offshore Ammonia,” *ACS Sustain. Chem. Eng.*, vol. 9, no. 43, pp. 14605–14617, 2021.

[28] N. Salmon and R. Bañares-Alcántara, “A global, spatially granular techno-economic analysis of offshore green ammonia production,” *J. Clean. Prod.*, vol. 367, p. 133045, 2022.

[29] A. Mason-Jones, D. M. O’Doherty, C. E. Morris, T. O’Doherty, C. B. Byrne, P. W. Prickett, R. I. Grosvenor, I. Owen, S. Tedds, and R. J. Poole, “Non-dimensional scaling of tidal stream turbines,” *Energy*, vol. 44, no. 1, pp. 820–829, 2012.

[30] M. Garcia-Sanz, “A Metric Space with LCOE Isolines for Research Guidance in wind and hydrokinetic energy systems,” *Wind Energy*, vol. 23, no. 2, pp. 291–311, 2020.

Chapter 4: Tidal Stream Phasing

Tidal stream energy is a predictable renewable energy source, and utilising the difference in phase of tidal stream currents in close-by locations can provide a more stable power profile. This stable power profile could be useful as ammonia production has limited flexibility, and although hydrogen production is more flexible, a stable power profile could avoid electrolyser oversizing. This chapter explores the effect of tidal stream phasing on both green ammonia and green hydrogen production in the English Channel. The coefficient of variation (CV) of the power profiles between three locations is used as a metric of tidal phasing, and the minimum is determined from locations in the English Channel appropriate for an Orbital O2 turbine. This minimum CV method is novel and can be applied to other tidal regions.

4.1. Introduction

Green ammonia production utilises green hydrogen (via electrolysis with renewable energy input) and nitrogen (via air separation with renewable energy input) as reactants in a Haber-Bosch reactor [1]. Ideally, green ammonia production should utilise a steady renewable energy input due to the limited operation flexibility of the Haber-Bosch reactor. In contrast, compared to the Haber-Bosch reactor, electrolysers do not have strict ramping constraints [2], so a steady renewable energy input is likely to be more beneficial for green ammonia production than for green hydrogen production. However, alkaline electrolysers operating in China (at Sinopec's large-scale Kuqa facility) have encountered unexpectedly low efficiencies due to the intermittent renewable input power [3]. Thus, a steady power profile may still be valuable for green hydrogen production.

Green ammonia and green hydrogen production studies are generally based on solar and wind renewable energy, which are variable renewable energy sources; wind is largely unpredictable.

The UK has an excellent tidal stream resource, which is largely unexploited due to historically high tidal stream turbine costs and grid capacity limitations in tidal hotspots such as Orkney (North Scotland) [4].

Tidal stream energy is variable but predictable. Tidal stream phasing, i.e. utilising tidal stream currents with a phase (time) variation in nearby locations, can provide a less variable and yet predictable power profile. Phasing reduces the maximum power and increases the minimum power of the aggregate power profile. The lower maximum power could ensure the equipment is less oversized, reducing the equipment CAPEX requirement, which could be cost beneficial to both green ammonia and green hydrogen production.

The author was the first to present an analysis of green ammonia production using tidal stream energy, with a case study in the Pentland Firth [5] (Chapter 3). Subsequently, two tidal stream phasing methods were explored by the author (in two papers) for green ammonia production: in the first one, correlation coefficients were used to identify anti-correlated tidal regions in Orkney and the Irish Sea - this was the first study to present an analysis of the benefit of tidal stream phasing on green ammonia production [6]; in the second one, a genetic algorithm was used to select tidal turbine locations which optimize the aggregate tidal stream power profile in four regions around the UK, i.e. automatically choosing turbine locations rather than choosing tidal regions manually through correlation coefficients – this was the first study to incorporate optimal tidal stream phasing with green ammonia production [7].

While these are both useful and successful techniques for incorporating tidal phasing, they have some important limitations. Firstly, the correlation coefficient method depends on how a tidal region is manually defined, that is, which turbine locations are considered within a tidal region. Since phasing is highly spatially dependent, grouping turbine locations into a tidal region has the potential to miss phasing opportunities. Secondly, the genetic algorithm is non-deterministic, which incorporates uncertainty into the modelling. The minimal CV method presented in this chapter avoids these two issues as turbine locations are analysed individually, and the method is deterministic. Moreover, the minimal CV method is simple and is a novel way of choosing turbine locations for green fuel production.

Although this is not the first study to model green hydrogen production from tidal stream energy (as mentioned in the literature review, section 2.2.5.2.), this is the first detailed study to model green hydrogen production from *phased* tidal stream energy and is adapted from a conference paper by the author [8] with more detail.

Apart from the paper presented by the author, which used a genetic algorithm to select tidal turbine locations [7], there are only two academic papers which optimize the location of tidal stream turbines to optimize the aggregate power profile by exploiting complementary phase differences – Neill et al. [9] and Giorgi and Ringwood [10], from 2014 and 2013 respectively. Giorgi and Ringwood [10] utilise a genetic algorithm over 11 locations around the island of Ireland, and Neill et al. [9] utilise a greedy algorithm over the northwest European shelf seas. The work described in this chapter utilises a smaller region than in [9] or [10] (thus reducing the cable costs), and utilises tidal stream energy for green ammonia/hydrogen production, rather than for the grid. Improvements of this work with respect to [9] and [10] include: i) using all water depths above the minimum operable turbine water depth (not constrained to 25–50 m as in [9]), since floating turbines are considered which can operate in deep water [11], and ii) no restriction on the minimum velocity, apart from the cut-in velocity of the tidal turbine (a minimum M2 current of 1.5–2.5 m/s is used in [9], and a minimum tidal current velocity of 2.0 m/s is used in [10]).

Previous literature on tidal phasing in the UK utilises between 100 MW [12] to several GW [13] of tidal stream power, from locations all around the UK, for the purpose of grid power demand (as detailed in the literature review). Realistically, local ammonia/hydrogen production from tidal stream power requires tidal sites close together. Thus, phasing potential is assessed for a given small area located around the UK. The UK is chosen as there are tidal stream velocities data available in this region - the Scottish shelf model (SSM) climatology version 2.01 [14] provides 3D tidal stream velocities at hourly and high spatial resolution around the UK. The PFOW model (used in Chapter 3) is part of the SSM but the PFOW model has a higher spatial resolution than the SSM and is exclusive to the Pentland Firth and Orkney waters. The English Channel has both tidal stream energy potential and phasing potential [9][12]. As discussed in the literature review, the Pentland Firth has high tidal stream energy potential but has limited phasing potential. Moreover, there are other areas around the UK which have some phasing potential but are relatively spread out (such as within the Irish Sea [11]). Thus, the English Channel will be the focus of this chapter.

4.2. Methodology

The tidal stream turbine is modelled as a horizontal axis, twin-rotor, Orbital O2 turbine. This turbine model was chosen firstly due to its low rated velocity of 2.5 m/s [15] at 2 MW rated power which allows a high quantity of energy to be extracted from the turbine over a spring-neap cycle, and secondly as it is a floating turbine, which utilises the fast currents near the sea surface and suits a large range of water depths [13]. The cut-in velocity is 1 m/s, the rated velocity is 2.5 m/s and the cut-off velocity is 4.5 m/s [16]. The Orbital O2 power curve is displayed in the Appendix (Figure B.2). Each turbine has a rotor diameter of 20 m and a minimum water depth of 23.2 m [16]. The Orbital O2 turbine is deployed at the EMEC Fall of Warness tidal test site [16], and is a part of the FORWARD2030 (Fast-tracking Offshore Renewable energy With Advanced Research to Deploy 2030MW of tidal energy before 2030) project [17].

Using the Scottish Shelf Model version 2.01 (SSM) [14], all nodes (hereafter called locations) in the English Channel with a minimum water depth above 28.2 m (23.2 m plus a 5 m bottom clearance [18]) and a capacity factor (CF) of 15-20% are considered (Figure 4.3). This CF range is chosen because phasing is only relevant if the constituent power profiles are of similar energy. Secondly, there is little phasing potential for high CF turbine locations around the UK [12] (and thus within the English Channel). 15% is the lower CF limit in a tidal phasing study in Japan [19]. Moreover, a turbine CF of 20% is used in another tidal phasing study [20].

Sigma layers are chosen (out of 20) to be suitable for the average location of the turbines in the water column. Moreover, the number of sigma layers is selected based on the vertical distance that the turbine fills in the water column. That is, the diameter of the turbine relative to the mean lowest water depth in the region. Since the turbines modelled are floating, sigma layers close to the top of the water column are chosen (low sigma layer values). The 3-D tidal stream velocities are larger near the top of the water column (near the surface) and lower near the bottom of the water column (by the seabed).

The number of turbines per location is chosen as the maximum allowable according to the turbine spacing constraint of 2.5D lateral by 10D downstream [18] (where D is rotor diameter for a single-rotor turbine. For the dual-rotor Orbital O2 device, D is taken as the lateral width of the device during operation, 45 m [16]). The area allocated per location in the SSM will differ, so the number of turbines per location will also differ. That is, there is one power profile allocated to each location, but more than one turbine could be allocated to each location.

The coefficient of variation (CV) has been used in the literature to assess the suitability of tidal sites to different turbines and as a metric of tidal phasing [21][19]. A phased profile has a low CV, with a low proportion of time at zero or maximum power, as the constituent power profiles have highs and lows at slightly different times (as seen in Figure 4.5). The CV is dimensionless and can be compared to other variable profiles (not just for tidal stream power profiles).

$$CV = \frac{\sigma_P}{\mu_P}$$

σ_P is the standard deviation, μ_P is the mean and P is the hourly tidal stream power profile over an operational year (1 year minus 2 weeks of maintenance time i.e. 8,424 hours).

In order to find three locations with complementary phasing, the aggregate power profiles of every combination of a trio of locations are considered, and the combination with the lowest CV over an operational year is chosen (positioning shown in Figure 4.4). This minimum CV method is a novel method for choosing turbine locations with complementary phasing. There are 229 turbine locations with a CF of 15-20% (Figure 4.3) - combining three power profiles out of 229 turbine locations results in almost 2 million different power profiles and almost 2 million different CV values. Three turbine locations are chosen to balance the optimization time and the phasing benefit. Increasing the number of turbine locations to be optimized increases the potential phasing benefit but increases the number of possible combinations exponentially, and thus increases the optimization time significantly. The purpose of this chapter is to show the potential phasing benefit to the LCOA/LCOH, and three turbine locations give a good picture of this. An onshore location that is suitable for a green ammonia/hydrogen plant is also identified in Figure 4.4 (i.e. on grassland [22] and avoiding protected land [23]).

To see the effect of phasing on the levelized cost of ammonia (LCOA) and the levelized cost of hydrogen (LCOH), the LCOA and LCOH from the three locations are determined separately (i.e. three power profiles and three plants) and then combined (i.e. one aggregate power profile and one plant). If the LCOA and LCOH from the combined power profile is less than the average LCOA and LCOH from the three separate power profiles, then phasing is useful.

Two major adjustments were made to the green ammonia model compared to Chapter 3. Firstly, the model incorporates green hydrogen production (separate to green ammonia production) – so both an LCOA and LCOH can be determined. Secondly, a demand profile for the product (ammonia or hydrogen) is incorporated, which requires storage of the product. The model was created by Carlo Palazzi, another DPhil student in the OXGATE group (developed using Calliope v0.6.10 [24] in Python). The model was adapted by the author to incorporate tidal stream energy as an energy input and to incorporate a cable cost. The model is an LP model, instead of an MILP model in the first chapter, as the ramping constraints were recast as linear constraints. The updated green ammonia flow diagram is displayed in Figure 4.1 and the green hydrogen flow diagram is displayed in Figure 4.2. The model overview is displayed in Figure D.1 and Figure D.2 in Appendix D. Model verification is in Appendix E.

Other minor adjustments to the model compared to Chapter 3 include: no curtailment, the fuel cell can support the electrolyser, battery and the HB+ASU (not just the HB+ASU), the HB ramping limits are 2% up and 2% down (rather than the 2% up and 20% down used in Chapter 3), which is a conservative modelling decision but affects the LCOA negligibly, the fuel cell efficiency is incorporated at 50% [25], the desalination energy is 4.2 kWh/t of water [25] (not 2 USD/t of water as in Chapter 3), and the hydrogen compression energy is incorporated at 2.016 kWh/kg [25].

The green ammonia and green hydrogen model is used to find the minimum cost of ammonia and hydrogen production. The time resolution of the model is one hour. One year of hourly tidal stream power data is incorporated with two weeks of maintenance time at the end of the year. Ammonia and hydrogen are collected from the plant every hour. A flat hourly hydrogen/ammonia demand profile is used in a green hydrogen/ammonia study in Queensland, Australia [25] and is chosen for this chapter to avoid large hydrogen/ammonia storage requirements, which could dwarf the costs of the plant itself and any potential phasing benefit.

Equipment CAPEX costs are displayed in Table A.1. The upper tidal CAPEX cost is used, which is a conservative modelling assumption. Operating costs are assumed to be 2% of CAPEX costs (as in Chapter 3). The Haber-Bosch (HB) reactor has a 20% minimum load [2]. The electrolyser is modelled as fully flexible. Hydrogen storage, battery storage and a fuel cell are incorporated for internal storage within the ammonia/hydrogen plants.

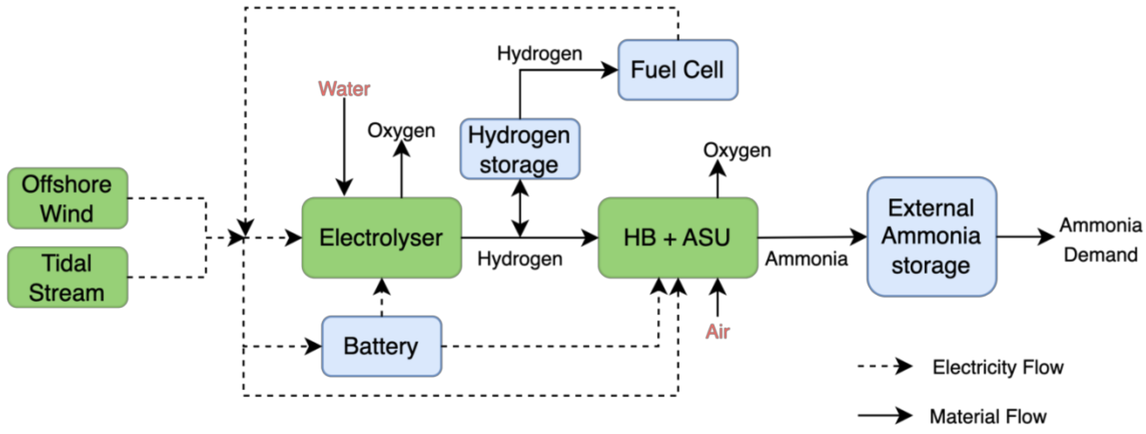

Figure 4.1: Updated flow diagram displaying the units involved in green ammonia production, electricity flow between them and material inputs and outputs. Energy storage units are in blue

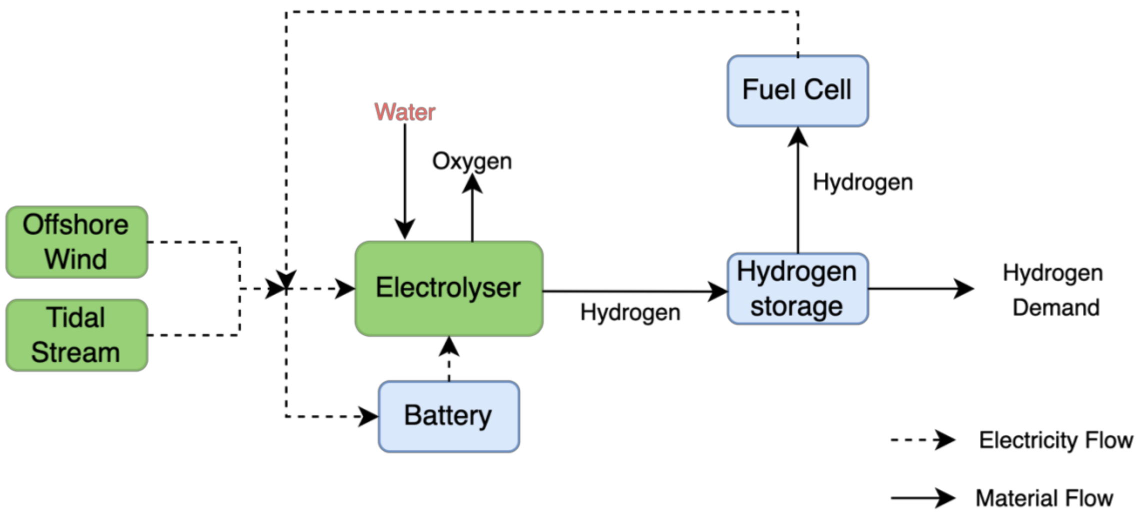

Figure 4.2: Flow diagram displaying the units involved in green hydrogen production, electricity flow between them and material inputs and outputs. Energy storage units are in blue

The three tidal stream turbine locations chosen will be separate (in distance) from each other and also from the ammonia/hydrogen plant. Therefore, as a post-optimization step, a cable cost from the ammonia/hydrogen plant to the tidal stream turbine locations must be factored into the LCOA and LCOH (Table 4.1). Subsea HVAC cabling is cheaper than subsea HVDC cabling for transmission distances lower than around 80 km [26]. The transmission distances in this chapter are not expected to be much larger than 80 km, so HVAC is chosen as the subsea cable type. The subsea HVAC cable cost is difficult to determine accurately as detailed costing information is not available publicly. In particular, little costing information is available for low-capacity cables (~30 MW). The subsea HVAC cable CAPEX equation, Eqn. A.2, was used and is displayed in Appendix A.

4.3. Results and Discussion

The CF of tidal stream turbines in the English Channel is spatially variable (Figure 4.3). However, the CF is not the only important metric to consider when choosing a tidal stream turbine location. The stability of the power profile is also important because of the limited operation flexibility of the Haber-Bosch reactor, as discussed in the introduction. Of all the locations shown in Figure 4.3, the three locations with the lowest combined CV are shown in Figure 4.4, along with the ammonia/hydrogen plant location. The phase difference between these three locations can be seen in the 50-hour power profiles in Figure 4.5. The combined power profile is relatively stable (Figure 4.6), as reflected in its CV value of 0.53, which is considerably lower compared to the CV of the three individual locations (1.13, 1.01 and 1.31 in Table 4.1). This power stability results in a cost reduction for green ammonia and green hydrogen production despite the fact that the locations are not next to each other, requiring separate cables to power the ammonia/hydrogen plant. Compared to separate power profiles from the three locations (with three separate plants) the combined power profile (feeding one plant) has a 6% lower LCOA and a 5% lower LCOH on average (Table 4.1). That is, for the same quantity of energy produced by 80 MW of tidal stream turbines, the stability of the power profile provided by phasing can provide a cost benefit to both green ammonia and green hydrogen production.

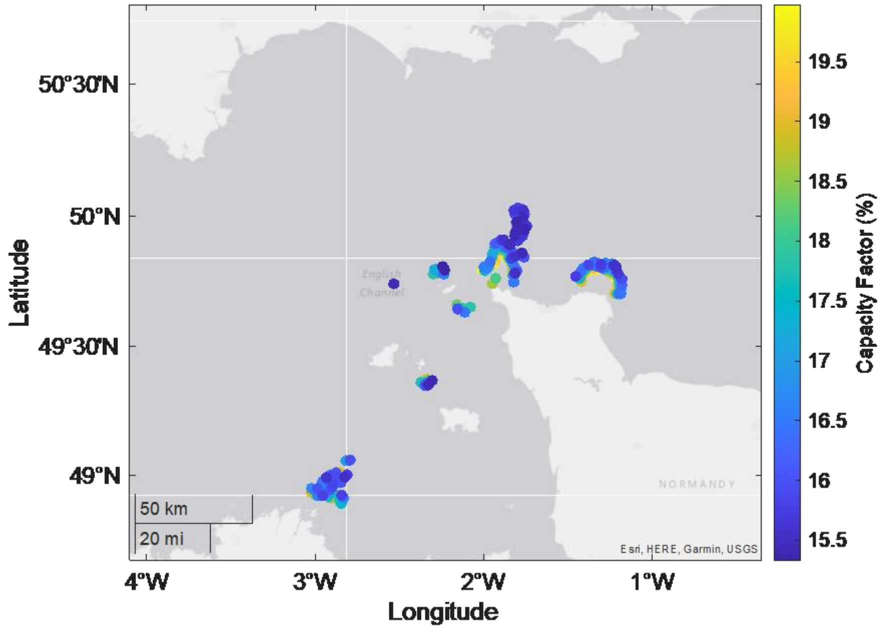

Figure 4.3: All tidal stream turbine locations in the English Channel with a minimum water depth > 28.2 m and a capacity factor range of 15-20% (for an Orbital O2 tidal turbine).

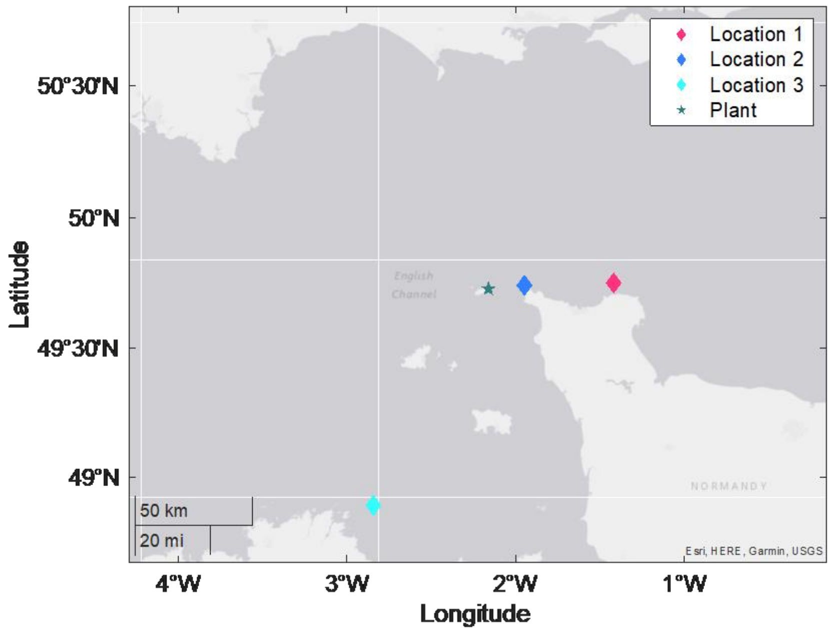

Figure 4.4: Positioning of the three turbine locations and the ammonia/hydrogen plant

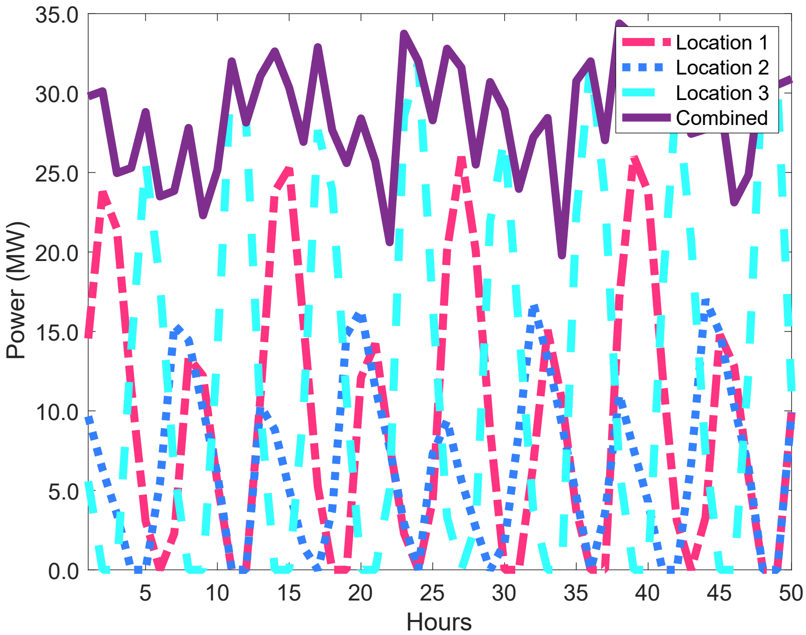

Figure 4.5: 50-hour sample of the power profiles from Location 1, Location 2, Location 3 and the combined (aggregate) power profile, visibly showing the phase difference between the three turbine locations.

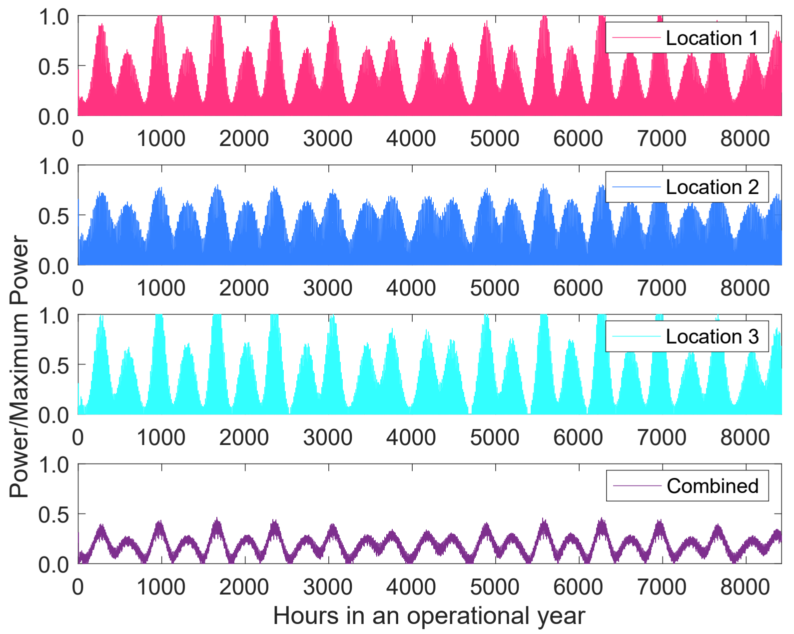

Figure 4.6: Power profiles from Location 1, Location 2, Location 3 and the combined (aggregate) power profile over an operational year

Table 4.1: The CV, yearly CF, power capacity, LCOA and LCOH corresponding to the power profiles from Location 1, Location 2 and Location 3, both separately and combined.

	LCOA (USD/t)	**LCOH (USD/t)**	**Yearly CF (%)**	**CV**	**Power (MW)**	**Cable length (km)**
Location 1	2,469	13,176	19	1.13	26	53.4
Location 2	2,391	12,681	19	1.01	22	15.4
Location 3	2,833	15,308	17	1.31	32	105.4
Combined power profiles (optimal case)	2,401	13,104	18	0.53	80	174.2
Separate power profiles (average of 3 locations)	2,564	13,722	-	-	-	-
Phasing benefit (% reduction)	6	5	-	-	-	-

The LCOA and LCOH for Location 2 are slightly lower than the optimal case due to the large cable cost for the optimal case and the particularly small cable cost for Location 2 (Table 4.1). If the cable cost is removed from the LCOA and LCOH, the levelized costs from the three locations separately are always higher than the three locations combined (the optimal, phased case). Since a limit is placed on the power capacity at each turbine location (due to the turbine spacing), utilising more power (and producing more ammonia/hydrogen) than from one turbine location requires utilising multiple turbine locations. Moreover, utilising turbine locations with a phase difference has a cost benefit.

It is important to stress that lower LCOA/LCOHs could be obtained from the higher CF tidal locations (CF > 0.2) within the region analysed. The objective of this chapter was not to find the lowest LCOA/LCOHs from tidal stream energy within the English Channel but to quantify the phasing benefit to ammonia/hydrogen production. It is likely that the highest CF tidal locations (CF > 0.2) will be deployed first, and could be used for green ammonia/hydrogen production or grid energy. Producing green ammonia/hydrogen from lower CF tidal locations (0.15 < CF < 0.2, as in this chapter) may enable the utilisation of otherwise unutilized tidal turbine locations.

Utilising phasing has a 5% cost benefit to green hydrogen production, as a 51% lower electrolyser capacity is required (Figure 4.7), as the phased power profile does not reach high power values, avoiding electrolyser oversizing. However, a 5% higher hydrogen storage capacity is required to meet the hourly hydrogen offtake. Interestingly, despite being available for use in the green hydrogen model (Figure 4.2), no battery or fuel cell capacity is utilized for the three locations – separately or combined. This is due to the assumed availability of a fully flexible electrolyser.

For green ammonia production, phasing ensures 30% less hydrogen storage, 67% less battery storage, 100% less fuel cell capacity and 48% less electrolyser capacity is required, resulting in a 6% lower LCOA (Figure 4.7). However, a 7% higher HB+ASU capacity is required, and a 10% higher ammonia storage capacity is required to meet the hourly ammonia offtake. Since the phased profile always has moderate power values, whereas the unphased power profiles reach near maximum power frequently, the flat hourly demand profile for ammonia requires slightly more ammonia production capacity and ammonia storage.

Utilising phasing has a slightly larger cost benefit to green ammonia production than to green hydrogen production due to the limited operation flexibility of the Haber-Bosch reactor (compared to the flexible electrolyser). Phasing reduces the hydrogen storage requirements for ammonia production, but not for hydrogen production.

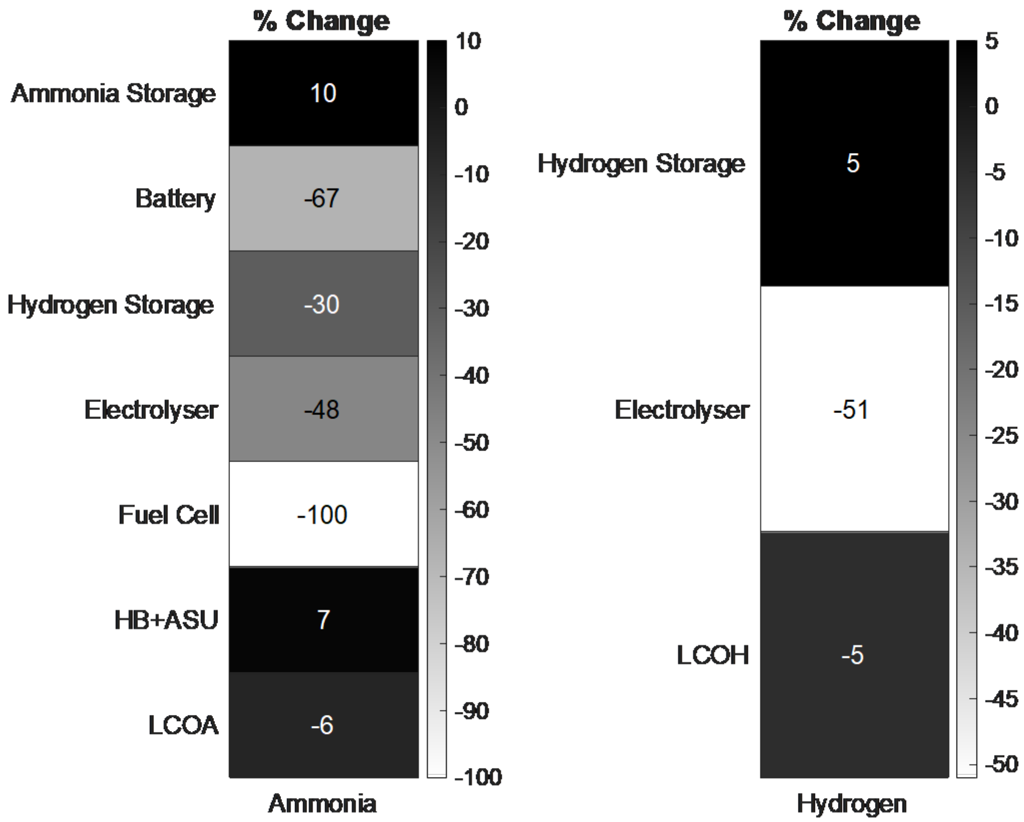

Figure 4.7: Percentage change in equipment capacities and levelized costs for the optimal case compared to the three separate plants for ammonia (left) and hydrogen (right).

Incorporating tidal phasing into green ammonia production has four main operational benefits. These comprise i) less reliance on energy storage to provide the minimum load of the HB process, ii) more consistent ammonia production, iii) lower equipment capacities, and iv) lower inventory improving process safety.

Firstly, phasing decreases the frequency and duration of low-power periods, which ensures that the minimum load of the HB process is more likely to be met by the input tidal power than by a battery or fuel cell (energy storage). Therefore, the energy storage requirement is reduced.

Secondly, phasing smooths the power profile, facilitating higher minimum powers and lower maximum powers, providing a less variable power profile over long time periods. This ensures that ammonia production is more consistent, rather than rated ammonia production for a period of time followed by no ammonia production for another period of time. Consistent ammonia production is attractive to ammonia off-takers, facilitating a consistent shipping schedule to offload ammonia, which may ease contract initiation and renewal.

Thirdly, since phasing lowers the maximum power to below the rated power, most equipment capacities are less oversized and thus have a higher load factor than if the maximum power was at rated power. This is particularly important for the electrolyser, which has the largest cost of the equipment in the plant (Figure 4.8).

Fourthly, phasing facilitates a simpler ammonia plant, improving process safety since less inventory, that is, smaller equipment and less energy storage, is required.

Incorporating tidal phasing into green hydrogen production has two main operational benefits. These comprise i) more consistent hydrogen production and ii) a lower electrolyser capacity.

On the other hand, drawbacks of utilising tidal phasing include: i) optimizing phasing tends to utilise turbines with a lower CF than the highest CF turbines resulting in a high tidal capacity required for a given ammonia/hydrogen production requirement, ii) tidal turbines may be further apart to exploit phase differences (than the highest CF turbines), which requires a longer cable, and iii) optimization modelling (to find the optimal turbine locations) may be computationally expensive and is dependent on the accuracy and resolution of the tidal stream velocity model used.

The largest contributors to the LCOA and LCOH in the optimal case are the cost of tidal capacity (~60%) and cabling (32%) (Figure 4.8). The electrolyser, storage and HB+ASU costs are not a significant proportion of the levelized costs. Cabling is significant but contributes less than the cost of tidal capacity.

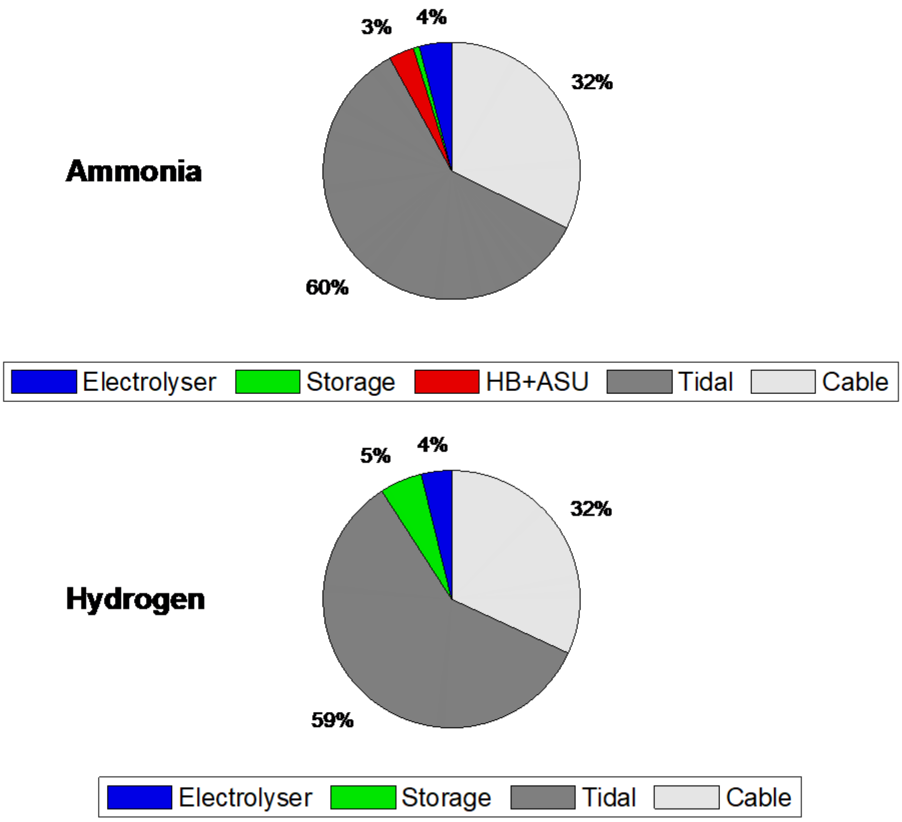

Figure 4.8: Contributions to the levelized costs of ammonia (top) and hydrogen (bottom) for the optimal case. The storage % is not shown for ammonia, as it is <1%.

It is acknowledged that a 5-6% reduction in levelized cost due to phasing is not a major decrease. Although the combined, phased power profile of the three locations does not reach zero power as frequently as the constituent profiles (Figure 4.6), the combined profile still reaches zero power during most neap tides in a year. Therefore, internal energy storage (hydrogen and battery storage) is still needed to provide the minimum load to the HB reactor (for ammonia production), and ammonia/hydrogen storage is needed to meet an hourly demand profile (for ammonia and hydrogen production). Therefore, the benefit of phasing is limited. However, these results are specific to the English Channel with an Orbital O2 turbine and a flat hourly ammonia/hydrogen demand. The results are likely to differ for a different region, a different type of turbine, and a different ammonia/hydrogen demand profile.

Tidal stream phasing could be useful in other tidal regions around the world, especially if the turbine locations are nearby and the CFs are high. The method of choosing three turbine locations by finding the minimum CV presented in this chapter could be applied to any trio of turbine locations globally.

An improvement to the optimization approach could be to include the cabling cost in the optimization of the LCOA and LCOH rather than including the cabling cost as a post-optimization cost addition. This approach may enable higher LCOA/LCOH reductions to be determined, as cabling is a large proportion of the levelized costs (Figure 4.8). However, this may only be useful if high CF turbine locations are utilised. That is, phasing may only be useful if the resultant LCOA is lower than the cost of conventional green ammonia (the cost of green ammonia today is 720-1,400 USD/t [1]). However, there is little phasing potential for high CF turbine locations around the UK [12]. There may be phasing potential for high CF turbine locations in other tidal regions around the world (such as around West Japan [19]), but if the turbine locations are not close-by, the additional cabling cost is unlikely to be worth the phasing benefit. If the turbines were connected to the grid, this may help to solve the large cable cost problem. However, phased tidal stream power on the grid may be best used for grid demand (such as electricity). Producing ammonia/hydrogen from the grid may miss some of the benefits of producing these energy vectors near the tidal hotspot. For tidal hotspots which are grid-constrained (such as Orkney [27]), there is a benefit to producing green ammonia/hydrogen where the tidal hotspots are and transporting the resulting ammonia/hydrogen to areas of demand. There is such a low deployment of tidal turbines globally (as detailed in the literature review) that grid-connected phased tidal stream power for green ammonia/hydrogen production is unlikely to be feasible at present or would produce a very small amount of product.

4.4. Limitations

While attention was given to ensuring the modelling decisions were reasonable, there are potential improvements that could be made.

The SSM has a 1993 tidal component [14]. However, it is recognised that, throughout the 18.6-year lunar cycle, the power will fluctuate. For example, Thiébot et al. [28] determined that the annual power variation over 18.6 years is +/- 10% for tidal sites in north-western Europe (Alderney Race, Ramsey Sound and Fromveur Strait). Moreover, the ammonia/hydrogen plant will be expected to run for 30 years, and the power variation year-on-year will affect the ammonia/hydrogen production and the resulting LCOA/LCOH.

The SSM has a temporal resolution of 1 hour [14]. This may limit the accuracy of the time difference between power profiles at different tidal locations (and the CV values). Moreover, tidal stream power phasing literature typically uses sub-hourly resolution tidal power data [20][9][13][12]. However, hourly resolution tidal power data is also reported in tidal stream power phasing literature [29][19][11][10][30]. Therefore, using power data at hourly resolution was deemed to be sufficient.

The spatial resolution in the area considered in the SSM is around 1 km [14], so the minimum water depth at each turbine location is hard to determine accurately. Therefore, sites with a minimum depth of less than 28.2 m may potentially not be excluded, which could mean that unrealistically shallow sites may have been included in the tidal power output.

Shipping routes and fishing areas were not excluded from the analysis as these areas can, in principle, be altered around high-energy tidal turbine sites. However, getting approval for tidal turbine sites (and associated cables) in shipping routes and fishing areas could be prohibitively time-consuming, and there could be significant opposition from local residents.

The CV values are determined for power profiles over a year using tidal velocity data with a 1993 tidal component [14]. It is acknowledged that the tidal stream velocity phase may vary slightly over 18.6 years, although any change would likely be on the order of minutes/seconds, not hours [28]. Thus, the CV values may change very slightly over the 30-year plant operation, but this is unlikely to affect the long-term viability of relying on tidal phasing for a consistent power profile. Climate change [31] could potentially influence the phase difference. However, the magnitude of phase difference change is difficult to determine and is likely to be highly region dependent. Moreover, using large-scale tidal arrays could alter the phase difference, but this would likely only be significant if tens of thousands of turbines are utilised [32].

Tidal stream power extraction can also alter tidal range, marine currents and ocean stratification which could potentially negatively affect ecosystems and marine animals [31]. The specific environmental impact of combining power capacity in different locations would need to be modelled. Since the power capacity analysed is relatively small, it is unlikely that the environmental impacts would be significant. A detailed analysis is out of the scope of this thesis.

To improve the modelling, multiple turbine types (varying in rated power, cut-in speed, diameter and position in the water column – i.e. fixed on the seabed or floating) could be incorporated, as suggested by Novo and Kyozuka [19]. Other modelling improvements include utilising accurate sigma (vertical) layers for the tidal stream velocity at every turbine location (rather than average sigma layers for the region as a whole) and incorporating a more conservative minimum operable water depth for each turbine [18]. Moreover, a distance restriction could be applied in the optimization (as suggested in [9]). This could be used to, for example, minimize the distance between the tidal turbines or minimize the distance between the ammonia/hydrogen plant location and the tidal turbines or both (with the objective of minimizing the cable cost).

The precision of the tidal model data is relatively good (as justified below), but higher spatio-temporal resolution tidal velocity and water depth data over more than a year, if available, would provide more credibility to the result that tidal phasing is beneficial for green ammonia/hydrogen production. The tidal model data precision in this work can be compared to the two other optimal-location tidal phasing papers, Neill et al. [9] and Giorgi and Ringwood [10]. The work presented in this chapter has i) A high spatial resolution: both [9] and [10] use the ROMS (Regional Ocean Modelling System) hydrodynamic model to provide tidal stream velocities. In [10], the horizontal resolution is 1.2 km, and the velocity is depth-averaged. Neill et al. [9] used 11 vertical layers, a longitude resolution of 1/24° (~3 km) and a latitude resolution of 1/32°–1/51° (~3 km). In the SSM, the spatial resolution is around 1 km, and the number of vertical (sigma) layers is 20 [14]. ii) More tidal constituents: eight are used in the SSM [33], compared to one (M2) in [9] and four in [10]. iii) A lower temporal resolution: velocities have a 10-minute temporal resolution in [10], and the temporal resolution is not stated in [9]. The SSM has a temporal resolution of one hour [14].

As well as the uncertainties in the LCOA/LCOH values already addressed (the 18.6-year lunar cycle and the spatiotemporal resolution of the tidal stream velocity data), other uncertainties include the accuracy of the tidal stream turbine power curve and equipment CAPEX. In particular, due to the novelty of the tidal turbine industry, the tidal CAPEX values are difficult to determine accurately [34]. A sensitivity analysis of these parameters on the LCOA/LCOH would identify the most important uncertainties. However, the percentage change in LCOA/LCOH between the unphased and phased scenarios is more informative than the actual LCOA/LCOH for this analysis.

It is acknowledged that wake and blockage effects are not incorporated into this chapter as the main focus of this chapter is phasing. If wake/blockage effects were incorporated, the LCOAs/LCOHs obtained would likely be higher, but the percentage change in LCOA/LCOH between the unphased and phased scenarios would likely be the same or very similar. Wake and blockage effects will be incorporated into the next chapter.

4.5. Conclusion

The novel minimum coefficient of variation (CV) method was used to determine which trio of tidal stream turbine locations to utilise within the English Channel (with a complementary phase difference). Overall, 80 MW of Orbital O2 turbines were utilized. The minimized CV (0.53) is due to the difference in phase (timing) of the three constituent power profiles, resulting in a more stable power profile. To determine if this stable power profile is beneficial to green ammonia and green hydrogen production, the levelized cost of green ammonia and green hydrogen production was determined in a model developed in Calliope [24]. This chapter utilises local, small-scale tidal power phasing for green fuel production, which is a novel concept. Utilising the phase difference between the three tidal stream turbine locations chosen (which give the minimized CV) reduces the LCOA by 6% and the LCOH by 5% after including the cable cost to the ammonia/hydrogen plant. Thus, phasing is important when considering which turbine locations to utilise for both green ammonia and green hydrogen production. However, the resultant LCOA is high (2,401 USD/t), as low CF turbine locations are used since most of the phasing potential within the English Channel is for low CF turbine locations. Thus, the LCOA is not cost-competitive with conventional ammonia. Cabling contributes to the levelized costs significantly, although less than the cost of tidal capacity. Tidal stream phasing could be more beneficial in other global tidal hotspots if the turbine locations are nearby and the CFs are high.

References

[1] IRENA and AEA, "Innovation Outlook: Renewable Ammonia," International Renewable Energy Agency, Abu Dhabi, Ammonia Energy Association, Brooklyn, 2022. [Online]. Available: https://www.irena.org/publications/2022/May/Innovation-Outlook-Renewable-Ammonia

[2] N. Salmon and R. Bañares-Alcántara, "Impact of grid connectivity on cost and location of green ammonia production: Australia as a case study," *Energy Environ. Sci.*, vol. 14, no. 12, pp. 6655–6671, 2021.

[3] L. Collins, "EXCLUSIVE | World's largest green hydrogen project 'has major problems due to its Chinese electrolysers': BNEF," Hydrogen Insight. [Online]. Available: https://www.hydrogeninsight.com/production/exclusive-worlds-largest-green-hydrogen-project-has-major-problems-due-to-its-chinese-electrolysers-bnef/2-1-1566679

[4] D. Coles, A. Angeloudis, D. Greaves, G. Hastie, M. Lewis, L. Mackie, J. McNaughton, J. Miles, S. Neill, M. Piggott, D. Risch, B. Scott, C. Sparling, T. Stallard, P. Thies, S. Walker, D. White, R. Willden, and B. Williamson, "A review of the UK and British Channel Islands practical tidal stream energy resource," *Proc. R. Soc. A*, vol. 477, no. 2255, p. 20210469, 2021.

[5] H. Driscoll, N. Salmon, and R. Bañares-Alcántara, "Technoeconomic evaluation of offshore green ammonia production using tidal and wind energy: a case study," *Energy Sources, Part A Recover. Util. Environ. Eff.*, vol. 45, no. 3, pp. 7222–7244, 2023.

[6] H. Driscoll, N. Salmon, and R. Bañares-Alcántara, "Exploiting the temporal characteristics of tidal stream power for green ammonia production," *Renew. Energy*, vol. 226, p. 120377, 2024.

[7] H. Driscoll, N. Salmon, and R. Bañares-Alcántara, "Optimal phasing of tidal stream

power around the British Isles and within the English Channel for green ammonia production,” *Renew. Energy*, vol. 241, p. 122335, 2025.

[8] H. Driscoll, C. Palazzi, and R. Bañares-Alcántara, “The Role of Tidal Stream Energy in Green Ammonia and Green Hydrogen Production in The English Channel,” in *OCEANS 2024 - Halifax*, 2024, pp. 1–4.

[9] S. P. Neill, M. R. Hashemi, and M. J. Lewis, “Optimal phasing of the European tidal stream resource using the greedy algorithm with penalty function,” *Energy*, vol. 73, pp. 997–1006, 2014.

[10] S. Giorgi and J. Ringwood, “Can Tidal Current Energy Provide Base Load?,” *Energies*, vol. 6, no. 6, pp. 2840–2858, 2013.

[11] M. Lewis, S. P. Neill, P. E. Robins, and M. R. Hashemi, “Resource assessment for future generations of tidal-stream energy arrays,” *Energy*, vol. 83, pp. 403–415, 2015.

[12] S. P. Neill, M. R. Hashemi, and M. J. Lewis, “Tidal energy leasing and tidal phasing,” *Renew. Energy*, vol. 85, pp. 580–587, 2016.

[13] A. S. Iyer, S. J. Couch, G. P. Harrison, and A. R. Wallace, “Variability and phasing of tidal current energy around the United Kingdom,” *Renew. Energy*, vol. 51, pp. 343–357, 2013.

[14] M. De Dominicis, R. O’Hara Murray, J. Wolf, and A. Gallego, “The Scottish Shelf Model 1990 – 2014 climatology version 2.01,” Marine Scotland. Accessed: Aug. 15, 2022. [Online]. Available: 10.7489/12037-1

[15] A. Alex, R. Petrone, B. Tala-Ighil, D. Bozalakov, L. Vandevelde, and H. Gualous, “Optimal techno-enviro-economic analysis of a hybrid grid connected tidal-wind-hydrogen energy system,” *Int. J. Hydrogen Energy*, vol. 47, no. 86, pp. 36448–36464, 2022.

[16] Orbital Marine Power Ltd., “Orbital O2 2MW Tidal Turbine,” Kirkwall, United

Kingdom, 2018. [Online]. Available: https://marine.gov.scot/sites/default/files/project_information_summary.pdf

[17] "Project overview," FORWARD2030. Accessed: Jul. 19, 2022. [Online]. Available: https://www.forward2030.tech/project-overview

[18] C. Legrand, *Assessment of tidal energy resource: Marine renewable energy guides*. London, UK: European Marine Energy Centre, 2009.

[19] P. G. Novo and Y. Kyozuka, "Tidal stream energy as a potential continuous power producer: A case study for West Japan," *Energy Convers. Manag.*, vol. 245, p. 114533, 2021.

[20] J. Hardisty, "Power intermittency, redundancy and tidal phasing around the United Kingdom," *Geogr. J.*, vol. 174, no. 1, pp. 76–84, 2008.

[21] Y. Wen and P. Lin, "Exploitation potential of tidal current energy in Southern China seas," *Energy Convers. Manag.*, vol. 267, p. 115901, 2022.

[22] "Land Cover Map 2021," Digimap. Accessed: Sep. 05, 2022. [Online]. Available: https://digimap.edina.ac.uk/roam/map/environment

[23] "Chapter 3 Coverage," Protected Planet. Accessed: Feb. 10, 2022. [Online]. Available: https://livereport.protectedplanet.net/chapter-3

[24] S. Pfenninger and B. Pickering, "Calliope: a multi-scale energy systems modelling framework," *J. Open Source Softw.*, vol. 3, no. 29, p. 825, 2018.

[25] A. Fletcher, H. Nguyen, N. Salmon, N. Spencer, P. Wild, and R. Bañares-Alcántara, "Queensland green ammonia value chain: Decarbonising hard-to-abate sectors and the NEM," Brisbane, Australia, 2023. [Online]. Available: https://www.griffith.edu.au/__data/assets/pdf_file/0035/1875167/No.2023-16-QLD-Green-Ammonia-Value-Chain-Main-Report.pdf

[26] B. Van Eeckhout, D. Van Hertem, M. Reza, K. Srivastava, and R. Belmans,

"Economic comparison of VSC HVDC and HVAC as transmission system for a 300 MW offshore wind farm," *Eur. Trans. Electr. Power*, vol. 20, no. 5, pp. 661–671, 2010.

[27] M. A. Almoghayer, D. K. Woolf, S. Kerr, and G. Davies, "Integration of tidal energy into an island energy system - A case study of Orkney islands," *Energy*, vol. 242, p. 122547, 2022.

[28] J. Thiébot, N. Guillou, D. Coles, and S. Guillou, "On nodal modulations of tidal-stream energy resource in north-western Europe," *Appl. Ocean Res.*, vol. 121, p. 103091, 2022.

[29] J. A. Clarke, G. Connor, A. D. Grant, and C. M. Johnstone, "Regulating the output characteristics of tidal current power stations to facilitate better base load matching over the lunar cycle," *Renew. Energy*, vol. 31, no. 2, pp. 173–180, 2006.

[30] D. Preziuso, G. García-Medina, R. O'Neil, Z. Yang, and T. Wang, "Evaluating the Potential for Tidal Phase Diversity to Produce Smoother Power Profiles," *J. Mar. Sci. Eng.*, vol. 8, no. 4, p. 246, 2020.

[31] M. De Dominicis, J. Wolf, and R. O'Hara Murray, "Comparative Effects of Climate Change and Tidal Stream Energy Extraction in a Shelf Sea," *J. Geophys. Res. Ocean.*, vol. 123, no. 7, pp. 5041–5067, 2018.

[32] R. O'Hara Murray and A. Gallego, "A modelling study of the tidal stream resource of the Pentland Firth, Scotland," *Renew. Energy*, vol. 102, no. B, pp. 326–340, 2017.

[33] M. De Dominicis, R. O'Hara Murray, and J. Wolf, "Multi-scale ocean response to a large tidal stream turbine array," *Renew. Energy*, vol. 114, pp. 1160–1179, 2017.

[34] Z. Goss, D. Coles, and M. Piggott, "Economic analysis of tidal stream turbine arrays: a review," *arXiv*, pp. 1–29, 2021. [Online]. Available: http://arxiv.org/abs/2105.04718

Chapter 5: Onshore green ammonia production using tidal stream energy: selection of global tidal hotspots

Chapter 3 demonstrated that tidal stream energy is a promising energy source for green ammonia production compared to offshore wind energy in the Pentland Firth. Nevertheless, the Pentland Firth is an exceptional tidal stream resource. This chapter assesses whether tidal stream energy can be beneficial compared to offshore wind energy in other tidal stream energy hotspots around the world, which vary in energy, depth and distance to shore.

5.1. Introduction

Chapter 3 demonstrated that adding tidal stream energy capacity to offshore wind energy capacity can reduce the LCOA by up to 18% in the Pentland Firth but did not determine the LCOA from solely tidal stream energy. Moreover, that chapter exclusively looked at *offshore* ammonia production and concluded that tidal stream energy hotspots are usually close to shore, so the cable cost from the tidal turbines to shore is likely to be lower than the offshore platform cost, so onshore ammonia production is likely to be cheaper than offshore ammonia production for tidal-ammonia. In turn, Chapter 4 demonstrated that tidal stream phasing can lower the LCOA by 6% and lower the LCOH by 5% in the English Channel but concluded that tidal stream phasing for green hydrogen and ammonia production has a limited use unless there is phasing potential among close-by turbine locations which have high CFs. This chapter incorporates tidal stream energy (unphased) and offshore wind energy in many tidal hotspots around the world and focuses on onshore ammonia production. Both tidal stream energy on its own and tidal stream energy with offshore wind energy are modelled for green ammonia production. Moreover, to ensure a more realistic green ammonia production cost, wake and blockage effects are accounted for within the LCOA and varying ammonia demand profiles are incorporated.

When green ammonia is produced, it will likely need to be stored before it is collected by a ship or a truck. In green ammonia production studies, the ammonia storage cost is usually not incorporated into the LCOA. Therefore, the LCOA without ammonia storage is determined first so that the LCOA is comparable to other studies. Then, an ammonia storage cost with an ammonia demand profile is incorporated for a more realistic production cost.

Available and suitable tidal stream velocity data around the world were searched for (Table 5.1 and Figure 5.1). The tidal data was obtained after contacting different tidal stream energy researchers worldwide. It should be noted that tidal stream velocity data is not freely available at high spatiotemporal resolution (unlike solar and wind data), so significant time and effort went into identifying useful tidal data and coordinating access to the data.
All tidal data is from models which use the hydrodynamic model FVCOM (Finite Volume Community Ocean Model). All tidal data is at hourly resolution over a year. The data for the Cook Inlet, Japan, and the Minas Passage were obtained via private communication and permission was given to use the data for the thesis.

Table 5.1: Main details of the tidal data used in this chapter. 2-D means depth-averaged.

Tidal site	**Tidal constituents**	**2-D or 3-D**	**Sigma layers**	**Spatial resolution (m)**	**Reference**	**Institution**
Pentland Firth, UK	8	3-D	10	100-150	PFOW model [1], [2] [3]	Marine Scotland, Scottish Government
Alderney Race, UK	8	3-D	20	1,000	SSM [4] [3]	
Cook Inlet, USA	13	3-D	10	100-300	Based on Wang and Yang [5]	Pacific Northwest National Laboratory
Hayasaki and Hayasui Straits, Japan	16	2-D	N/A	200-500	Based on Novo and Kyozuka [6]	Nagasaki University
Minas Passage, Canada	5	2-D	N/A	150 (regular grid)	Data not available publicly	Fundy Ocean Research Centre for Energy

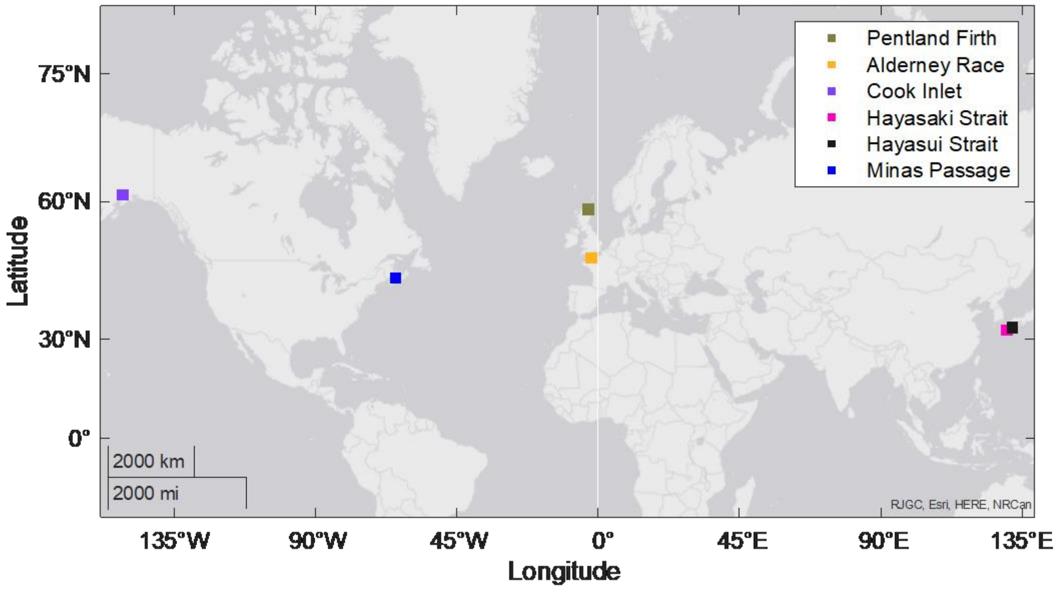

Figure 5.1: Location of tidal sites considered in this chapter

5.1.1. Blockage effects

The presence of turbines will decrease the flow velocity relative to when no turbines are present [7] - this effect is referred to as the blockage effect in this chapter. This velocity reduction depends on many factors. For example, the number of rows of turbines, blockage (turbine swept area/cross-sectional area of the channel), the number of tidal constituents, the tidal regime (diurnal, mixed diurnal, semi-diurnal or mixed semi-diurnal) and channel geometry [8]. Generally, increasing blockage and increasing the number of rows of turbines tends to increase the velocity reduction [8].

Blockage effects are also present for wind turbines but are much less important than the impact of wake effects on wind power reduction [9]. Thus, in this chapter, blockage effects are incorporated for tidal stream power but are not incorporated for wind power. The general impact of wake effects on tidal and wind power is discussed in section 2.4, and the modelling approach taken to account for wake effects is discussed in section 5.1.2. The modelling approach taken to account for blockage effects is discussed in this section.

Each site considered does not occupy the whole cross-section of the channel, only a small fraction (i.e. low blockage) since only the highest energy turbine locations are considered. However, occupying the whole cross-section will optimise the power per turbine, avoiding energy losses from flow diversion [1].

At maximum power extraction, when the whole channel is occupied by turbines, the transport reduction (volume flow rate reduction) with turbines compared to when no turbines are present could be 29% according to Garrett and Cummins [7], 38% in the Pentland Firth, UK [1], 36% in the Naru Strait, Japan [10], or 42% in the Johnstone Strait, Canada [11]. Assuming the area of the channel is constant, these transport reduction values are taken as velocity reduction values. The velocity reduction in each site in this chapter is likely to be significantly less than 29-42% since the power (200 MW) is small compared to the maximum power in each site (Table 5.2). The relationship between mean power extraction and transport reduction is non-linear – transport reduction increases more as power extraction approaches its maximum (compared to low to medium power extraction values) [12].

O'Hara Murray and Gallego [1] modelled the impact of power extraction (using 2 MW tidal stream turbines) on the transport reduction in the Pentland Firth for two different scenarios – scenario A, when the whole channel is occupied by turbines, and scenario B when a fraction of the channel is occupied by turbines (avoiding low water depths). Scenario B is more similar to the scenarios modelled in this chapter. In scenario A, at maximum power extraction (10.8 GW), 31,420 turbines cause a transport reduction of 38%. This is a very large number of turbines, causing a large transport reduction. In scenario B, 5,636 turbines cause a 6.8% transport reduction. Since this chapter considers only 100 turbines in each site (considerably less than 5,636), it is assumed that the velocity reduction will be less than 6.8%.

A 5% velocity reduction will be implemented in each site to account for the presence of turbines on the flow. A 5% velocity reduction is likely to be conservative as 200 MW is significantly less than the maximum power in each site, and there is a non-linear relationship between power extraction and transport reduction. The velocity reduction is likely to be different in each site as each has a different channel geometry, number of tidal constituents incorporated and turbine arrangement (number of rows of turbines). However, determining an accurate value of velocity reduction for each site is out of the scope of the thesis. O'Hara Murray and Gallego [1] also show that the change in velocity magnitude due to power extraction within the Pentland Firth is not spatially uniform – in some regions it increases and in some regions it decreases. Thus, applying a blanket velocity reduction within a channel is an approximation.

Table 5.2: Maximum tidal stream power in each tidal site

Tidal site	**Maximum Power (GW)**	**Reference**
Pentland Firth	10.8	[1]
Alderney Race	1.7	[13]
Cook Inlet	18	[5]
Hayasaki Strait	>> 0.2	[14]
Hayasui Strait	>> 0.2	[14]
Minas Passage	7	[15]

5.1.2. Wake effects

Wake effects refer to the reduction in velocity downstream of the turbines. It is known that the velocity exiting a turbine will be lower than the velocity entering it [16]. Although a 10D downstream spacing is applied, at 10D, the flow may not have fully recovered [17]. To account for this, a power reduction factor is incorporated on top of the 5% velocity reduction from blockage.

The power reduction factor due to wake effects (that is, power with wake effects over power with no wake effects) is around 0.90–0.95 [18][19] for a wind farm, and is approximated as 0.90 for all tidal and wind farms in this chapter. It is acknowledged that the fluid flow behavior will differ in a tidal stream turbine farm compared to a wind farm [20][21]. However, due to the lack of deployment of tidal turbines compared to wind turbines [22], and the complexity of modelling wake effects from tidal turbines [23], wake effect assumptions are drawn from wind farms in this chapter.

5.2. Methodology

1) Convert the hourly tidal stream velocity values in each tidal site to hourly tidal stream power values using the Orbital O2 power curve (Figure B.2 in the Appendix).

2) Identify 200 MW of the highest energy tidal stream power in each tidal site. 100, 2 MW tidal stream turbines are considered in each site, as approximately 200 MW of tidal stream power is required to produce 100,000 tons of ammonia per year (Chapter 3). For tidal data available in 3-D, appropriate sigma layers are chosen for the average location of the turbine in the water column within the site (as done in Chapter 4). The same turbine spacing constraint (2.5D lateral by 10D downstream where D = 45 m) and the same water depth constraint (> 28.2 m) as in Chapter 4 are incorporated.

3) Obtain an hourly offshore wind power profile at each tidal site representing a high and low wind year between 1991-2020 (as in Chapter 3). The hourly offshore wind velocities are obtained from ERA5 data [24] and converted to power using the same method as in Chapter 3 (DTU 10 MW wind turbine power curve).

4) The total power from a tidal/wind farm, P_T, will be affected by wake effects (η) and blockage effects (γ). P_T is defined as $P_T = P \times n$, where n is the number of turbines in a farm. P is the power of an individual turbine which is modified by η overall and modified by γ in the velocity term:

$$P = \eta \times \left(\frac{1}{2}\rho A C_p\right) \times (\gamma \times u)^3$$

where ρ is the density of fluid, A is the swept area of turbine, C_p is the power coefficient and u is the fluid velocity.

As justified in the introduction to this chapter, $\eta = 0.9$ for both wind and tidal.

However, $\gamma = 0.95$ for tidal and $\gamma = 1$ for wind (that is, no blockage effect is incorporated for wind).

It should be noted that the equation for P is the same as in the previous two chapters, however, it is altered by η and γ for this chapter.

The same blockage and wake correction factors are applied to all turbines in the farm (spatially constant coefficients). This is an approximation to account for a lowered power output in the presence of turbines compared to no turbines present. Two parameters (η and γ) are incorporated to highlight that two separate power reduction processes are occurring.

5) Choose a plant location onshore, close to the tidal site. Avoid protected land [25], hills and buildings.

6) Use the green ammonia model (as in Chapter 4) to find the LCOA for tidal+wind (reporting the tidal fraction utilized for both the high and low wind year) and tidal-only for each tidal site. Equipment CAPEX costs (Table A.1) and operating assumptions are the same as in Chapter 4. The upper tidal CAPEX cost is used. No ammonia storage cost is incorporated to ensure the LCOAs are comparable to other green ammonia production studies.

   As in Chapter 4, as a post-optimization step, the subsea HVAC cable CAPEX is incorporated into the LCOA using Eqn. A.2 (Appendix A).

   The same ammonia production rate (t/y) is kept for the tidal+wind cases and for the tidal-only case - this approximation was also made in Chapter 3. The tidal stream power profile is fixed for the tidal+wind cases and for the tidal-only case, but the tidal capacity calculated by the green ammonia model will vary for the tidal+wind cases (between 0 and 200 MW). In the tidal-only case, the tidal capacity is always 200 MW. This effectively changes the turbine spacing constraint, that is, reduces the number of turbines that each turbine location can represent in the tidal+wind cases compared to the tidal-only case.

7) Sensitivity analysis: Vary the demand profile (frequency of product collection) from one collection per hour to one collection per year and find the resulting tidal-only LCOA and tidal-only LCOH for the Minas Passage. The LCOH is determined for comparison to the LCOA to show the effect of the vast difference in storage cost between ammonia and hydrogen.

8) Sensitivity analysis: Vary the tidal stream velocity reduction percentage (that is, vary γ) and find the tidal-only LCOA for the Minas Passage. No ammonia demand profile is incorporated, and the ammonia storage cost is zero.

5.3. Results and Discussion

The Pentland Firth and the Minas Passage are the best tidal sites of the six analysed, as shown in their yearly power profiles (Figure 5.2), where the power is infrequently close to zero and as displayed in their high capacity factors (Figure 5.3 bottom).

The turbine location arrangement and plant location in each site is shown in Figure 5.4. Each turbine location is representative of one or more turbines, depending on the area of the turbine location (variable) and the turbine spacing constraint (constant).

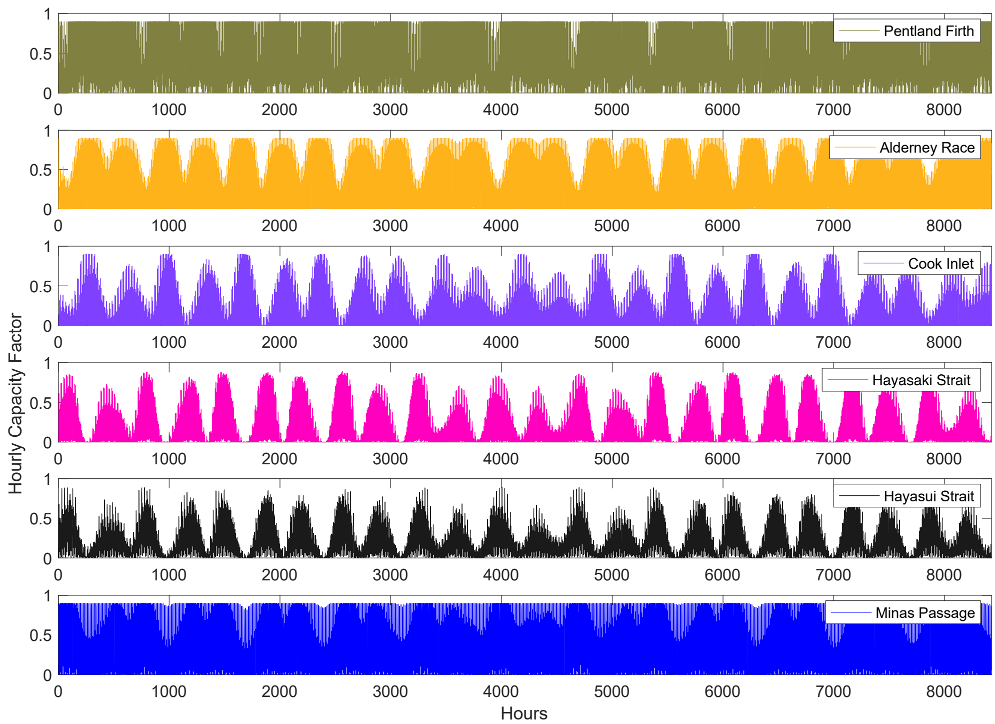

Figure 5.2: Hourly tidal stream power capacity factor profiles over an operational year in each of the six tidal sites analysed. Each profile is representative of 200 MW.

In the Alderney Race and the Hayasui Strait, some tidal capacity is chosen over wind capacity despite the lower capacity factor of the tidal resource at these sites (Figure 5.3) and the higher

CAPEX cost of tidal. In the Pentland Firth, the Cook Inlet, the Hayasaki Strait and the Minas Passage, despite the higher CAPEX cost of tidal, tidal capacity is mostly chosen over wind capacity as the tidal resource has a higher capacity factor than the wind resource at these sites. In the Pentland Firth, for the tidal+wind (high) scenario, the tidal fraction is only 0.14 due to the close capacity factor of wind (high) compared to tidal.

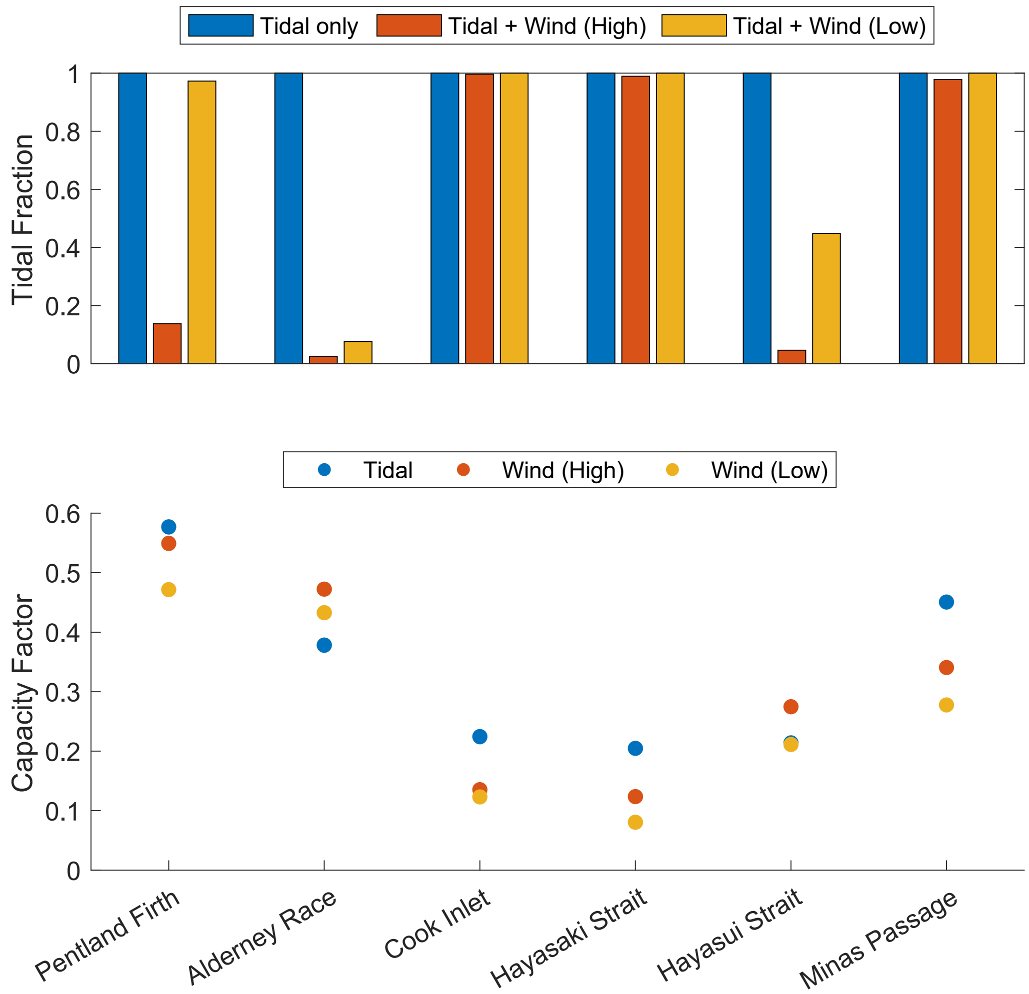

Figure 5.3: Bottom: Yearly capacity factors for 200 MW of tidal stream power and offshore wind (high and low wind years) in each site. Top: Tidal fraction chosen by the cost model for the tidal+wind (high and low) cases in each site. Tidal fraction is tidal capacity/tidal+wind capacity. A tidal fraction of 1 in the tidal only case is shown for comparison.

Figure 5.4: Turbine location arrangement and capacity factors in each tidal site. Each tidal site represents 200 MW. The production plant locations are represented by a star, and the turbine locations are represented by coloured circles (colour varies depending on the capacity factor).

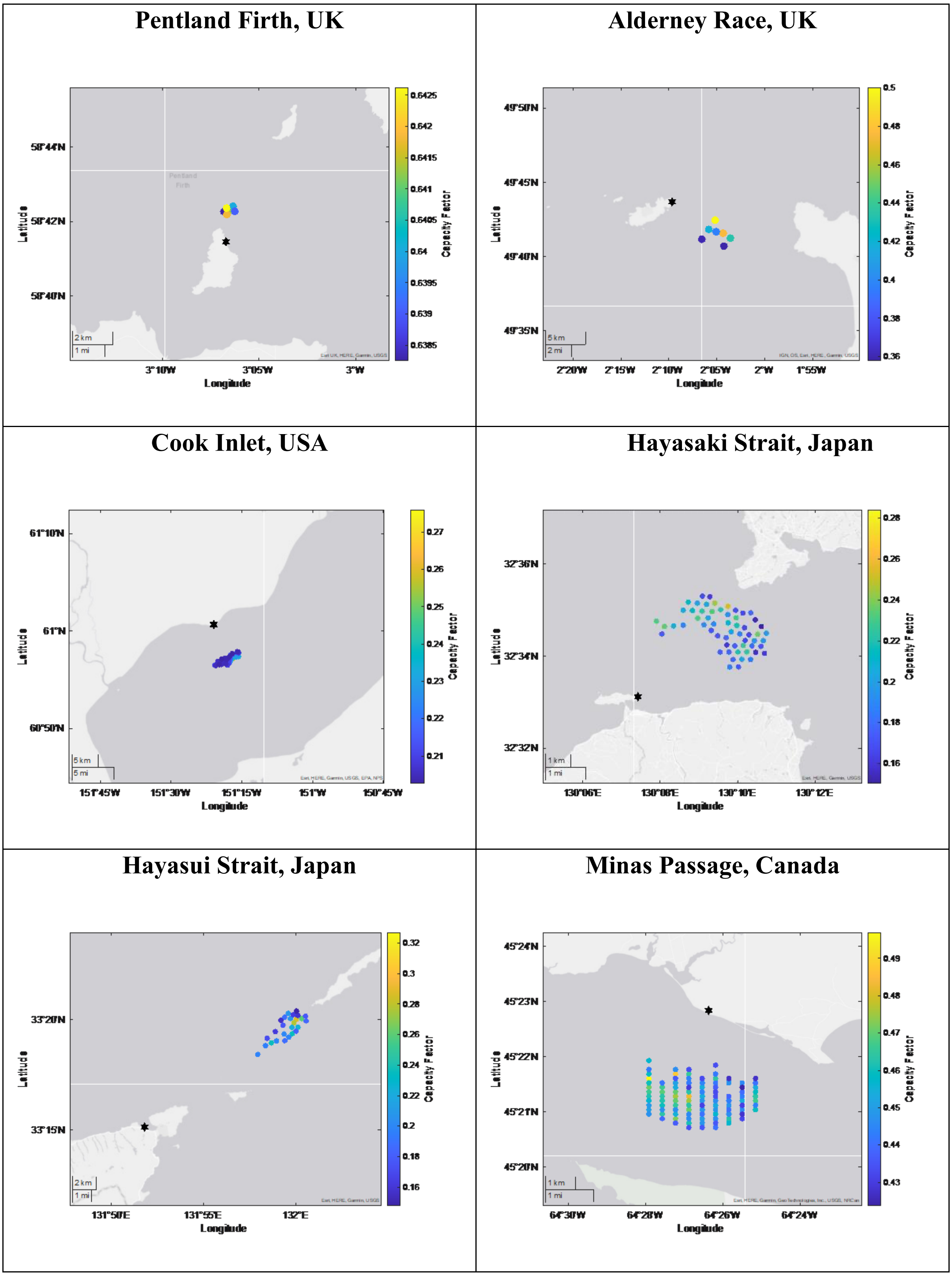

5.3.1. LCOAs

Figure 5.5 and Table 5.3 show that, at each site, the tidal+wind cases either have the same LCOA (0% change) or a lower LCOA compared to the tidal-only case. Including wind gives the largest LCOA reduction for the Alderney Race and the Hayasui Strait, as the wind capacity factors are above the tidal capacity factors in these sites (Figure 5.3). The tidal+wind (high) cases have a lower LCOA than the tidal+wind (low) cases, as the tidal+wind (high) cases have a higher wind fraction (lower tidal fraction), and wind has a lower CAPEX compared to tidal.

As shown in Chapter 3 for the Pentland Firth, the LCOA for tidal+wind using 30 years of wind data (1991-2020) would be in between the LCOA values for the tidal+wind (high) and tidal+wind (low) cases which use single wind years (between 1991 and 2020). However, the LCOA depends on which 30 years of historical wind data are used.

The long-term unpredictability of wind means that the real LCOA from a wind-based green ammonia plant would be higher than that predicted with perfect forecasting. Salmon and Bañares-Alcántara [26] demonstrated that the LCOA from a wind-dominated green ammonia plant which uses Model Predictive Control (MPC) with a 24-hour forecast would be around 20% larger than the LCOA with perfect forecasting. This LCOA increase would be site-specific and would also depend on the minimum operating rate of the Haber-Bosch, the plant equipment costs and the MPC tuning parameters.

A potential 20% increase in LCOA due to imperfect forecasting could mask any decrease in LCOA that ammonia production using tidal+wind offers compared to using just tidal (6% to 25% in Table 5.3). Moreover, Hatton et al. [27] demonstrated that the LCOA from offshore wind in the UK could become up to 8% more expensive with climate change (for 2061–2080 compared to 1981–2000) as more wind capacity is needed for the same output of ammonia due to higher wind variability or a lower energy resource (or both).

The 2020 LCOA for conventional green ammonia (solar and wind onshore) is 720-1,400 USD/t, and the historical (2000-2020) market price for brown ammonia is 100-600 USD/t [28]. The tidal-only LCOA is close to being competitive against brown ammonia in the Pentland Firth (618 USD/t). The tidal-only LCOA (Table 5.3) is competitive against conventional green ammonia in the Pentland Firth (618 USD/t), the Alderney Race (941 USD/t) and the Minas Passage (784 USD/t). In the Hayasui Strait, adding wind capacity (on a high wind year) to tidal capacity can make the LCOA (1,260 USD/t) competitive with conventional green ammonia (Figure 5.5).

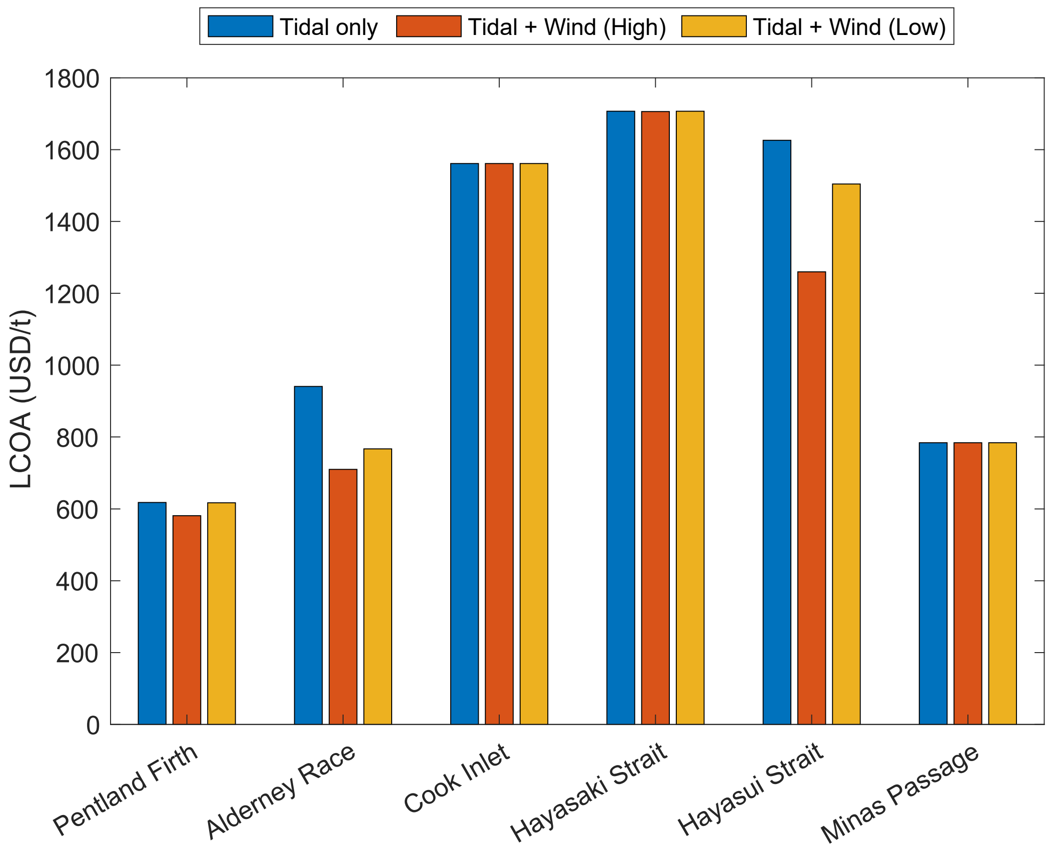

Figure 5.5: LCOA for the tidal-only case and for the tidal+wind cases in each tidal site.

Table 5.3: LCOA for the tidal-only case and the change in LCOA for the tidal+wind cases compared to the tidal-only case

	Tidal only LCOA (USD/t)	Tidal+wind (High) (LCOA % change compared to Tidal only)	Tidal+wind (Low) (LCOA % change compared to Tidal only)
Pentland Firth	618	-6	0
Alderney Race	941	-25	-18
Cook Inlet	1561	0	0
Hayasaki Strait	1707	0	0
Hayasui Strait	1626	-23	-7
Minas Passage	784	0	0

5.3.2. Sensitivity analysis: Demand profile

For green ammonia production, varying the collection of ammonia from once per hour (8,424 collections/year) to once per year increases the LCOA by 21% (Figure 5.6). For green hydrogen production, varying the collection of hydrogen from once per hour to once per year increases the LCOH by almost 950%. This large increase in LCOH compared to LCOA for the same change in product collection frequency is due to the very small ammonia storage cost compared to the hydrogen storage cost. A collection of once per year is an extreme case – a more frequent collection of product may be more realistic, such as once per month. Varying the collection frequency from once per hour (8,424 collections/year) to once per month (12 collections/year) increases the LCOA by 2% and increases the LCOH by almost 75%.

Thus, the ammonia collection frequency for green ammonia production is not an important parameter for the LCOA, but the hydrogen collection frequency for green hydrogen production is an important parameter for the LCOH. Green ammonia production may be better suited to remote areas which may have a low product collection frequency (such as the tidal sites modelled).

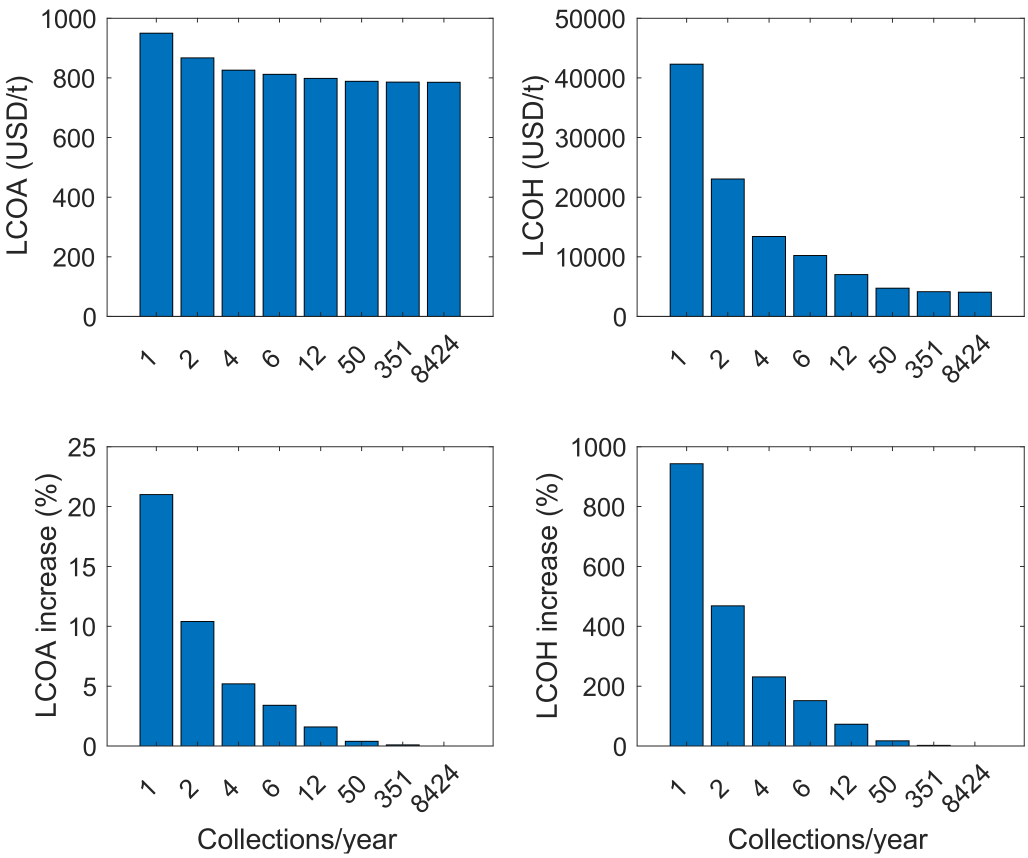

Figure 5.6: The tidal-only LCOA and tidal-only LCOH for the Minas Passage with different collection frequencies of ammonia and hydrogen, respectively (top panels). The increase in the LCOA and LCOH compared to a collection frequency of 8,424 collections/year (one collection per hour) is shown on the lower panels.

5.3.3. Sensitivity analysis: Velocity reduction

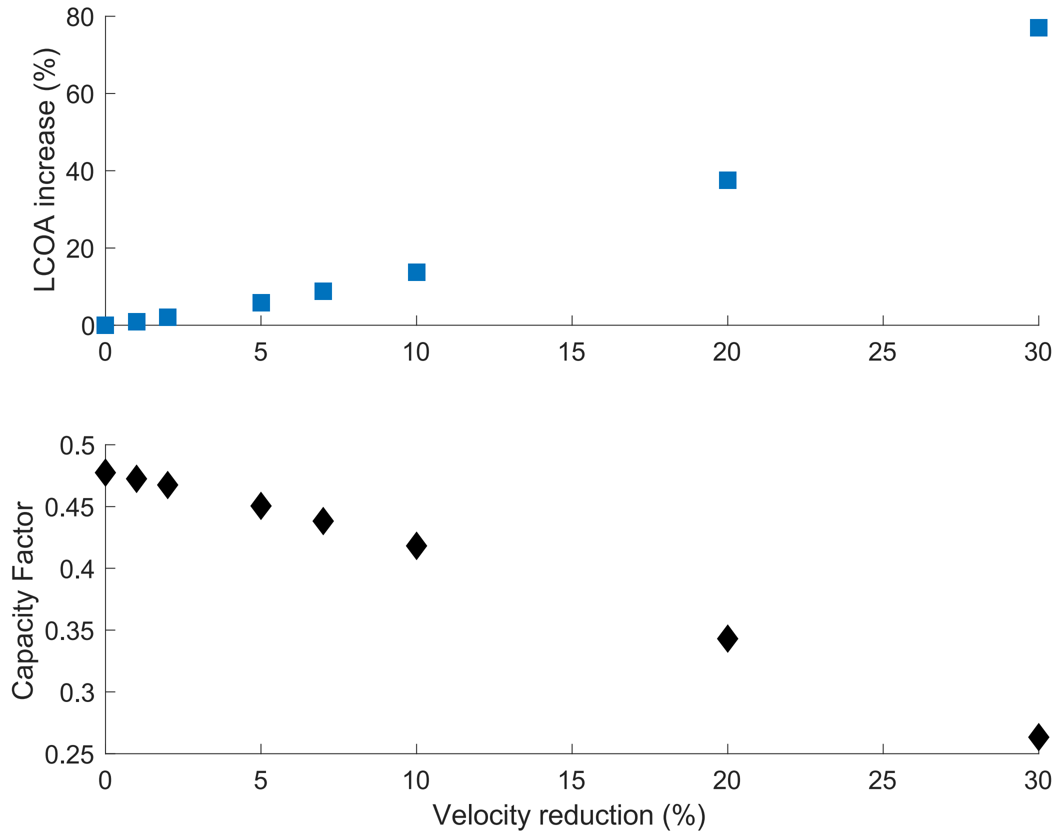

Figure 5.7: The LCOA increase and capacity factor variation with tidal stream velocity reduction (from the ambient flow with no turbines present) for the Minas Passage. Each case is tidal-only with zero ammonia storage cost.

At low velocity reductions, the LCOA increase is important but not significant. For example, the LCOA increase is 2%, 6% and 9% for a velocity reduction of 2%, 5% and 7%, respectively (Figure 5.7). However, the LCOA increase is almost 80% for the extreme case of a velocity reduction of 30%. The non-linear relationship between LCOA increase and velocity reduction is likely because tidal stream power is proportional to velocity cubed.

Interestingly, for most velocity reductions modelled, the capacity factor of the tidal resource is above that of the wind resource in the Minas Passage (0.28 for the low wind year and 0.34 for the high wind year - Figure 5.3). However, in the 30% velocity reduction scenario, the capacity factor of tidal is 0.26 (Figure 5.7), which is lower than the capacity factor of wind. Thus, for ammonia production in the Minas Passage, tidal will likely be chosen over wind for low to moderate velocity reductions.

Using a 5% velocity reduction (a value of the blockage effect correction factor, γ, of 0.95) for the modelling in this chapter is reasonable as low velocity reductions do not increase the LCOA significantly or decrease the capacity factor significantly. Using a velocity reduction of, say, 2% or 7% would not change the conclusions of this chapter.

5.3.4. Site comparisons

To give an insight into the plant equipment contributions to the LCOA values (in Figure 5.5), percentage stacked bars of the LCOA in the tidal only case, the tidal + wind (high) case and the tidal + wind (low) case are shown in Figure 5.8, Figure 5.9 and Figure 5.10, respectively, for each site.

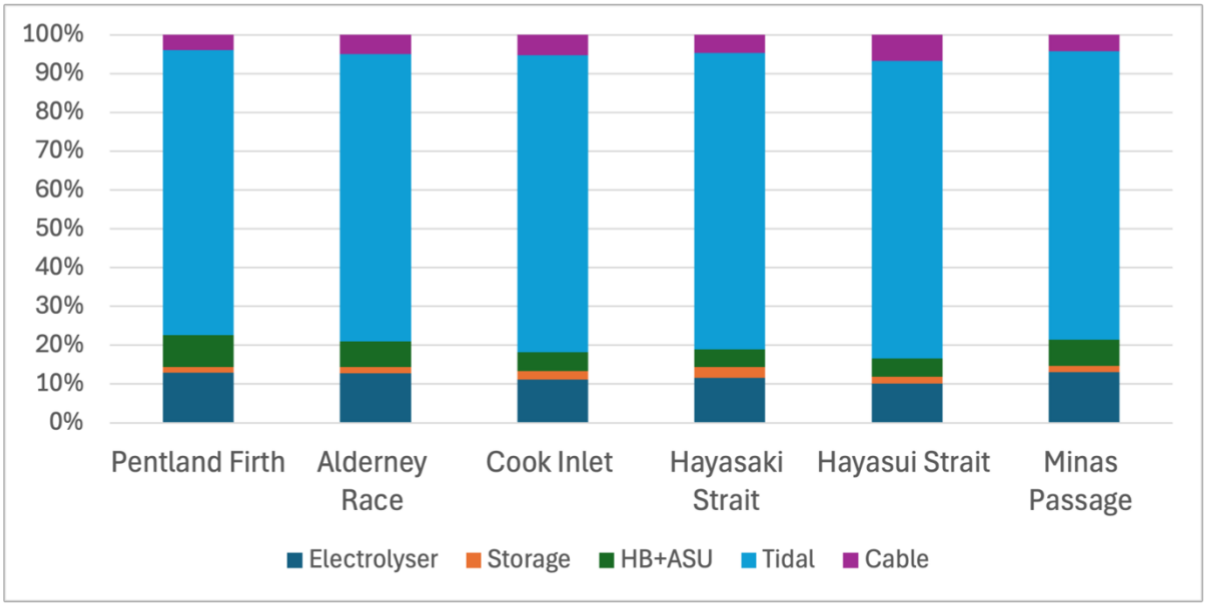

Figure 5.8: Percentage contribution of equipment to the LCOA at each site (tidal only case).

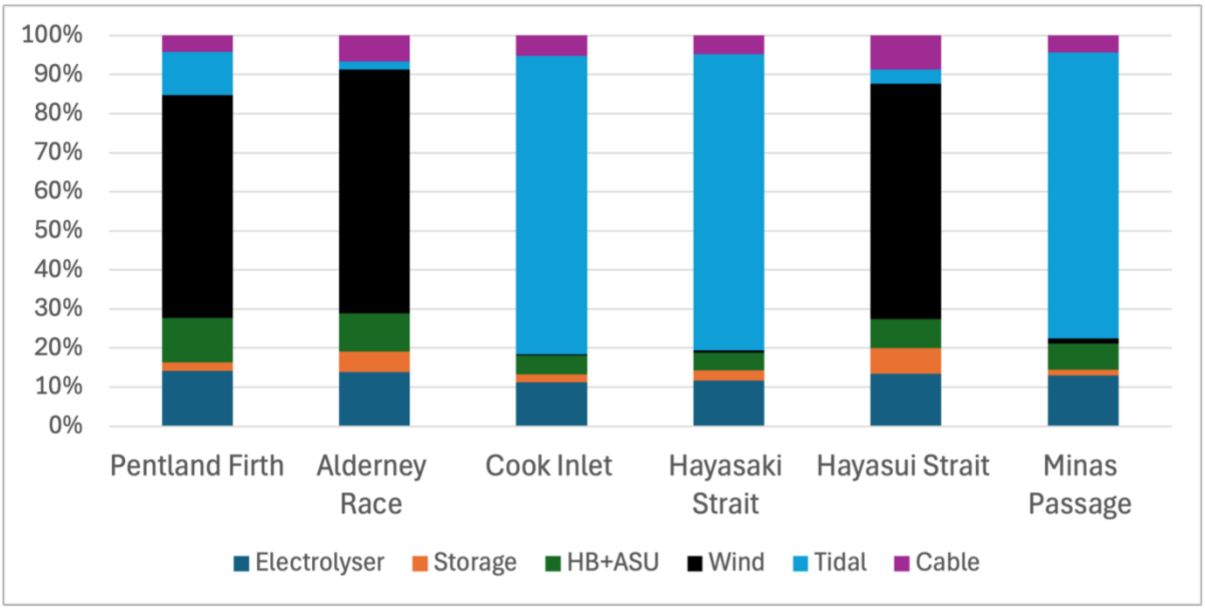

Figure 5.9: Percentage contribution of equipment to the LCOA at each site (tidal + wind (high) case)

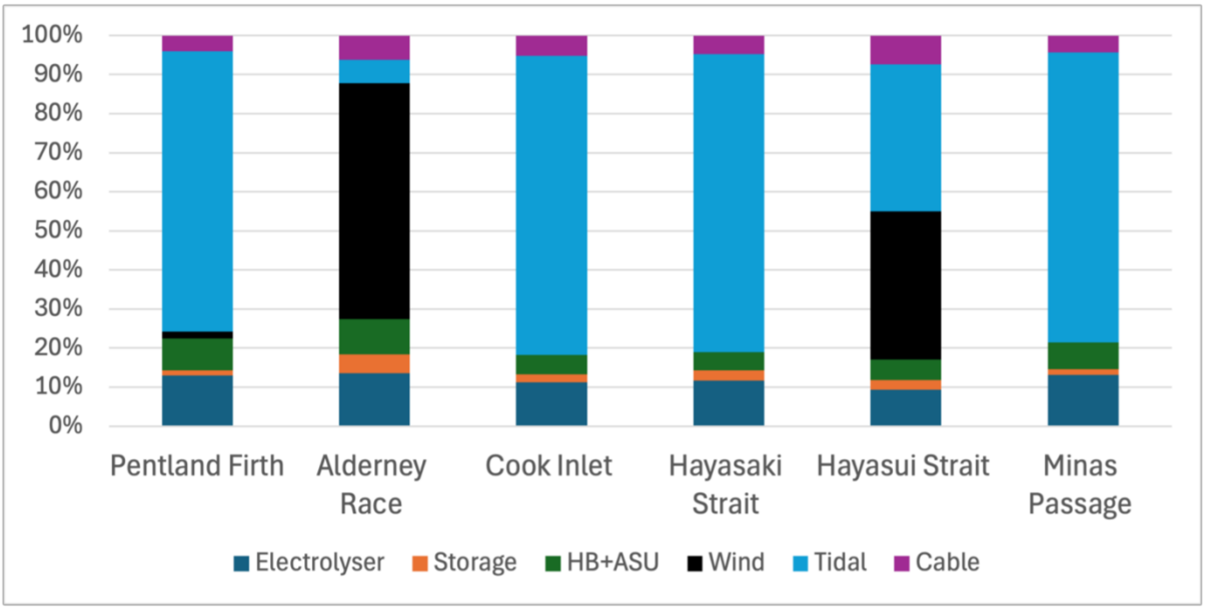

Figure 5.10: Percentage contribution of equipment to the LCOA at each site (tidal + wind (low) case)

At each site, the renewables component is the largest proportion of the LCOA, and the storage component is a low proportion. This is also the case in Chapters 3 and 4 (implied in Figure 3.13 and shown in Figure 4.8).

The cable cost varies at each site, contributing a different proportion of the LCOA at each site. The cable component is a lower proportion of the LCOA compared to Chapter 4 (Figure 4.8), as the ammonia plant to turbine distance is smaller in Chapter 5 compared to Chapter 4.

The wind-dominated scenarios have a higher storage proportion of the LCOA compared to the tidal-dominated scenarios, as in Chapter 3 (implied in Figure 3.13).

5.3.4.1. Pentland Firth comparison

The LCOA from the Pentland Firth site (taking the Tidal + Wind (High) case with the upper value of the tidal turbine CAPEX) is 826 USD/t in Chapter 3 (Figure 3.9), and 581 USD/t in Chapter 5 (Figure 5.5).

This 245 USD/t LCOA difference is due to the change in OPEX definition (149 USD/t decrease), as justified in Appendix E (Section E.10), and secondly due to the use of an HVAC offshore cable instead of an expensive offshore ammonia platform (96 USD/t decrease). The contribution of the ammonia plant equipment CAPEX (excluding cable/ammonia platform) to the LCOA is unchanged.

Although the change in OPEX definition (in particular, the inclusion of the annuity factor) causes a significant change to the LCOA, it should be noted that, as well as the OPEX, other parameters in the LCOA can vary, which can significantly affect the LCOA value. For example, the discount rate (2-12% [29]), the plant lifetime (20 years [30] to 30 years [31]) and the maintenance time (14 days per year [31] to 20 days per year [29]). The change in OPEX definition in the model used in Chapter 4 and Chapter 5 provides more detail compared to the more simplified and more conservative model used in Chapter 3.

5.3.5. Low renewable energy generation periods

This section analyses how the storage requirements are distributed throughout high and low renewable energy generation periods. The lowest LCOA scenario in Chapter 5, Pentland Firth: Tidal + Wind (High), is taken as an example (Figure 5.11) – this scenario is also used as the example for the verification of the model in Appendix E. The period from 3100 to 4600 hours is chosen because it displays a variety of low-energy behaviours, varying in length and depth (low or zero/near zero).

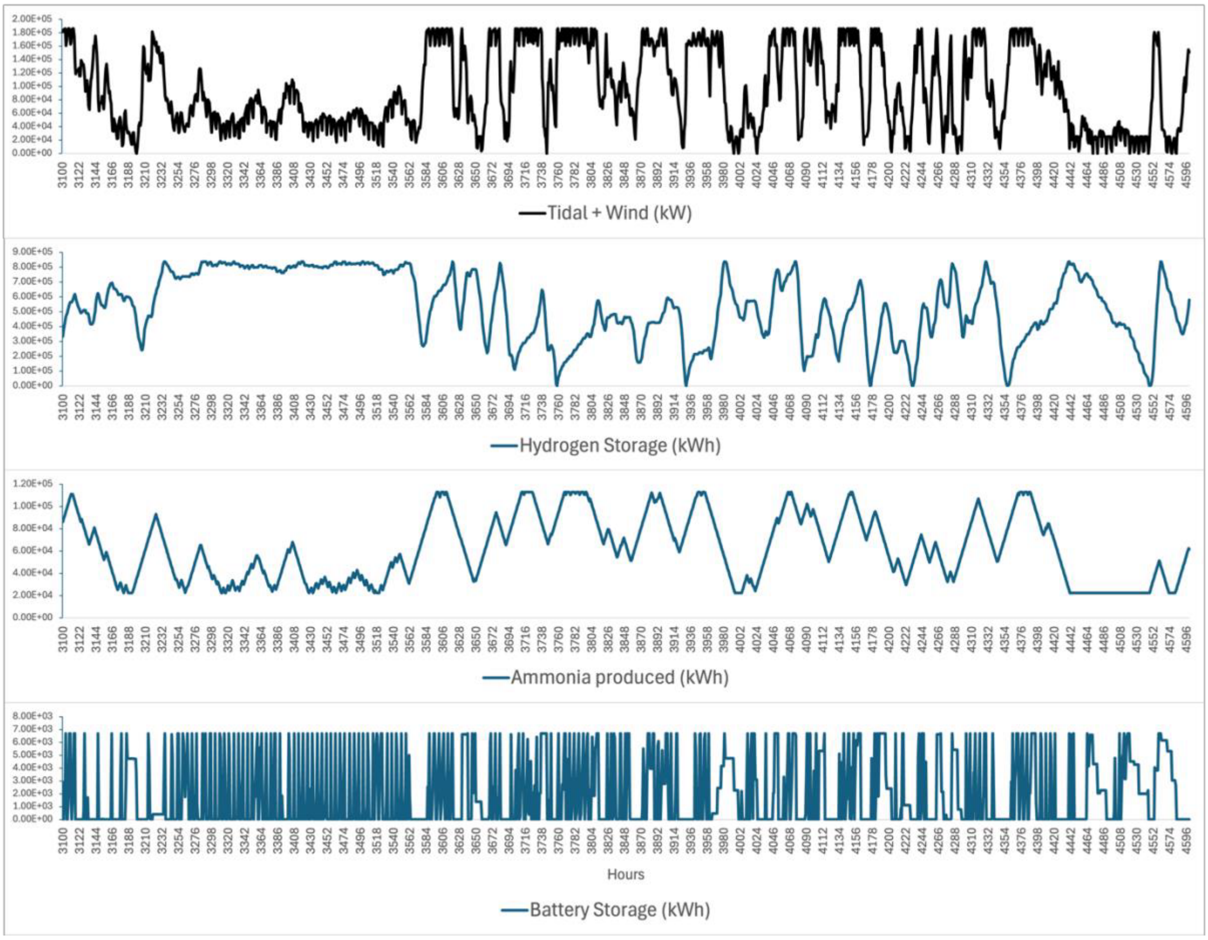

Figure 5.11: The hourly tidal + wind power profile, and corresponding hourly hydrogen storage level, ammonia production and battery storage level for the Pentland Firth: Tidal + Wind (High) example over 3100 to 4600 hours.

The storage (hydrogen and battery) reaches its maximum value many times over the operational year. If the storage was oversized to account for just one specific low renewable energy generation period, it would only reach the maximum value once (just before that low-energy period). The fuel cell is infrequently used (Figure E.11), as the cheaper battery can also provide back-up power to other plant equipment.

The battery storage provides power to other plant equipment when there are short-term fluctuations in the tidal + wind power profile. The battery storage is depleted more frequently than the hydrogen storage. The battery storage is depleted from small decreases in the tidal + wind power profile.

The hydrogen storage level generally drops when the input power profile drops significantly for a short period, to support the HB, which is not fully flexible. For example, at 3930 hours, the input power profile drops significantly, the hydrogen storage level drops to zero, and the HB operates at a lower level. The hydrogen storage level decreases significantly when the input power profile drops to zero/near zero for a long period. The HB operates at or near its minimum load, and hydrogen storage is necessary to support HB operation. That is, the hydrogen requirement for the HB cannot be solely met by the input energy. For example, between 4440-4550 hours. The hydrogen storage level is not depleted during prolonged, low energy periods (that are not zero/near zero) as the HB turns down to a low level, and the hydrogen requirement for the HB can mostly be met by the input energy. For example, between 3250-3550 hours.

The yearly mean energy available (yearly CF) from tidal/wind dictates how much ammonia can be produced per year, which strongly affects the LCOA. The higher the yearly CF, the more ammonia is produced per year, and the lower the LCOA and vice versa (Figure 5.12 – shown relative to the Pentland Firth).

Storage never takes a significant proportion of the LCOA, even in the wind-dominated cases (Figure 5.9). Thus, the yearly CF is more important than the presence of low renewable energy generation periods for LCOA determination.

However, the ideal renewable power profile would have both a high yearly CF and minimal low-energy generation periods. Moreover, the yearly CF is not the only important driver of the LCOA - a very large cable cost can also significantly influence the LCOA.

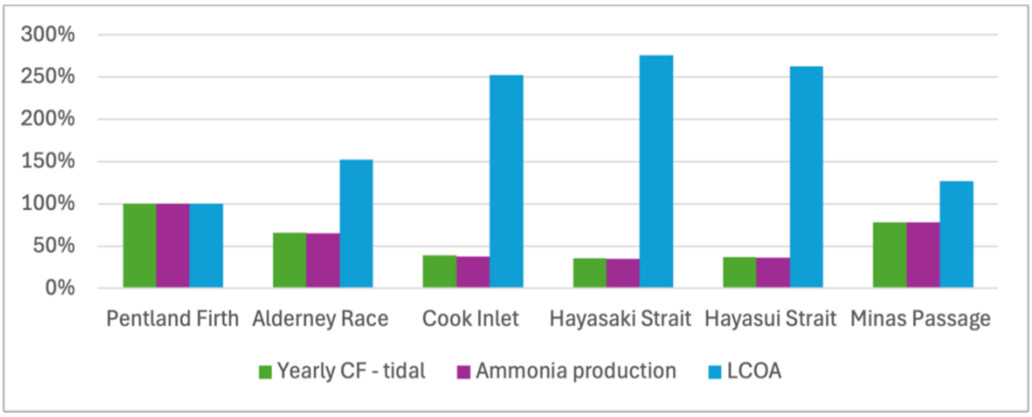

Figure 5.12: Yearly CF, ammonia production per year and LCOA for the tidal only case at each site, relative to the Pentland Firth for comparison

5.4. Limitations

The tidal data in each tidal site (Table 5.1) have a different number of tidal constituents and varying spatial resolution (in both the vertical and horizontal directions). Thus, the accuracy of the LCOA will vary between each tidal site. To be clear, the higher the number of tidal constituents and the better the spatiotemporal resolution, the more accurate the LCOA. Since depth-averaged velocities were used for the Hayasaki Strait, the Hayasui Strait and the Minas Passage, the real power available is underestimated in these sites (and the LCOA is overestimated). It would be beneficial to use 3-D velocities to more accurately model the tidal stream power in these sites. As mentioned in the introduction of this chapter, available tidal stream velocity data worldwide is limited, and the highest spatiotemporal resolution data was sought for the thesis after contacting multiple research centres/universities (institutions shown in the last column of Table 5.1).

It should be noted that, in the Pentland Firth and the Hayasui Strait, the water depths are close to 60 m, which is the maximum depth for fixed offshore wind [32]. Thus, floating offshore wind may be more appropriate for these two sites. However, since floating offshore wind is more expensive than fixed offshore wind, more tidal capacity would be chosen by the model in these two sites (than that shown in the top of Figure 5.3).

There is a computational limitation to running 30 years of hourly tidal and wind power data (which was used in Chapter 3) using the green ammonia model in this chapter. Instead, a single high and low wind year between 1991-2020 is used for the tidal+wind cases. This is a reasonable modelling decision as it is useful to show the range of difference in LCOA between the tidal+wind cases and the tidal-only case for two extreme cases of wind power (high and low), to emphasise that wind is variable.

5.5. Conclusion

The LCOA using tidal stream energy and onshore green ammonia production was determined for six major tidal sites worldwide, covering the UK (Pentland Firth and Alderney Race), the USA (Cook Inlet), Japan (Hayasaki Strait and Hayasui Strait) and Canada (Minas Passage). The tidal sites with the lowest LCOA from tidal stream energy are the Pentland Firth and the Minas Passage. Adding offshore wind at the location of the tidal sites to tidal stream energy reduced the LCOA for the Pentland Firth (0-6%), Alderney Race (18-25%) and the Hayasui Strait (7-23%) (Table 5.3).

For the tidal+wind cases, the tidal fractions utilised by the green ammonia model were reported along with the CFs of the tidal, wind (high) and wind (low) power profiles at each tidal site (Figure 5.3). Some tidal capacity is chosen over wind capacity in all sites despite the higher tidal CAPEX compared to wind CAPEX (Table A.1) and the lower CF of tidal compared to wind in the Alderney Race and the Hayasui Strait.

Both wake and blockage effects were incorporated (as a power reduction), as well as tidal turbine spacing and depth constraints. A sensitivity analysis was performed on the product collection frequency for both green ammonia production and green hydrogen production for the Minas Passage (Figure 5.6). The frequency of ammonia collection has an insignificant impact to the LCOA in comparison to the impact of the frequency of hydrogen collection to the LCOH. A sensitivity analysis was also performed on the effect of blockage effects on the LCOA for the Minas Passage (Figure 5.7). For low velocity reductions (2-7%), the blockage effect does not increase the LCOA significantly, justifying the use of a 5% velocity reduction used in this chapter.

Overall, green ammonia production from tidal stream energy is promising in all tidal sites analysed, even when the CF of tidal is lower than wind in the site. When the predictability benefits of tidal over wind are incorporated, tidal stream energy could be even more promising. However, better spatiotemporal resolution tidal data in more tidal sites worldwide would be needed to better establish the benefit of tidal stream energy over offshore wind.

References

[1] R. O'Hara Murray and A. Gallego, "A modelling study of the tidal stream resource of the Pentland Firth, Scotland," *Renew. Energy*, vol. 102, no. B, pp. 326–340, 2017.

[2] R. O'Hara Murray and L. Campbell, "Pentland Firth and Orkney Waters Climatology 1.02," Marine Scotland. Accessed: Jan. 06, 2022. [Online]. Available: 10.7489/12041-1

[3] M. De Dominicis, R. O'Hara Murray, and J. Wolf, "Multi-scale ocean response to a large tidal stream turbine array," *Renew. Energy*, vol. 114, pp. 1160–1179, 2017.

[4] M. De Dominicis, R. O'Hara Murray, J. Wolf, and A. Gallego, "The Scottish Shelf Model 1990 – 2014 climatology version 2.01," Marine Scotland. Accessed: Aug. 15, 2022. [Online]. Available: 10.7489/12037-1

[5] T. Wang and Z. Yang, "A Tidal Hydrodynamic Model for Cook Inlet, Alaska, to Support Tidal Energy Resource Characterization," *J. Mar. Sci. Eng.*, vol. 8, no. 4, p. 254, 2020.

[6] P. G. Novo and Y. Kyozuka, "Tidal stream energy as a potential continuous power producer: A case study for West Japan," *Energy Convers. Manag.*, vol. 245, p. 114533, 2021.

[7] C. Garrett and P. Cummins, "The power potential of tidal currents in channels," *Proc. R. Soc. A Math. Phys. Eng. Sci.*, vol. 461, no. 2060, pp. 2563–2572, 2005.

[8] M. D. Patel, "The Impact of Real-world Constraints on Tidal Stream Energy Resource Assessments (PhD Thesis)," University of Oxford, 2024.

[9] D. Foxwell, "Understanding blockage will help industry raise its game," Riviera Maritime Media. Accessed: Nov. 19, 2024. [Online]. Available: https://www.rivieramm.com/news-content-hub/news-content-hub/understanding-blockage-will-help-industry-raise-its-game-56712

[10] S. Waldman, S. Yamaguchi, R. O'Hara Murray, and D. Woolf, "Tidal resource and interactions between multiple channels in the Goto Islands, Japan," *Int. J. Mar. Energy*, vol. 19, pp. 332–344, 2017.

[11] G. Sutherland, M. Foreman, and C. Garrett, "Tidal current energy assessment for Johnstone Strait, Vancouver Island," *Proc. Inst. Mech. Eng. Part A J. Power Energy*, vol. 221, no. 2, pp. 147–157, 2007.

[12] S. Draper, T. A. A. Adcock, A. G. L. Borthwick, and G. T. Houlsby, "Estimate of the tidal stream power resource of the Pentland Firth," *Renew. Energy*, vol. 63, pp. 650–657, 2014.

[13] R. Campbell, A. Martinez, C. Letetrel, and A. Rio, "Methodology for estimating the French tidal current energy resource," *Int. J. Mar. Energy*, vol. 19, pp. 256–271, 2017.

[14] P. Garcia-Novo, S. Waldman, Y. Kyozuka, and D. Sakaguchi, "Estimation of the Technical Resource for Tidal Stream Energy in South-West Japan," in *2024 13th International Conference on Renewable Energy Research and Applications (ICRERA)*, 2024, pp. 1492–1498.

[15] R. H. Karsten, J. M. McMillan, M. J. Lickley, and R. D. Haynes, "Assessment of tidal current energy in the Minas Passage, Bay of Fundy," *Proc. Inst. Mech. Eng. Part A J. Power Energy*, vol. 222, no. 5, pp. 493–507, 2008.

[16] R. Vennell, "Tuning turbines in a tidal channel," *J. Fluid Mech.*, vol. 663, pp. 253–267, 2010.

[17] T. Stallard, R. Collings, T. Feng, and J. Whelan, "Interactions between tidal turbine wakes: experimental study of a group of three-bladed rotors," *Philos. Trans. R. Soc. A*, vol. 371, no. 1985, p. 20120159, 2013.

[18] L. Zhao, L. Xue, Z. Li, J. Wang, Z. Yang, and Y. Xue, "Progress on Offshore Wind Farm Dynamic Wake Management for Energy," *J. Mar. Sci. Eng.*, vol. 10, no. 10, p.

1395, 2022.

[19] J. K. Lundquist, K. K. DuVivier, D. Kaffine, and J. M. Tomaszewski, “Costs and consequences of wind turbine wake effects arising from uncoordinated wind energy development,” *Nat. Energy*, vol. 4, no. 1, pp. 26–34, 2019.

[20] R. Vennell, S. W. Funke, S. Draper, C. Stevens, and T. Divett, “Designing large arrays of tidal turbines: A synthesis and review,” *Renew. Sustain. Energy Rev.*, vol. 41, pp. 454–472, 2015.

[21] T. A. A. Adcock, S. Draper, R. H. J. Willden, and C. R. Vogel, “The Fluid Mechanics of Tidal Stream Energy Conversion,” *Annu. Rev. Fluid Mech.*, vol. 53, pp. 287–310, 2021.

[22] D. Coles, A. Angeloudis, D. Greaves, G. Hastie, M. Lewis, L. Mackie, J. McNaughton, J. Miles, S. Neill, M. Piggott, D. Risch, B. Scott, C. Sparling, T. Stallard, P. Thies, S. Walker, D. White, R. Willden, and B. Williamson, “A review of the UK and British Channel Islands practical tidal stream energy resource,” *Proc. R. Soc. A*, vol. 477, no. 2255, p. 20210469, 2021.

[23] P. Stansby and T. Stallard, “Fast optimisation of tidal stream turbine positions for power generation in small arrays with low blockage based on superposition of self-similar far-wake velocity deficit profiles,” *Renew. Energy*, vol. 92, pp. 366–375, 2016.

[24] H. Hersbach, B. Bell, P. Berrisford, G. Biavati, A. Horányi, J. Muñoz Sabater, J. Nicolas, C. Peubey, R. Radu, I. Rozum, D. Schepers, A. Simmons, C. Soci, D. Dee, and J.-N. Thépaut, “ERA5 hourly data on single levels from 1979 to present,” Copernicus Climate Change Service (C3S) Climate Data Store (CDS). Accessed: Mar. 10, 2022. [Online]. Available: 10.24381/cds.adbb2d47

[25] “Chapter 3 Coverage,” Protected Planet. Accessed: Feb. 10, 2022. [Online]. Available: https://livereport.protectedplanet.net/chapter-3

[26] N. Salmon and R. Bañares-Alcántara, "Impact of process flexibility and imperfect forecasting on the operation and design of Haber–Bosch green ammonia," *RSC Sustain.*, vol. 1, no. 4, pp. 923–937, 2023.

[27] L. Hatton, R. Bañares-Alcántara, S. Sparrow, F. Lott, and N. Salmon, "Assessing the impact of climate change on the cost of production of green ammonia from offshore wind," *Int. J. Hydrogen Energy*, vol. 49, pp. 635–643, 2024.

[28] IRENA and AEA, "Innovation Outlook: Renewable Ammonia," International Renewable Energy Agency, Abu Dhabi, Ammonia Energy Association, Brooklyn, 2022. [Online]. Available: https://www.irena.org/publications/2022/May/Innovation-Outlook-Renewable-Ammonia

[29] R. M. Nayak-Luke and R. Bañares-Alcántara, "Techno-economic viability of islanded green ammonia as a carbon-free energy vector and as a substitute for conventional production," *Energy Environ. Sci.*, vol. 13, no. 9, pp. 2957–2966, 2020.

[30] A. Fletcher, H. Nguyen, N. Salmon, N. Spencer, P. Wild, and R. Bañares-Alcántara, "Queensland green ammonia value chain: Decarbonising hard-to-abate sectors and the NEM," Brisbane, Australia, 2023. [Online]. Available: https://www.griffith.edu.au/__data/assets/pdf_file/0035/1875167/No.2023-16-QLD-Green-Ammonia-Value-Chain-Main-Report.pdf

[31] N. Salmon and R. Bañares-Alcántara, "Impact of grid connectivity on cost and location of green ammonia production: Australia as a case study," *Energy Environ. Sci.*, vol. 14, no. 12, pp. 6655–6671, 2021.

[32] H. Wang, P. Daoutidis, and Q. Zhang, "Harnessing the Wind Power of the Ocean with Green Offshore Ammonia," *ACS Sustain. Chem. Eng.*, vol. 9, no. 43, pp. 14605–14617, 2021.

Chapter 6: Conclusion

6.1. Thesis summary

The thesis has assessed the feasibility of utilising tidal stream energy for green ammonia production, which has not been done before. Ammonia production from tidal stream energy was compared to ammonia production from a cheaper and more established offshore energy technology, offshore wind energy. The levelized cost of ammonia (LCOA) was compared, and the optimal fraction of power capacity (tidal plus wind) that the green ammonia model allocated to tidal stream energy was also compared. Firstly, the Pentland Firth was chosen as a case study as it is a globally excellent tidal hotspot (Chapter 3). Then, many tidal hotspots around the world were explored in Chapter 5. In Chapter 4, tidal stream phasing was used to see if it could reduce the LCOA and LCOH (the levelized cost of hydrogen), which is a novel concept. Offshore green ammonia production was analysed in Chapter 3, and onshore green ammonia production was analysed in Chapter 4 and Chapter 5.

To address the thesis title, "*Assessing the feasibility of utilising tidal stream energy for green ammonia production*", the answers to the research objectives are explained:

1. **To show that tidal stream energy is a useful energy source for green ammonia production**

   The tidal-only LCOA in the Pentland Firth, the Alderney Race, and the Minas Passage is shown to be competitive compared to the LCOA from conventional green ammonia (Chapter 5).

2. **To show that tidal stream phasing is beneficial for green ammonia production**

   The second research chapter (Chapter 4) demonstrated that incorporating tidal phasing can decrease the LCOA by 6% (and decrease the LCOH by 5%) in the English Channel.

3. **To show that tidal stream energy is complementary to offshore wind energy for green ammonia production**

   The first research chapter (Chapter 3) demonstrated that adding unphased tidal stream energy to offshore wind energy for green ammonia production offshore decreased the LCOA by up to 18% in the Pentland Firth.

   The third research chapter (Chapter 5) demonstrated that some tidal stream energy capacity is chosen over the cheaper energy resource, offshore wind energy (Figure 5.3), for green ammonia production in six tidal stream energy hotspots worldwide: the Pentland Firth (UK), the Alderney Race (UK), the Cook Inlet (USA), the Hayasaki Strait (Japan), the Hayasui Strait (Japan) and the Minas Passage (Canada).

   Moreover, in the Pentland Firth, the Cook Inlet, the Hayasaki Strait and the Minas Passage, the capacity factor is larger for tidal stream energy than for offshore wind energy. Thus, at these sites, tidal stream energy is a better resource.

   Therefore, the thesis has shown that tidal stream energy can be complementary to offshore wind energy and competitive compared to offshore wind energy for green ammonia production.

Each research chapter introduced more modelling complexity as the research developed over time.

The green ammonia model determined the minimum LCOA using a MILP model in Chapter 3 [1] and an LP model in Chapter 4 and Chapter 5. These two models were developed by other DPhil students in the OXGATE group. The LP model has two major differences from the first model – it incorporates a demand profile and finds the LCOH as well as the LCOA.

Tidal turbine depth constraints and tidal turbine spacing constraints were introduced in Chapter 4 and retained in Chapter 5.

Wake and blockage effects were introduced in Chapter 5, lowering the tidal/wind power output.

In Chapter 3, the middle three sigma layers are used for tidal stream velocities, and a fixed-bottom AR2000 turbine is used. In Chapter 4 and Chapter 5, sigma layers are selected based on the mean position of the turbines in the water column in that region, which is more accurate, and a floating Orbital O2 turbine is used. The use of a floating turbine enables larger velocities to be used, as the turbines are higher up in the water column. Moreover, the Orbital O2 turbine has a lower rated velocity of 2.5 m/s, compared to 3.05 m/s for the AR2000, allowing more energy to be produced (both turbines have a rated power of 2 MW).

The main focus of the thesis is green ammonia, so green hydrogen was not included in every part of the thesis. Green hydrogen is used as a comparison to green ammonia in Chapter 4 in terms of the relative benefit of tidal phasing and in Chapter 5 in terms of the relative increase in production cost when the product collection frequency is altered.

6.2. Main conclusions

Firstly, the main benefit of tidal stream energy for green ammonia production is likely to be predictability rather than its ability to provide a consistent power profile through phasing. While phasing is region-specific, tidal stream energy is predictable worldwide. Within the English Channel (Chapter 4), phasing only has a slightly better cost benefit to ammonia production (6%) versus hydrogen production (5%), as although the HB is inflexible, the internal storage costs are not a major contribution to the LCOA or LCOH, but the cable costs are. Tidal stream phasing analysis was not continued in other chapters as phasing is determined to be mostly useful for high-energy turbine locations that are close together. The focus of the thesis was not to find where phasing has the most potential for green ammonia production around the world but to show the effect of phasing on the LCOA and LCOH, which is a novel concept.

Secondly, for global green ammonia production, the main useful offshore energy resource would likely be offshore wind, as tidal stream energy is more geographically constrained compared to offshore wind. However, the thesis has shown that tidal stream energy can provide a competitive LCOA compared to conventional green ammonia, particularly when combined with offshore wind. Furthermore, the tidal-only LCOA in the Pentland Firth is near the historical brown ammonia market price. Moreover, tidal stream energy can be particularly beneficial for regions where offshore wind has a lower energy potential, such as the Cook Inlet.

Thirdly, ammonia is a useful green fuel as it is cheap to store in comparison with hydrogen. If the product collection frequency (demand) varies, this does not have a major impact on the LCOA but does have a major and significant impact on the LCOH (section 5.3.2.). Tidal stream energy tends to be in relatively remote locations, so the product collection at a nearby site for a green fuel produced by tidal stream energy may be infrequent, favouring ammonia. Moreover, tidal stream energy may be far from grid connections or in a grid-constrained region, such as Orkney. Thus, an energy vector such as ammonia could be essential in enabling that energy to be utilised.

Fourthly, onshore green ammonia production from tidal stream energy is likely to be more cost-effective than offshore green ammonia production from tidal stream energy, which requires an offshore platform. This is because tidal hotspots tend to be close to shore, requiring a relatively short cable.

Overall, this thesis has shown that tidal stream energy is a cost-effective way to produce ammonia and is particularly promising in the Pentland Firth, the Alderney Race and the Minas Passage. Tidal stream energy is different from other renewable energy sources as it is predictable and has the ability to produce a consistent power profile by utilizing phase (time) differences of tidal currents in nearby locations, which is beneficial for inflexible green ammonia production. The remoteness of tidal stream energy makes green ammonia an ideal energy vector for these locations, as it is cheap to store and transport. Methods of decarbonisation, such as green ammonia, are essential to help combat climate change. Tidal stream energy provides a novel and valuable pathway for green ammonia production.

6.3. Main limitations and further work

The limitations of each research chapter are presented at the end of each research chapter. In this section, the main limitations of the thesis as a whole are discussed, and further work is addressed.

In the green ammonia model used in the latter two research chapters, the cable cost is a post-optimization addition to the LCOA and is not incorporated within the minimum cost optimization of the LCOA.

Further work should incorporate the cable cost within the optimization of the LCOA.

The green ammonia model uses perfect forecasting. This is not a problem for tidal as it is predictable, but it will underestimate the LCOA for wind.

Further work could use an imperfect forecasting model to quantify the impact of the unpredictability of wind on the LCOA in each region analysed (with MPC).

A single year of tidal power data is incorporated into each chapter. Although 30 years of tidal power were incorporated in Chapter 3, this was the same yearly power profile repeated 30 times.

Further work could quantify the impact of the 18.6-year lunar cycle on the LCOA, ideally with tidal power data over 18.6 years or more.

In general, if available, better spatiotemporal resolution tidal power data and wind power data over a longer time period (> 1 year) would increase the accuracy of the LCOA. For tidal stream velocity data, incorporating more tidal constituents would increase the accuracy of the LCOA.

The equipment CAPEX values have a degree of uncertainty, particularly the tidal turbine CAPEX value (as previously discussed).

Further work could incorporate a sensitivity analysis on all CAPEX values (not just the tidal turbine CAPEX value as in Chapter 3) and the discount rate, resulting in an LCOA range for each case.

Further work could also incorporate CAPEX costs in the future. A lower tidal turbine CAPEX value is expected in the future (as tidal deployment is expected to increase), which may result in a more competitive LCOA compared to wind or solar-powered green ammonia as well as to grey ammonia.

If CAPEX costs in the future are incorporated, climate change should also be incorporated using a future climate scenario for both the wind and tidal power data. In particular, the frequency and duration of wind droughts should be addressed, as this could cause a large increase in LCOA if there is no power input to the plant for extended periods of time.

A constant power coefficient was incorporated for both wind power and tidal power (Appendix B). However, as mentioned in Chapter 3, the power coefficient could be a function of velocity. More advanced power modelling code for tidal turbines would provide a more accurate LCOA.

It is out of the scope of this thesis to determine an accurate power profile accounting for the interaction between all tidal turbines in the arrays in each region analyzed, as this would be very computationally expensive (3D hydrodynamic modelling, such as O'Hara Murray and Gallego [2], is likely required), and also a research area under development. Moreover, there is very little publicly available data on power production from operating tidal stream arrays. It should be noted that other tidal stream energy studies, such as Neill et al. [3] and

Giorgi and Ringwood [4] did not explicitly incorporate wake effects or blockage effects in their modelling of tidal energy.

However, further work could incorporate more accurate and spatially variable wake effects and blockage effects for both tidal stream energy and wind energy, as this would provide a more accurate LCOA and LCOH.

References

[1] N. Salmon and R. Bañares-Alcántara, "Impact of grid connectivity on cost and location of green ammonia production: Australia as a case study," *Energy Environ. Sci.*, vol. 14, no. 12, pp. 6655–6671, 2021.

[2] R. O'Hara Murray and A. Gallego, "A modelling study of the tidal stream resource of the Pentland Firth, Scotland," *Renew. Energy*, vol. 102, no. B, pp. 326–340, 2017.

[3] S. P. Neill, M. R. Hashemi, and M. J. Lewis, "Optimal phasing of the European tidal stream resource using the greedy algorithm with penalty function," *Energy*, vol. 73, pp. 997–1006, 2014.

[4] S. Giorgi and J. Ringwood, "Can Tidal Current Energy Provide Base Load?," *Energies*, vol. 6, no. 6, pp. 2840–2858, 2013.

Appendix A: Equipment CAPEX details

Table A.1: CAPEX values for equipment used in the technoeconomic Python model for green ammonia production. 2020 USD is used. (*) denotes that the CAPEX value is justified in Appendix A.

Equipment	CAPEX	Reference
HB+ASU	7,444 USD kW^{-1}	[1]
Hydrogen storage	500 USD kg^{-1}	[2]
Fuel cell	960 USD kW^{-1}	[2]
Electrolyser	770 USD kW^{-1}	[3]
Battery interface (Lithium Ion)	271 USD kW^{-1}	[4]
Battery storage (Lithium Ion)	500 USD $kW^{-1}h^{-1}$	[1]
Offshore platform*	120 M USD	[5]
Tidal stream turbine* (Generic 2 MW)	2,200 USD kW^{-1} (lower) 2,900 USD kW^{-1} (upper)	[6]
Wind turbine* (Generic Offshore)	2,372 USD kW^{-1}	[7]
Ammonia storage	2,100 USD/t	[8]

Tidal turbine CAPEX

The tidal turbine CAPEX estimate is from Goss et al. [6] and is dependent on the number of turbines in the array and the capacity of each turbine. For 50-100, 2 MW turbines, the average typical and conservative CAPEX/MW is 2.2 and 2.9 M USD/MW, respectively. It is acknowledged that current tidal CAPEX values are higher than these values due to the current low deployment of tidal stream in the UK (on the order of 10 MW) [9]. However, for 100-200 MW, the tidal CAPEX is expected to be considerably less than current values (due to the high learning rate of 26% below 100 MW [9]).

Wind turbine CAPEX

Fixed-bottom wind turbines are appropriate for water depths <60 m [5]. There are locations in the Pentland Firth with water depths of <60 m (Figure C.2 – Appendix C). Thus, the wind turbine CAPEX is estimated from the worldwide average installed cost of fixed-bottom offshore wind turbines [7] (cabling, representing ~17% of the total CAPEX is not included).

Offshore platform CAPEX

The capital cost of an offshore platform for ammonia production is difficult to estimate, due to its novelty. Wang et al. [5] use a cost correlation, altered from newbuild, jackup platform offshore oil rigs in Kaiser et al. [10] (in the region considered, the water depths are < 168 m, thus fixed jackup platforms are appropriate).

The capital cost (C in USD) varies with water depth (b in metres) and plant capacity (D in t/day) as shown in Eqn. A.1.

$$C = \left(1 + \frac{0.25D}{3000}\right) \times (7.37 \times 10^7 + 8.61 \times 10^3 b^2) \qquad \textit{(Eqn. A.1)}$$

$D = 285\ t/day$ for 100,000 ton NH_3/year (1 operational year is 8,424 hours). $b = \sim 70\ m$ in the region of the Pentland Firth considered. Thus, $C = 120\ M\ USD$.

Cable CAPEX

Wang et al. [5] use a fixed and variable capital cost for a subsea HVAC cable (for power capacities between 0 and 1,200 MW), as shown in Eqn. A.2:

$$Cost_{Cable} = 2.77 \times 10^7 + 7.36 \times d \times P_t \times 1{,}000 \qquad \textit{(Eqn. A.2)}$$

$Cost_{Cable}$ is the cable cost in USD, d is distance in km and P_t is power capacity in MW.

<u>Appendix B: Power calculation for Wind and Tidal turbines</u>

<u>Tidal Turbine power calculation</u>

The power curve for an AR2000 2 MW tidal turbine (Figure B.1) is determined from the following constraints:

If $u_s \leq u \leq u_r$, $P = \frac{1}{2}\rho A C_p u^3$

If $u < u_s$, $P = 0\ W$,

If $u > u_r$, $P = P_r$

Where P_r is maximum power, u_r is rated velocity and u_s is cut-in velocity. For the AR2000 2 MW tidal turbine: $u_r = 3.05\ m/s$ and $u_s = 1\ m/s$ [11]. The parameters values are:

$\rho = 1{,}027\ kg/m^3$ [11] and $A = \pi r^2 = \pi(\frac{20}{2}\ m)^2$ (radius, r, of the turbine is 10 m [12]) and $C_p = 0.437$ as calculated below:

$$C_p = \frac{P_r}{\frac{1}{2}\rho A {u_r}^3} = \frac{2\ MW}{\frac{1}{2} \times 1{,}027\ \frac{kg}{m^3} \times (\frac{1}{4}\pi \times (20\ \text{m})^2) \times \left(3.05 \frac{m}{s}\right)^3 \times 10^{-6} \frac{MW}{W}}$$

$$= 0.437\ (3dp)$$

The power coefficient, C_p, is assumed to be the same from the cut-in velocity to the rated velocity. The cut-out velocity is not always required for tidal stream turbines but is required for wind turbines since the range of tidal current speeds is not as large as wind speeds [13].

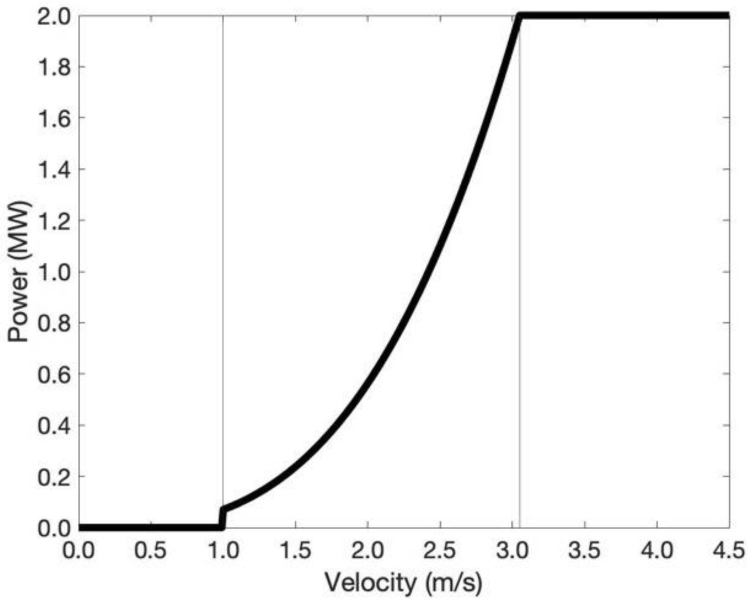

Figure B.1: Power curve for an AR2000 2 MW tidal turbine

The power curve for an Orbital O2 2 MW tidal turbine (Figure B.2) is determined from the following constraints:

If $u_s \leq u \leq u_r$, $P = 2\left(\frac{1}{2}\rho A C_p u^3\right)$, note the multiplier '2' is used to account for 2 rotors.

If $u < u_s$, $P = 0\ W$,

If $u_r < u < u_o$, $P = 2(P_r)$

If $u \geq u_o$, $P = 0\ W$

Where u_o is cut-out velocity. For the Orbital O2 2 MW tidal turbine: $u_r = 2.5\ m/s$, $u_s = 1\ m/s$ and $u_o = 4.5\ m/s$ [14]. The diameter of each rotor is 20 m [14]. $C_p = 0.397$ as calculated below:

$$C_p = \frac{P_r}{\frac{1}{2}\rho A {u_r}^3} = \frac{1\ MW}{\frac{1}{2} \times 1{,}027\ \frac{kg}{m^3} \times (\frac{1}{4}\pi \times (20\ \mathrm{m})^2) \times \left(2.5\frac{m}{s}\right)^3 \times 10^{-6}\frac{MW}{W}}$$

$$= 0.397\ (3dp)$$

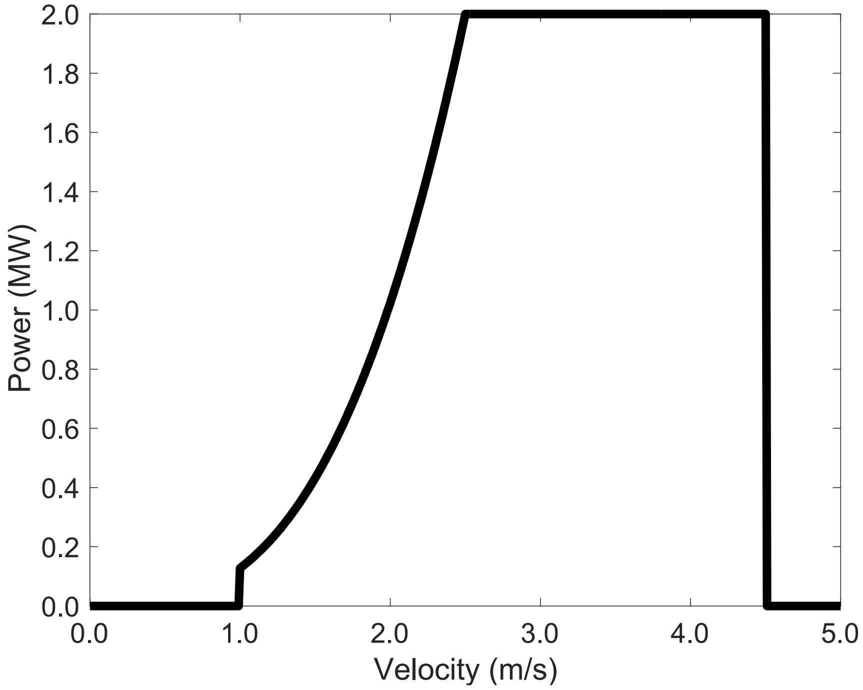

Figure B.2: Power curve for an Orbital O2 2 MW tidal turbine

Wind Turbine power calculation

The power curve for a DTU 10 MW wind turbine (Figure B.3) is determined according to the following constraints:

If $u_s \leq u \leq u_r$, $P = \frac{1}{2}\rho A C_p u^3$

If $u < u_s$, $P = 0\ W$,

If $u_r < u < u_o$, $P = P_r$,

If $u \geq u_o$, $P = 0\ W$

where u_o is cut-out velocity. For the DTU 10 MW wind turbine: $u_r = 11.4\ m/s$, $u_s = 4\ m/s$ and $u_o = 25\ \mathrm{m/s}$ [15]. The parameters values are: $\rho = 1.225\ \frac{kg}{m^3}$ (the density of air is assumed to not vary with time which is typical in wind power literature [16]), $A = \pi r^2 = \pi(\frac{178.3}{2}\ m)^2$ (radius, r, of the turbine is $\frac{178.3}{2}m$ [15]) and $C_p = 0.441$ as calculated below:

$$C_p = \frac{P_r}{\frac{1}{2}\rho A {u_r}^3} = \frac{10\ MW}{\frac{1}{2} \times 1.225\ \frac{kg}{m^3} \times (\frac{1}{4}\pi \times (178.3\ \mathrm{m})^2) \times \left(11.4\frac{m}{s}\right)^3 \times 10^{-6}\frac{MW}{W}}$$

$$= 0.441\ (3dp)$$

For both the tidal turbine and the wind turbine, the velocity is determined using $u = \sqrt{{u_{north}}^2 + {u_{east}}^2}$. u_{north} and u_{east} are the velocity values in the northern and eastern directions, respectively.

The power coefficient, C_p, is assumed to be the same from the cut-in velocity to the rated velocity.

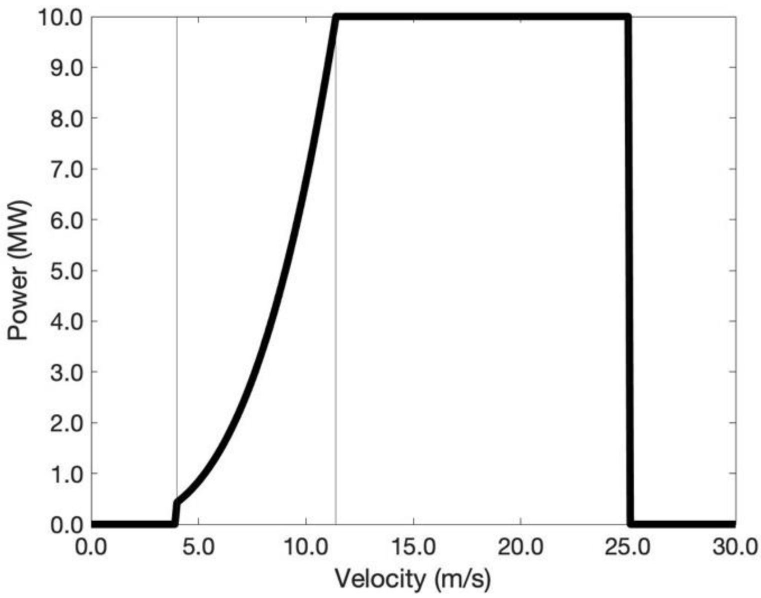

Figure B.3: Power curve for a DTU 10 MW wind turbine

Appendix C: Layout of Tidal Turbines and Water Depth in Pentland Firth (Chapter 3)

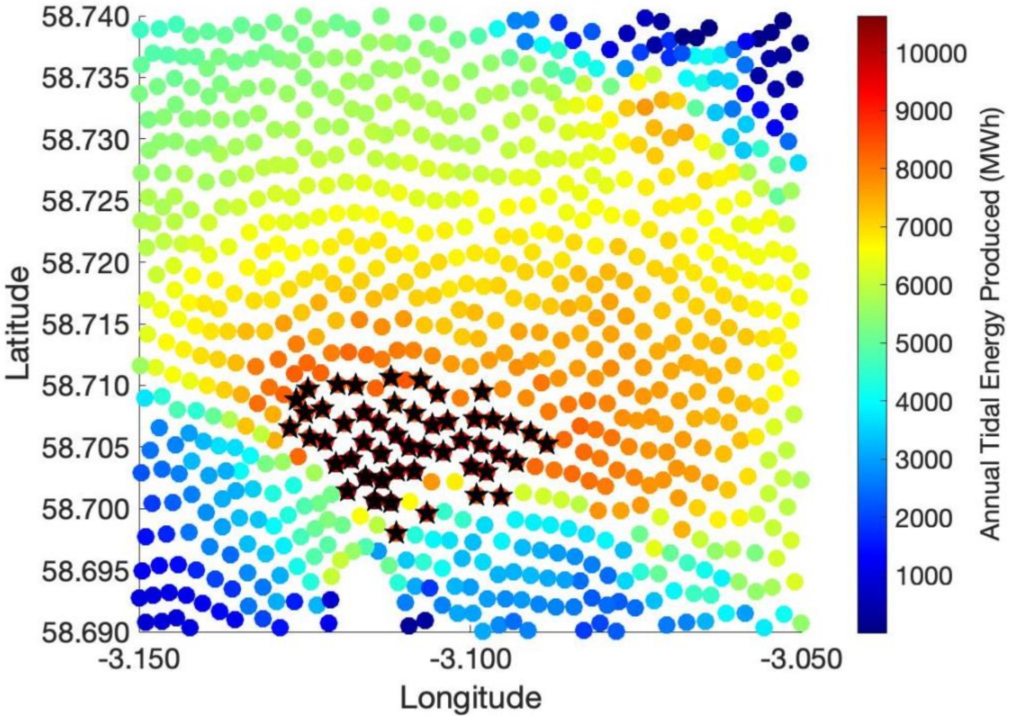

Figure C.1: Tidal turbine layout for the wind+tidal scenarios of Study 1 and Study 2 (Chapter 3)

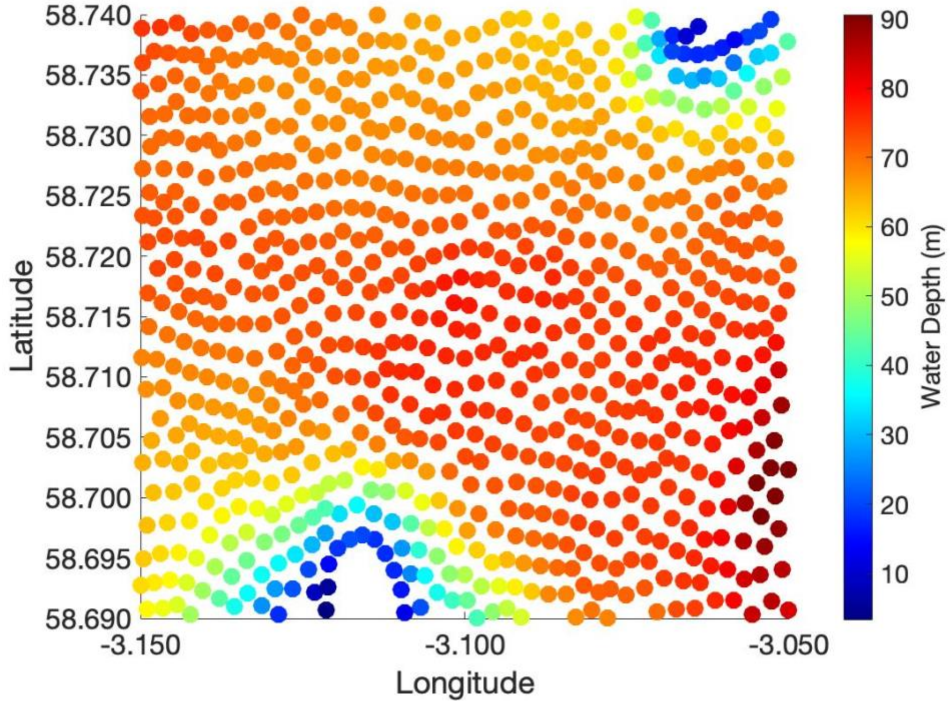

Figure C.2: Water depth in a region of the Pentland Firth (depth data from the PFOW model [17], [18])

Appendix D: Overview of the green ammonia and green hydrogen model (Chapter 4 and Chapter 5)

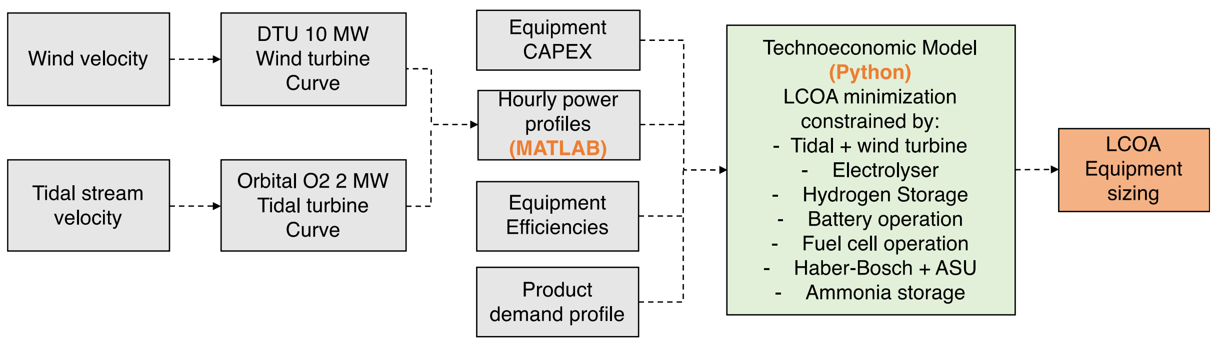

Figure D.1: Overview of the green ammonia model used in Chapters 4-5

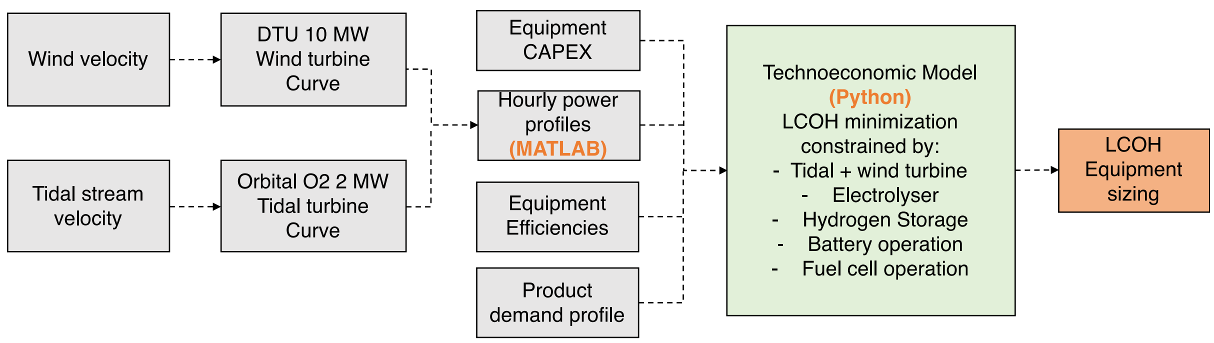

Figure D.2: Overview of the green hydrogen model used in Chapters 4-5

Appendix E: Techno-economic model

E.1. Main points

- The verification of the ammonia model is outlined in this section. The flow diagram for the ammonia model is displayed in Figure 4.1 (and Figure 3.4).
- The differences between the ammonia models used in Chapter 3 and Chapters 4/5 are already discussed in Section 4.2. The equations and efficiencies stated in Appendix E are for the model used in Chapters 4/5. For the model used in Chapter 3, the equations are equivalent, but there is no ammonia storage, so Eqn. E.8 and Eqn. E.9 are not incorporated.
- **Pentland Firth: Tidal + Wind (High) (as analysed in Chapter 5) is chosen as an example for verification of the model (as this has the lowest LCOA).**
- Power supply units: Tidal Stream and Offshore Wind
- Storage units: Battery storage, hydrogen storage and ammonia storage
- Conversion units: Electrolyser, Fuel Cell and HB+ASU
- Energy flows (kWh) represent either electrical energy, hydrogen or ammonia.
- Ammonia and hydrogen energy flows are on a HHV basis.

  Where $\mathrm{HHV_{H2}} = 39.4\ \mathrm{kWh/kg}$ and $\mathrm{HHV_{NH3}} = 6.25\ \mathrm{kWh/kg}$ [8].
- Water, oxygen and air flows are not directly modelled
- Balance equations are shown in equations E.1, E.2, E.7 and E.9:

  To verify that the left-hand side equals the right-hand side, the values of each term are summed over an operational year and plotted in a bar chart (Figures E.1, E.2, E.7 and E.9). The left bar represents the left-hand side of the equation, and the right bar represents the right-hand side of the equation.

- Capacity constraints are shown in equations E.3-E.6, E.8, E.10-14:

  To verify that these constraints are met, hourly profiles over an operational year are shown in Figures E.3-E.6, E.8, E.10-13.

- The flow diagram for the hydrogen model used in Chapters 4/5 is displayed in Figure 4.2. The main difference from the ammonia model is that no HB+ASU or ammonia storage is required.

E.2. Power supply

The electricity flow at any time from wind and tidal combined (minus curtailment, $\zeta(t)$) must equal the total electricity consumed by the HB+ASU, battery and electrolyser minus the electricity produced by the fuel cell and battery:

$$CFa(Wind,t)\cdot\sigma_R(Wind) + CFa(Tidal,t)\cdot\sigma_R(Tidal) - \zeta(t) = Electricity_{in}(HB+ASU,t) + Electricity_{in}(Battery,t) + Electricity_{in}(Electrolyser,t) - Electricity_{out}(Fuel\ Cell,t) - Electricity_{out}(Battery,t) \quad \forall\, t \in S_t \qquad \textit{(Eqn. E.1)}$$

CFa is the hourly capacity factor (power/rated power). $CFa(Wind,t)$ and $CFa(Tidal,t)$ are inputs to the techno-economic model.

There is no curtailment, $\zeta(t) = 0$, for chapter 4 and chapter 5.

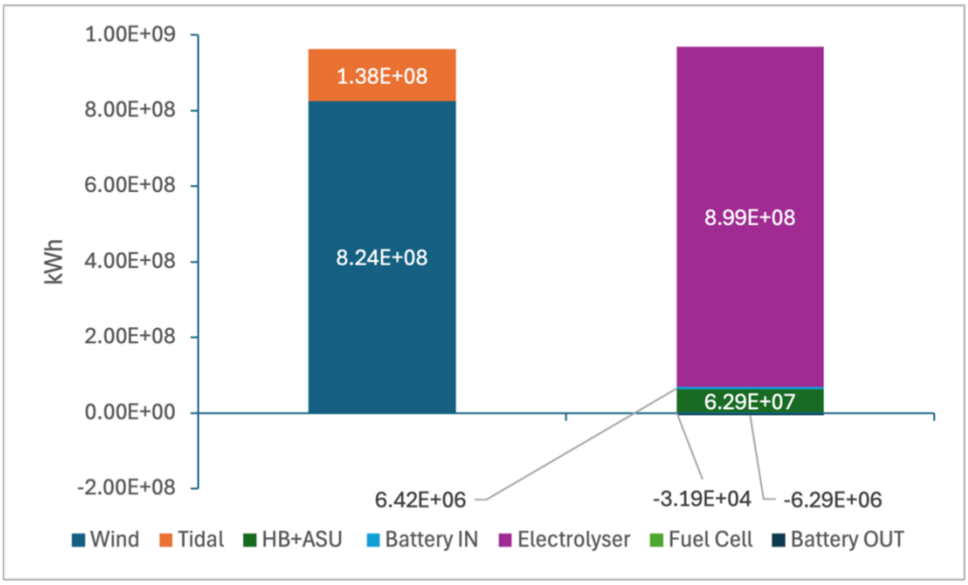

Figure E.1: Power supply verification. Total value of the left-hand side terms (left) and right-hand side terms (right) of Eqn. E.1 over an operational year for the Pentland Firth: Tidal + Wind (High) example.

E.3. Battery storage

Energy flow in: Electrical energy

Energy flow out: Electrical energy

Efficiency: 0.98 kWh/kWh [1]

Discharge loss: 5% a month [1], which is 0.0000694 fraction/hour

The battery storage (kWh) at any time, $storage(Battery, t)$, is equal to the storage at the previous time step multiplied by the storage loss, plus the electricity flow in, minus the electricity flow out:

$$storage(Battery, t) = (1 - 0.0000694) \cdot storage(Battery, t-1) + 0.98 \cdot Electricity_{in}(Battery, t) - Electricity_{out}(Battery, t) \quad \forall\, t \in S_t \qquad \textit{(Eqn. E.2)}$$

As a sense check, it should be noted that the bar representing the total electricity flow out of the battery in Figure E.2 (-6.29E+06) is the same as the bar representing the total electricity flow out of the battery in Figure E.1 (-6.29E+06).

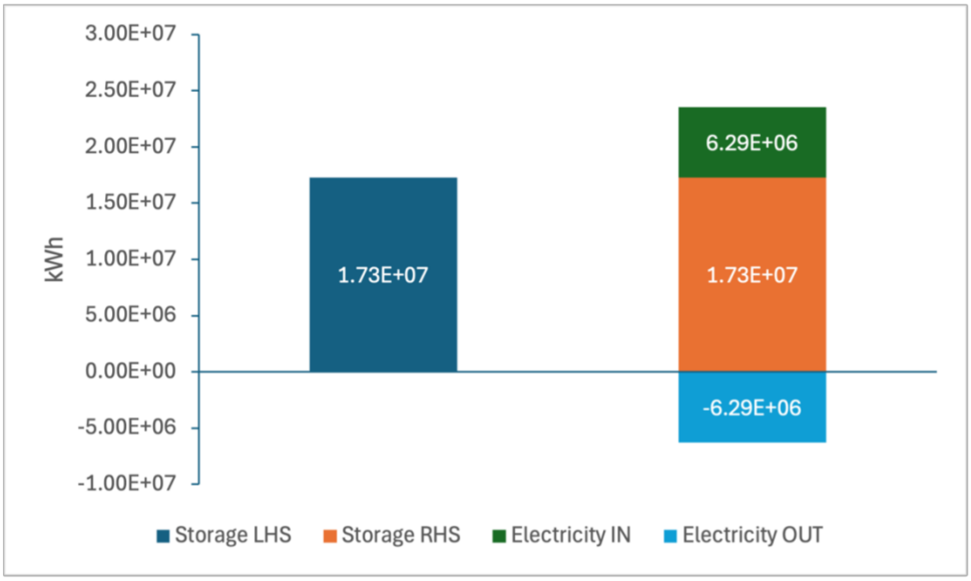

Figure E.2: Battery storage verification. Total value of the left-hand side term (left) and right-hand side terms (right) of Eqn. E.2 over an operational year for the Pentland Firth: Tidal + Wind (High) example.

The battery storage capacity, $\sigma_{SC}(Battery)$, should be larger than or equal to the battery storage at any time:

$$storage(Battery, t) \leq \sigma_{SC}(Battery) \qquad \forall t \in S_t \qquad \text{(Eqn. E.3)}$$

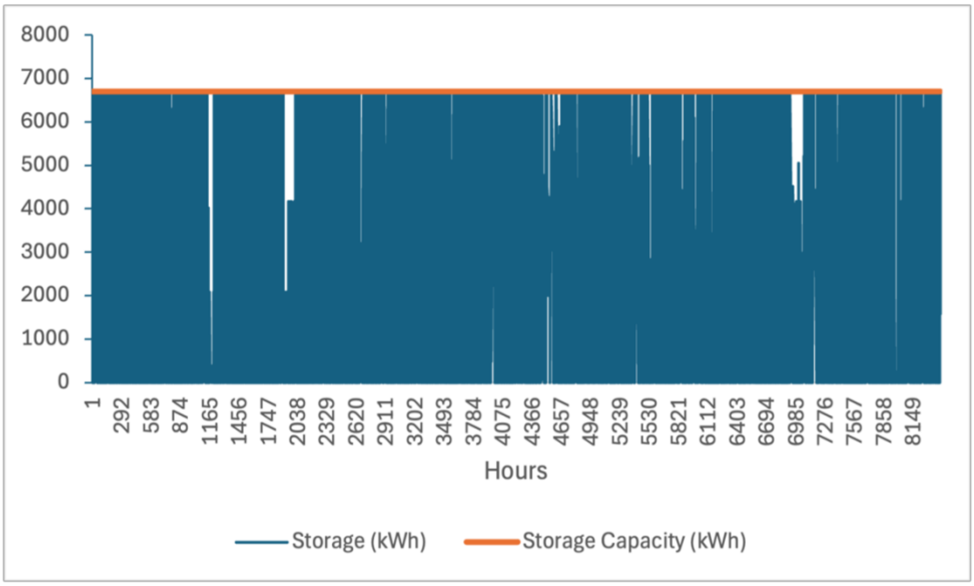

Figure E.3: Battery storage capacity verification. Representation of Eqn. E.3 over an operational year for the Pentland Firth: Tidal + Wind (High) example

The power capacity of the battery, $\sigma_C(Battery)$, should be larger than or equal to the electricity flow into the battery:

$$Electricity_{in}(Battery, t) \leq \sigma_C(Battery) \qquad \forall t \in S_t \qquad \textit{(Eqn. E.4)}$$

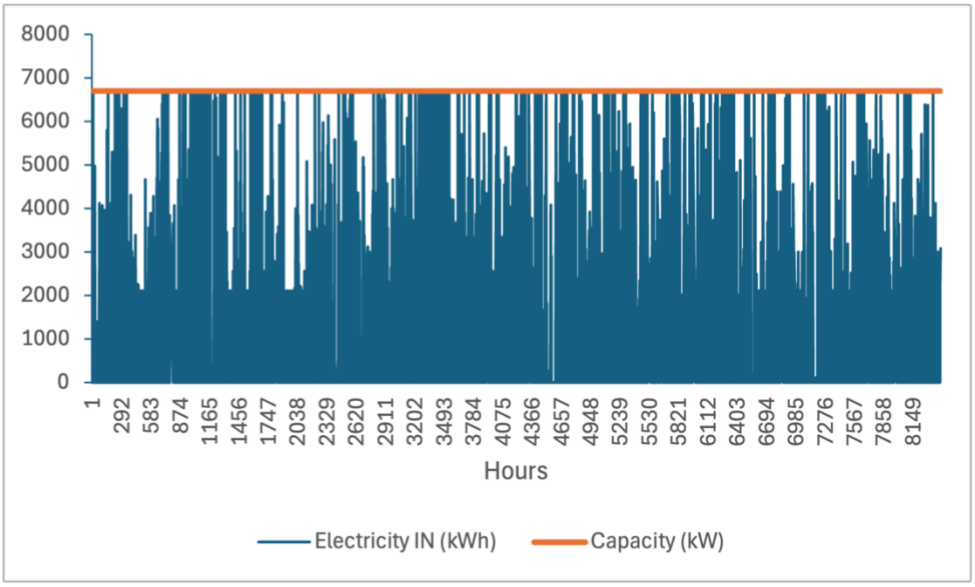

Figure E.4: Electricity into the battery. Representation of Eqn. E.4 over an operational year for the Pentland Firth: Tidal + Wind (High) example

The power capacity of the battery should be larger than or equal to the electricity flow out of the battery:

$$Electricity_{out}(Battery, t) \leq \sigma_C(Battery) \qquad \forall t \in S_t \qquad \textit{(Eqn. E.5)}$$

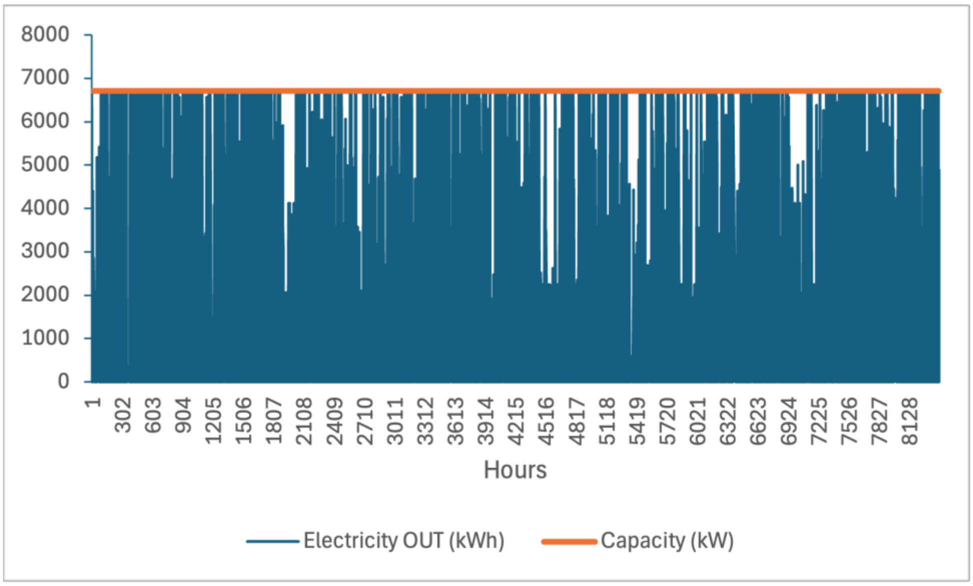

Figure E.5: Electricity out of the battery. Representation of Eqn. E.5 over an operational year for the Pentland Firth: Tidal + Wind (High) example

E.4. Hydrogen storage

Energy flow in: Hydrogen

Energy flow out: Hydrogen

Efficiency: $1 - \frac{2.016\ \mathrm{kWh/kg}}{\mathrm{HHV_{H2}}} = 0.949\,\frac{\mathrm{kWh}}{\mathrm{kWh}}$

2.016 kWh/kg [8] accounts for hydrogen compression.

The hydrogen storage capacity, $\sigma_{SC}(H2\ store)$, should be larger than or equal to the hydrogen storage at any time:

$$storage(H2\ store, t) \leq \sigma_{SC}(H2\ store) \qquad \forall t \in S_t \qquad \textit{(Eqn. E.6)}$$

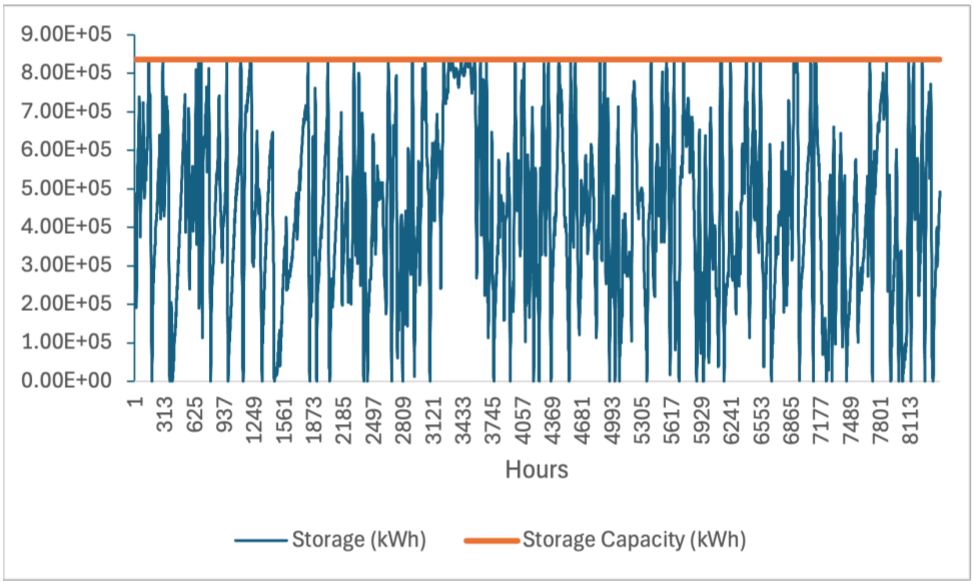

Figure E.6: Hydrogen storage capacity verification. Representation of Eqn. E.6 over an operational year for the Pentland Firth: Tidal + Wind (High) example

The hydrogen storage (kWh) at any time, $storage(H2\ store, t)$, is equal to the hydrogen storage at the previous time step, plus the hydrogen flow in, minus the hydrogen flow out:

$$storage(H2\ store, t) = storage(H2\ store, t-1) + 0.949 \cdot Hydrogen_{in}(H2\ store, t) - Hydrogen_{out}(H2\ store, t) \quad \forall\ t \in S_t \qquad \text{(Eqn. E.7)}$$

$Hydrogen_{in}(H2\ store, t)$ is from the electrolyser and $Hydrogen_{out}(H2\ store, t)$ goes to either the fuel cell or the HB.

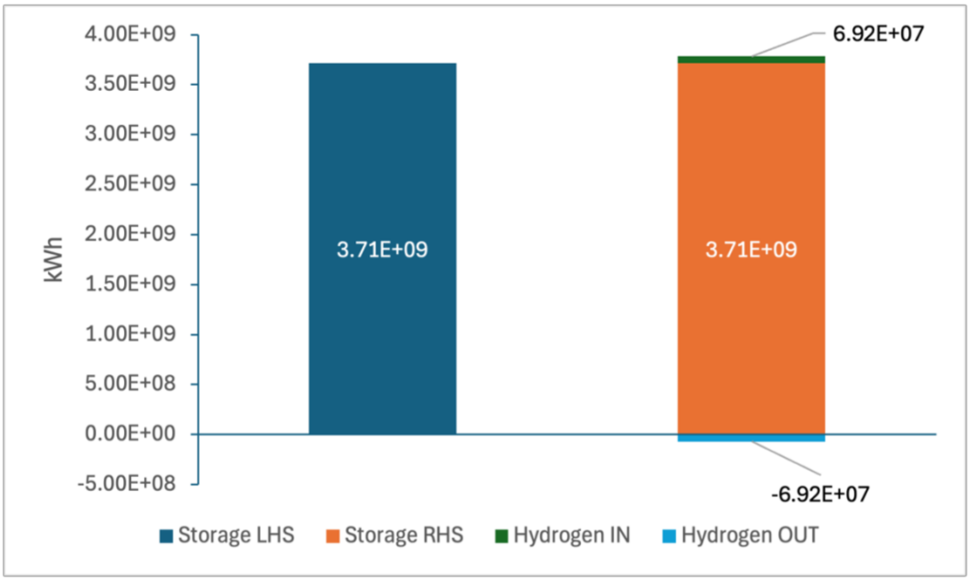

Figure E.7: Hydrogen storage verification. Total value of the left-hand side term (left) and right-hand side terms (right) of Eqn. E.7 over an operational year for the Pentland Firth: Tidal + Wind (High) example.

E.5. Ammonia storage

Energy flow in: Ammonia

Energy flow out: Ammonia

Efficiency: 1

The ammonia storage capacity, $\sigma_{SC}(NH3\ store)$, should be larger than or equal to the ammonia storage at any time:

$$storage(NH3\ store, t) \leq \sigma_{SC}(NH3\ store) \qquad \forall t \in S_t \qquad \text{(Eqn. E.8)}$$

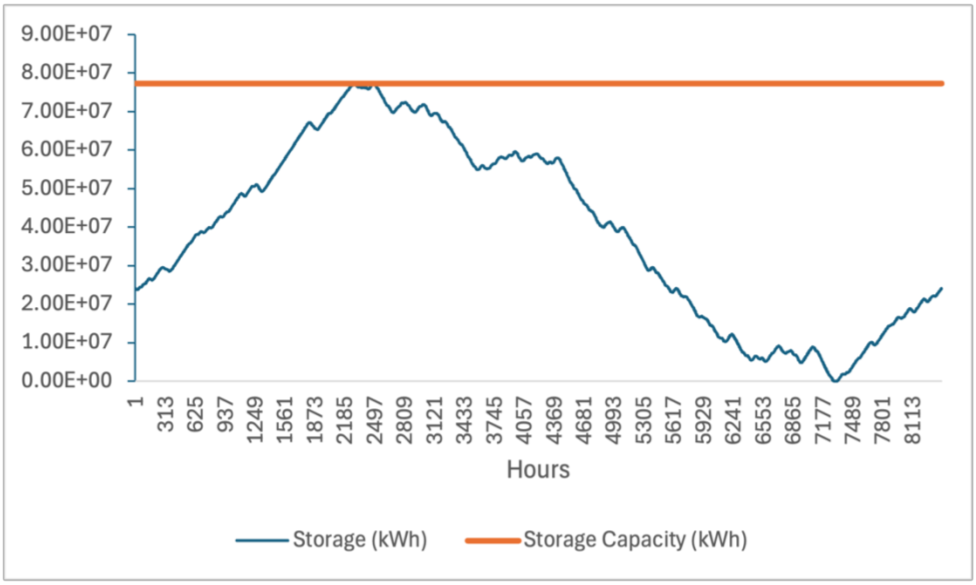

Figure E.8: Ammonia storage capacity verification. Representation of Eqn. E.8 over an operational year for the Pentland Firth: Tidal + Wind (High) example

The ammonia storage (kWh) at any time, $storage(NH3\ store, t)$, is equal to the ammonia storage at the previous time step, plus the ammonia flow in, minus the ammonia flow out:

$$storage(NH3\ store, t) = storage(NH3\ store, t-1) + Ammonia_{in}(NH3\ store, t) - Ammonia_{out}(NH3\ store, t) \quad \forall\, t \in S_t \qquad \textit{(Eqn. E.9)}$$

$Ammonia_{in}(NH3\ store, t)$ is the ammonia output from the Haber-Bosch reactor, i.e. $Ammonia_{out}(HB + ASU, t)$.

$Ammonia_{out}(NH3\ store, t)$ is the ammonia demand profile.

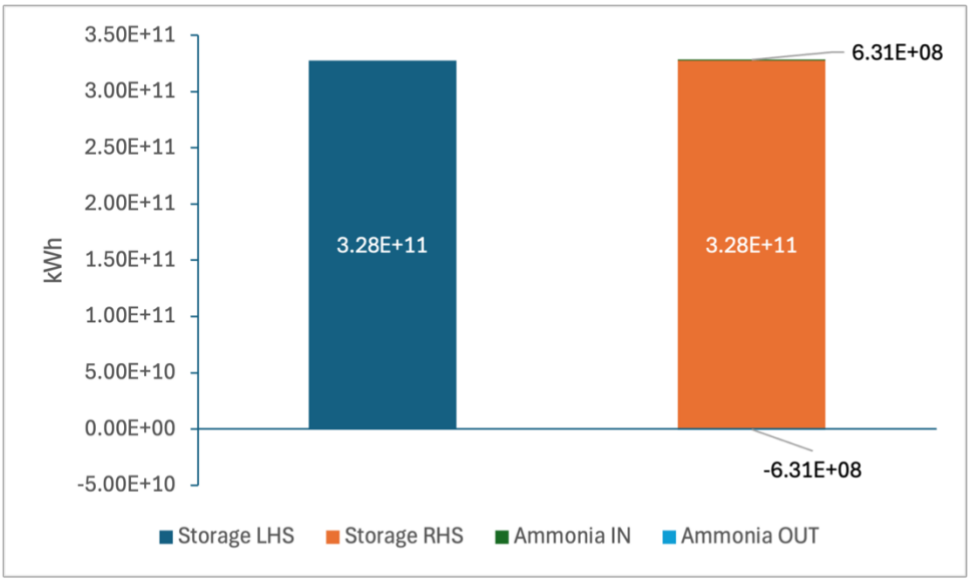

Figure E.9: Ammonia storage verification. Total value of the left-hand side term (left) and right-hand side terms (right) of Eqn. E.9 over an operational year for the Pentland Firth: Tidal + Wind (High) example.

E.6. Electrolyser

Energy flow in: Electrical energy

Energy flow out: Hydrogen

Conversion: $Hydrogen_{out}(Electrolyser, t) = 0.7874 \cdot Electricity_{in}(Electrolyser, t) \quad \forall\, t \in S_t$

Conversion value: $\frac{HHV_{H2}}{50\frac{kWh\ Electricity}{kg\ H2} + \left(9\frac{kg\ H20}{kg\ H2} \cdot 0.0042\frac{kWh\ Electricity}{kg\ H20}\right)} = 0.7874\ \frac{\text{kWh H2}}{\text{kWh Electricity}}$

$50\frac{kWh\ Electricity}{kg\ H2}$ [1] accounts for the electrolyser efficiency.

$9\ \frac{kg\ H20}{kg\ H2}$ [8] and $0.0042\ \frac{kWh\ Electricity}{kg\ H20}$ [8] account for the electricity requirement for water

The electrolyser capacity, $\sigma_C(Electrolyser)$, should be larger than or equal to the electricity flow (kWh) in at any time:

$$Electricity_{in}(Electrolyser, t) \leq \sigma_C(Electrolyser) \quad \forall\, t \in S_t \qquad \textit{(Eqn. E.10)}$$

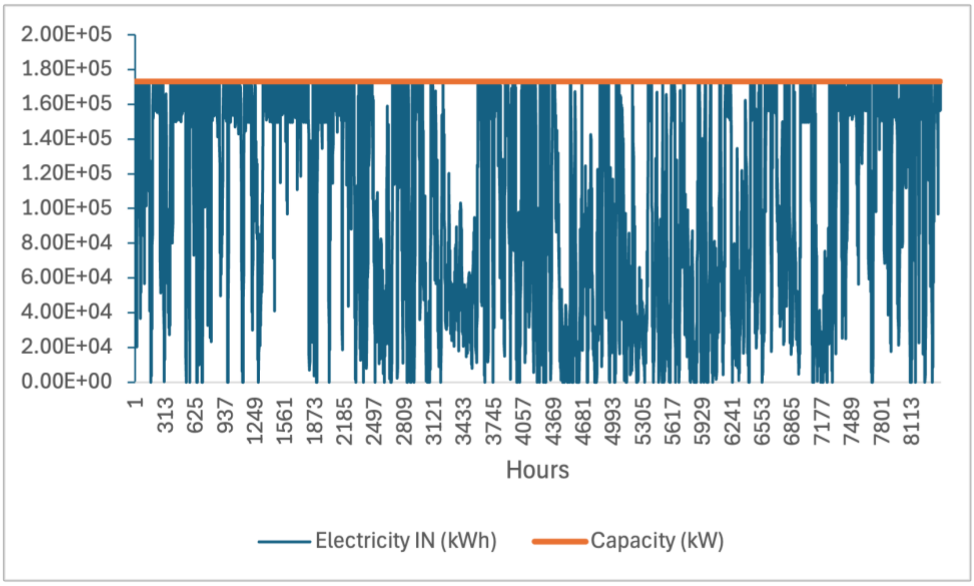

Figure E.10: Electrolyser capacity verification. Representation of Eqn. E.10 over an operational year for the Pentland Firth: Tidal + Wind (High) example

E.7. Fuel Cell

Energy flow in: Hydrogen

Energy flow out: Electrical energy

Conversion: $Electricity_{out}(Fuel\ Cell, t) = 0.5 \cdot Hydrogen_{in}(Fuel\ Cell, t) \quad \forall\ t \in S_t$

Conversion value: 50% efficiency, i.e. 0.5 $\frac{kWh\ Electricity}{kWh\ H2}$ [8].

The fuel cell capacity, σ_{FC}, should be larger than or equal to the electricity flow (kWh) out at any time:

$$Electricity_{out}(Fuel\ Cell, t) \leq \sigma_{FC} \quad \forall\ t \in S_t \qquad \text{(Eqn. E.11)}$$

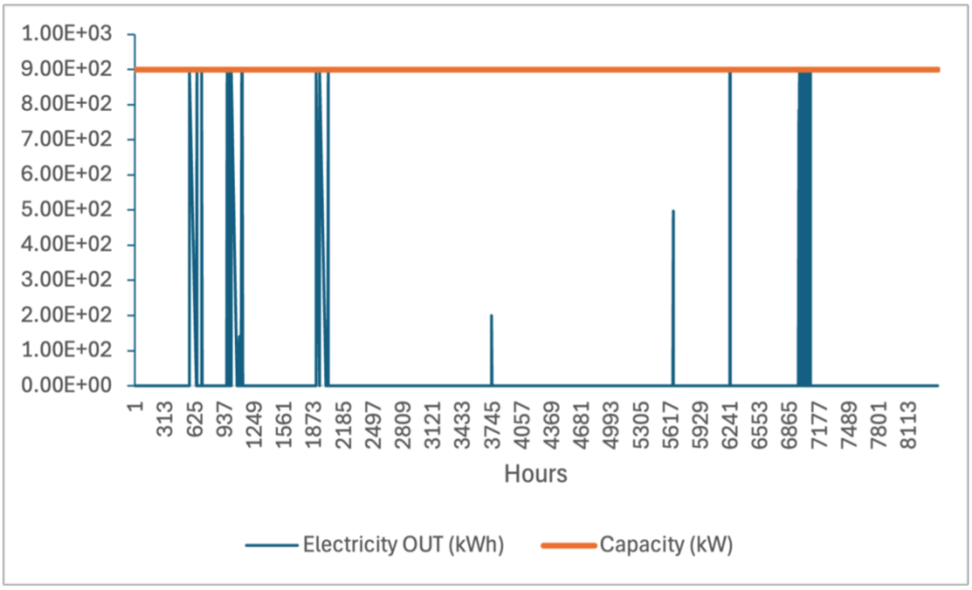

Figure E.11: Fuel cell capacity verification. Representation of Eqn. E.11 over an operational year for the Pentland Firth: Tidal + Wind (High) example

E.8. HB+ASU

Energy flow in: Electrical energy and hydrogen

Energy flow out: Ammonia

Hydrogen required: $Hydrogen_{in}(HB + ASU, t) = (0.284 \cdot HHV_{H2}) \cdot Electricity_{in}(HB + ASU, t) \quad \forall\, t \in S_t$

Ammonia produced: $Ammonia_{out}(HB + ASU, t) = (1.61 \cdot HHV_{NH3}) \cdot Electricity_{in}(HB + ASU, t) \quad \forall\, t \in S_t$

Conversion values: 1.61 kg NH3/kWh Electricity [1] and 0.284 kg H2/kWh Electricity

(using stoichiometry: 17/3 kg NH3/kg H2)

The HB+ASU capacity, $\sigma_C(HB + ASU)$, should be larger than or equal to the electricity flow (kWh) in at any time:

$$Electricity_{in}(HB + ASU, t) \leq \sigma_C(HB + ASU) \quad \forall\, t \in S_t \qquad \text{(Eqn. E.12)}$$

HB+ASU minimum load constraint:

$$Electricity_{in}(HB + ASU, t) \geq G_{HB_{Min}} \cdot \sigma_C(HB + ASU) \quad \forall\, t \in S_t \qquad \text{(Eqn. E.13)}$$

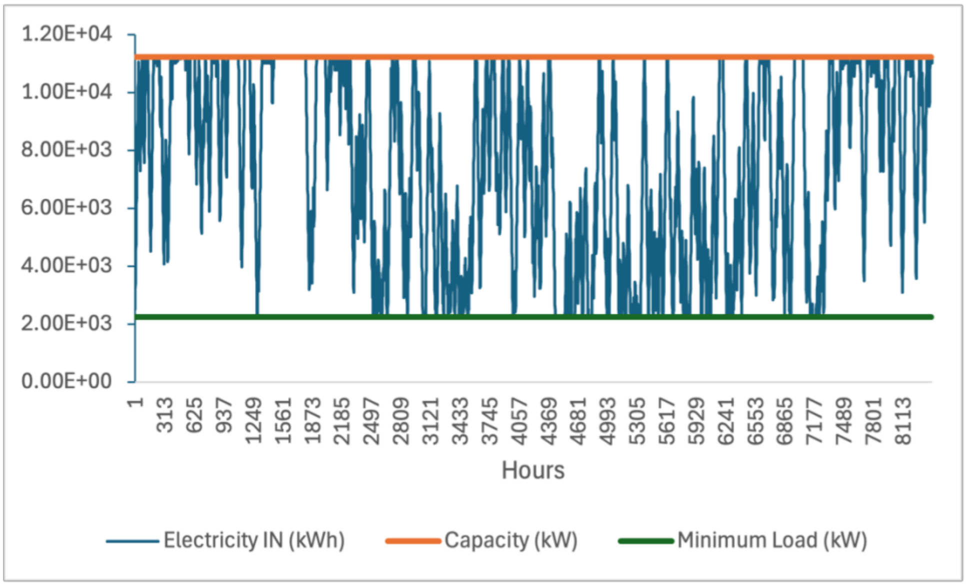

Figure E.12: HB+ASU capacity and minimum load verification. Representation of Eqn. E.12 and Eqn. E.13 over an operational year for the Pentland Firth: Tidal + Wind (High) example

HB+ASU ramping constraint:

$$-G_{HB_{Rampdown}} \cdot \sigma_C(HB + ASU) \leq Electricity_{in}(HB + ASU, t) - Electricity_{in}(HB + ASU, t - 1) \leq$$

$$G_{HB_{Rampup}} \cdot \sigma_C(HB + ASU) \qquad \forall t \in S_t \qquad \textit{(Eqn. E.14)}$$

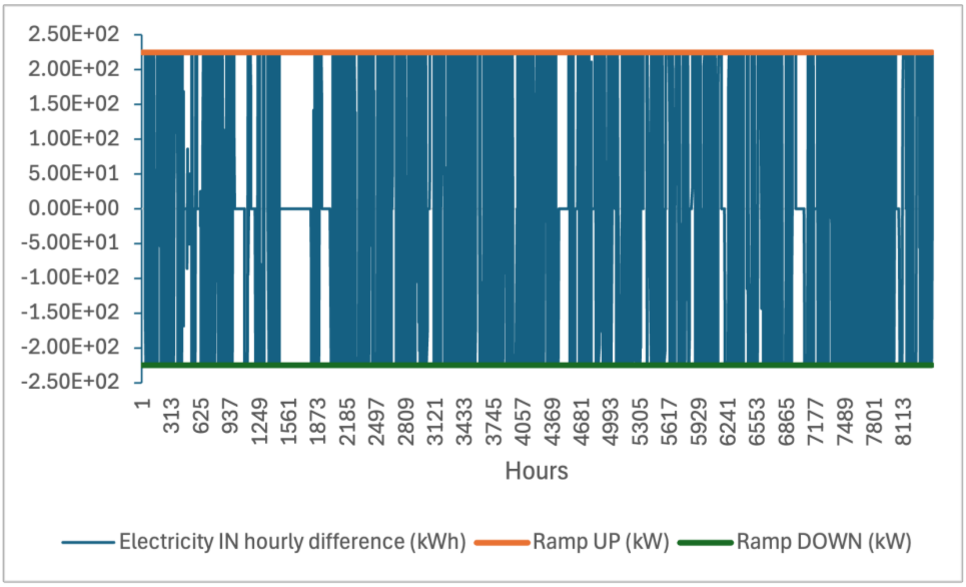

Figure E.13: HB+ASU ramping constraint verification. Representation of Eqn. E.14 over an operational year for the Pentland Firth: Tidal + Wind (High) example

The ramp down and ramp up limits are $G_{HB_{Rampdown}} = G_{HB_{Rampup}} = 2\%$ of rated capacity per hour. The minimum load is $G_{HB_{Min}} = 20\%$ of rated capacity [1].

The yearly ammonia production in tonnes is: $F = \frac{\sum_{t \in S_t} Ammonia_{out}(HB+ASU,t)}{1000\,\frac{kg}{t} \cdot HHV_{NH3}}$

E.9. Variable Correlation

To check the operation of the ammonia plant on an hourly basis, the input tidal + wind profile is shown in Figure E.14 with the corresponding hydrogen output from the electrolyser, battery storage level, hydrogen storage level, ammonia production from the HB and ammonia storage level. These values are shown over the first 700 hours (around 29 days) to account for two spring-neap cycles.

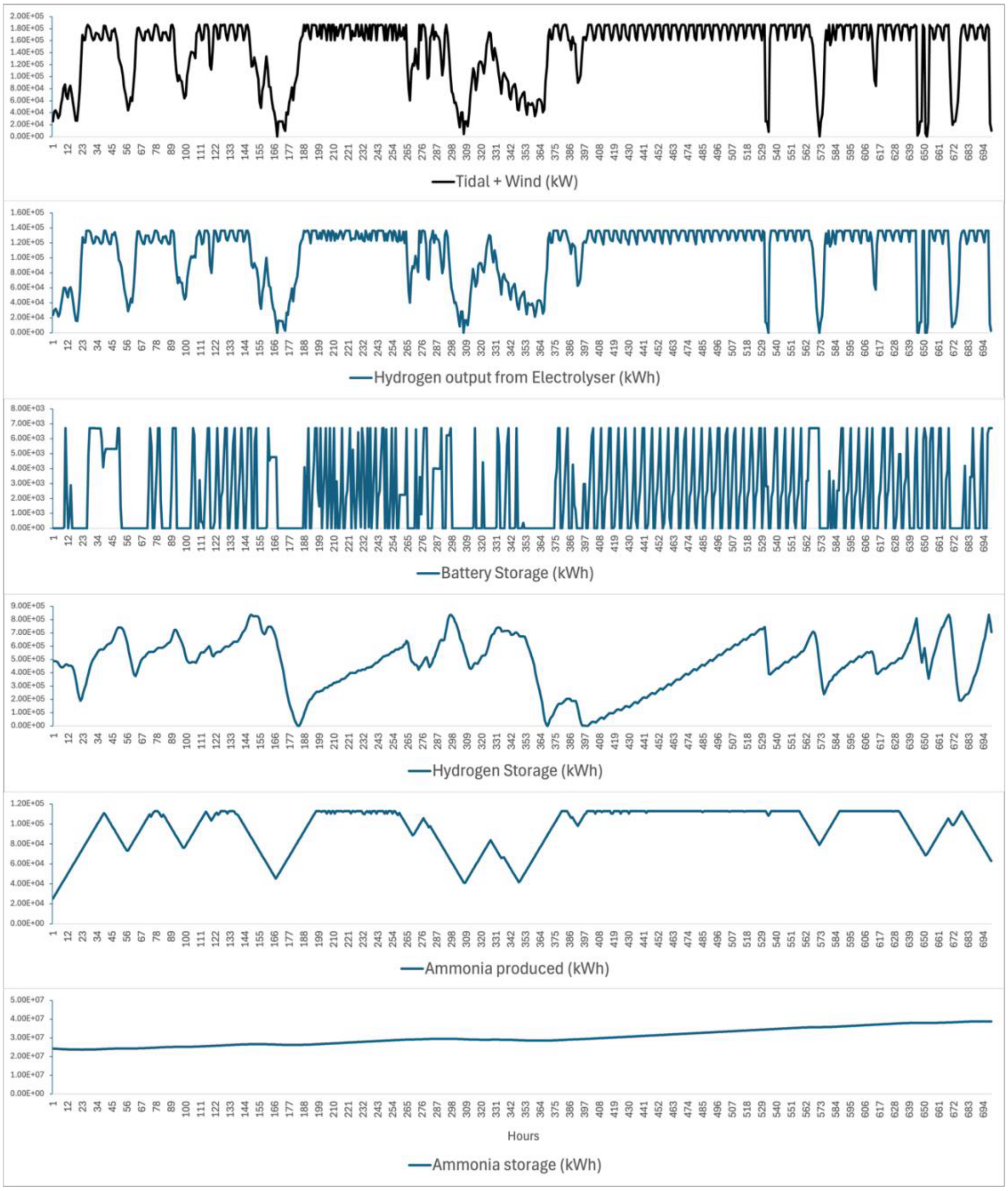

Figure E.14: Ammonia plant variable correlation for the first 700 hours of the Pentland Firth: Tidal + Wind (High) example

Due to the ramping constraints of the HB, the ammonia production doesn't follow the input power profile exactly (that is, it is smoother), whereas the hydrogen output from the electrolyser follows more closely the input power profile, as no ramping constraints are incorporated for the electrolyser. The ammonia production never reaches zero due to the minimum load restriction of the HB, whereas the hydrogen output from the electrolyser does reach zero, as no minimum load restriction is incorporated for the electrolyser.

The hydrogen and battery storage are used to back up the HB system. Their levels generally decrease when the input power profile decreases, and their levels generally increase when the input power profile is steady or increasing. The battery storage is distinct from the other variables as it has many charging and discharging cycles. The hydrogen storage follows a similar trend to the hydrogen output from the electrolyser, but it is slightly delayed since it functions as a storage component. The ammonia storage is external – it does not back up the HB system (Figure 4.1), so it does not correlate as closely with the input tidal + wind profile.

E.10. Levelized costs definitions

For Chapter 3: Eqn. 1 (p.65) represents the LCOA, Eqn. 2 (p.65) represents the CAPEX and Eqn. 3 (p.66) represents the OPEX.

For Chapter 4 and Chapter 5: Eqn. 1 (p.65) also represents the LCOA, but the CAPEX and OPEX equations are slightly altered to reflect the different scenarios modelled in these chapters.

In the CAPEX equation (Eqn. E.15), the offshore platform cost is removed as it is not required, and the offshore cable cost, $Cost_{Cable}$, is added:

$$CAPEX = \sum \sigma_R \, Cost_R + \sum \sigma_C \, Cost_C + \sum \sigma_{SC} \, Cost_{SC} + \sigma_{FC} Cost_{FC} + Cost_{Cable} \qquad \textit{(Eqn. E.15)}$$

In the OPEX equation (Eqn. E.16), the cost of water is removed as it is instead incorporated into the electrolyser energy conversion value (Section E.6. in Appendix E). This results in a negligible difference to the LCOA.

The operating and maintenance cost, $Cost_{OM}$, is 2% of the CAPEX **per year** [1][2]. This could be interpreted as $Cost_{OM} CAPEX$ (as in Chapter 3). The annuity factor $\left(\frac{i(1+i)^{PL}}{(1+i)^{PL-1}}\right)$ is added to the OPEX equation in Chapter 4 and Chapter 5 to explicitly make the CAPEX an annual cost.

$$OPEX = Cost_{OM}\left(\left(\frac{i(1+i)^{PL}}{(1+i)^{PL-1}}\right) \times CAPEX\right) \qquad \textit{(Eqn. E.16)}$$

In Chapter 3, the ammonia production is fixed at 100,000 t/year. In Chapter 4 and Chapter 5, the ammonia production per year is variable.

Glossary

Acronyms

ASU	Air separation unit
CAPEX	Capital cost
CF	Capacity factor
CfD	Contracts for Difference
CV	Coefficient of variation
ERA5	ECMWF (European Centre for Medium-Range Weather Forecasts) Reanalysis v5
FORWARD2030	Fast-tracking Offshore Renewable energy With Advanced Research to Deploy 2030MW of tidal energy before 2030
FPV	Floating photo voltaic
FVCOM	Finite Volume Community Ocean Model
HB	Haber-Bosch
HVAC	High voltage alternating current
LCOA	Levelized cost of ammonia
LCOE	Levelized cost of energy
LCOH	Levelized cost of hydrogen
LP	Linear programming
MILP	Mixed-integer linear program
MPC	Model Predictive Control
OPEX	Operating cost
OTEC	Ocean thermal energy conversion
PFOW	Pentland Firth and Orkney Waters

SSM	Scottish shelf model

Symbols

A	Swept area of turbine (m^2)
$Ammonia_{in}$ $Ammonia_{out}$	Ammonia flow into/out of plant equipment at each hour (kWh)
b	Water depth (m)
C	Capital cost of offshore platform (USD)
$CF(x, y)$	Conversion factor for the mass ratio of x to y
$CFa(Wind, t)$ $CFa(Tidal, t)$	Hourly capacity factor of wind/tidal at each hour
$Cost_C$	Cost of the component (USD/MW)
$Cost_{Cable}$	Cable cost (USD)
$Cost_{FC}$	Cost of fuel cell (USD/MW)
$Cost_{OM}$	Operating and maintenance costs (% of CAPEX)
$Cost_P$	Cost of offshore platform (USD)
$Cost_R$	Cost of renewable power (USD/MW)
$Cost_{SC}$	Cost of the storage component (USD/MWh for battery, USD/t for hydrogen)
$Cost_W$	Cost of desalinated water (USD/t)
C_p	Power coefficient
CV	Coefficient of variation (no unit)
d	Distance (km)
D	Plant capacity (t/day)

$Electricity_{in}$ $Electricity_{out}$	Electricity flow into/out of plant equipment at each hour (kWh)
F	Yearly ammonia production (tons/year)
$G_{HB_{Min}}$	Minimum load of the HB (% of rated capacity)
$G_{HB_{Rampup}}$ $G_{HB_{Rampdown}}$	HB ramp up and down limits (% of rated capacity per hour)
h	Wind turbine hub height (m)
h_{ref}	Reference height (m)
HHV_{H2} HHV_{NH3}	Higher heating value of hydrogen and ammonia (kWh/kg)
$Hydrogen_{in}$ $Hydrogen_{out}$	Hydrogen flow into/out of plant equipment at each hour (kWh)
i	Discount rate (%)
n	Number of turbines in a farm (no unit)
P	Power (MW)
PL	Plant lifetime (years)
P_r	Maximum power (MW)
P_T	Total power (MW)
r	Radius of turbine (m)
S_t	Time steps – 8,424 hours
$storage(Battery, t)$ $storage(H2\ store, t)$ $storage(NH3\ store, t)$	Level of battery storage, hydrogen storage and ammonia storage at each hour (kWh)
u	Fluid velocity (m/s)

u_{north}, u_{east}	Velocity in the northern and eastern directions (m/s)
u_o	Cut-out velocity (m/s)
u_r	Rated velocity (m/s)
u_{ref}	Reference velocity (m/s)
u_s	Cut-in velocity (m/s)
α	Hellmann exponent
σ_C	Installed capacity of the component (MW)
σ_{FC}	Installed capacity of the fuel cell (MW)
σ_P	Standard deviation (MW)
σ_R	Installed capacity of the renewable energy source (MW)
σ_{SC}	Installed capacity of the storage component (MWh for battery, t for hydrogen)
ρ	Density of fluid (kg/m^3)
μ_P	Mean (MW)
η	Wake effect correction factor (no unit)
γ	Blockage effect correction factor (no unit)
$\zeta(t)$	Curtailment at each hour (kWh)

References

[1] N. Salmon and R. Bañares-Alcántara, "Impact of grid connectivity on cost and location of green ammonia production: Australia as a case study," *Energy Environ. Sci.*, vol. 14, no. 12, pp. 6655–6671, 2021.

[2] R. M. Nayak-Luke and R. Bañares-Alcántara, "Techno-economic viability of islanded green ammonia as a carbon-free energy vector and as a substitute for conventional production," *Energy Environ. Sci.*, vol. 13, no. 9, pp. 2957–2966, 2020.

[3] IRENA (International Renewable Energy Agency), "Global Renewables Outlook: Energy transformation 2050," Abu Dhabi, United Arab Emirates, 2020. [Online]. Available: https://www.irena.org/publications/2020/Apr/Global-Renewables-Outlook-2020

[4] Z. Cesaro, M. Ives, R. Nayak-Luke, M. Mason, and R. Bañares-Alcántara, "Ammonia to power: Forecasting the levelized cost of electricity from green ammonia in large-scale power plants," *Appl. Energy*, vol. 282, p. 116009, 2021.

[5] H. Wang, P. Daoutidis, and Q. Zhang, "Harnessing the Wind Power of the Ocean with Green Offshore Ammonia," *ACS Sustain. Chem. Eng.*, vol. 9, no. 43, pp. 14605–14617, 2021.

[6] Z. Goss, D. Coles, and M. Piggott, "Economic analysis of tidal stream turbine arrays: a review," *arXiv*, pp. 1–29, 2021. [Online]. Available: http://arxiv.org/abs/2105.04718

[7] IRENA (International Renewable Energy Agency), "Renewable Power Generation Costs in 2021," Abu Dhabi, United Arab Emirates, 2022. [Online]. Available: https://www.irena.org/publications/2022/Jul/Renewable-Power-Generation-Costs-in-2021

[8] A. Fletcher, H. Nguyen, N. Salmon, N. Spencer, P. Wild, and R. Bañares-Alcántara, "Queensland green ammonia value chain: Decarbonising hard-to-abate sectors and the

NEM," Brisbane, Australia, 2023. [Online]. Available: https://www.griffith.edu.au/__data/assets/pdf_file/0035/1875167/No.2023-16-QLD-Green-Ammonia-Value-Chain-Main-Report.pdf

[9] D. Coles, A. Angeloudis, D. Greaves, G. Hastie, M. Lewis, L. Mackie, J. McNaughton, J. Miles, S. Neill, M. Piggott, D. Risch, B. Scott, C. Sparling, T. Stallard, P. Thies, S. Walker, D. White, R. Willden, and B. Williamson, "A review of the UK and British Channel Islands practical tidal stream energy resource," *Proc. R. Soc. A*, vol. 477, no. 2255, p. 20210469, 2021.

[10] M. J. Kaiser, B. Snyder, and A. G. Pulsipher, "Offshore Drilling Industry and Rig Construction Market in the Gulf of Mexico," U.S. Dept. of the Interior, Bureau of Ocean Energy Management, Gulf of Mexico OCS Region, New Orleans, LA. OCS Study BOEM 2013-0112, 2013. [Online]. Available: https://www.lsu.edu/ces/publications/2013/2013-0112.pdf

[11] M. Lewis, R. O'Hara Murray, S. Fredriksson, J. Maskell, A. de Fockert, S. P. Neill, and P. E. Robins, "A standardised tidal-stream power curve, optimised for the global resource," *Renew. Energy*, vol. 170, pp. 1308–1323, 2021.

[12] J. I. Encarnacion, C. Johnstone, and S. Ordonez-Sanchez, "Design of a Horizontal Axis Tidal Turbine for Less Energetic Current Velocity Profiles," *J. Mar. Sci. Eng.*, vol. 7, no. 7, p. 197, 2019.

[13] M. Liu, W. Li, R. Billinton, C. Wang, and J. Yu, "Probabilistic modeling of tidal power generation," in *2015 IEEE Power & Energy Society General Meeting*, 2015, pp. 1–5.

[14] Orbital Marine Power Ltd., "Orbital O2 2MW Tidal Turbine," Kirkwall, United Kingdom, 2018. [Online]. Available: https://marine.gov.scot/sites/default/files/project_information_summary.pdf

[15] C. Bak, F. Zahle, R. Bitsche, T. Kim, A. Yde, L. C. Henriksen, M. H. Hansen, J. P. A. A. Blasques, M. Gaunaa, and A. Natarajan, “The DTU 10-MW Reference Wind Turbine,” 2013. [Online]. Available: https://backend.orbit.dtu.dk/ws/portalfiles/portal/55645274/The_DTU_10MW_Reference_Turbine_Christian_Bak.pdf

[16] A. Ulazia, G. Ibarra-Berastegi, J. Sáenz, S. Carreno-Madinabeitia, and S. J. González-Rojí, “Seasonal correction of offshore wind energy potential due to air density: Case of the Iberian Peninsula,” *Sustainability*, vol. 11, no. 13, p. 3648, 2019.

[17] R. O’Hara Murray and A. Gallego, “A modelling study of the tidal stream resource of the Pentland Firth, Scotland,” *Renew. Energy*, vol. 102, no. B, pp. 326–340, 2017.

[18] R. O’Hara Murray and L. Campbell, “Pentland Firth and Orkney Waters Climatology 1.02,” Marine Scotland. Accessed: Jan. 06, 2022. [Online]. Available: 10.7489/12041-1

Publications and Presentations

Some parts of the three first-author journal papers and the one first-author conference paper were used in the thesis. In these four papers, the second author is included to acknowledge that their green ammonia model was used (but adapted by myself). The third (and last) author is my supervisor. A final paper will be written based on Chapter 5.

Journal Papers

- H. Driscoll, N. Salmon, and R. Bañares-Alcántara, "Technoeconomic evaluation of offshore green ammonia production using tidal and wind energy: a case study," *Energy Sources, Part A Recover. Util. Environ. Eff.*, vol. 45, no. 3, pp. 7222–7244, 2023.

- H. Driscoll, N. Salmon, and R. Bañares-Alcántara, "Exploiting the temporal characteristics of tidal stream power for green ammonia production," *Renew. Energy*, vol. 226, p. 120377, 2024.

- H. Driscoll, N. Salmon, and R. Bañares-Alcántara, "Optimal phasing of tidal stream power around the British Isles and within the English Channel for green ammonia production," *Renew. Energy*, vol. 241, p. 122335, 2025.

Conference Paper

- H. Driscoll, C. Palazzi, and R. Bañares-Alcántara, "The Role of Tidal Stream Energy in Green Ammonia and Green Hydrogen Production in The English Channel," in *OCEANS 2024 - Halifax*, 2024, pp. 1–4.

Conferences

- 1st Symposium on Ammonia Energy, Cardiff, UK, September 2022. Presented
- World Hydrogen Intelligence Day, Rotterdam, Netherlands, October 2023. Attended
- Worcester Energy Day, University of Oxford, UK, February 2024. Presented.
- OCEANS conference, Halifax, Canada, September 2024. Presented

Research visits

- Research visit to the European Marine Energy Centre (EMEC) in Orkney, UK, September 2023.

Poster presentations

- Launch event for Zero-carbon Energy Research Oxford (ZERO) and The Energy Systems Accelerator (Mini-TESA), University of Oxford, UK, May 2022
- Chemical engineering day, Department of Engineering, University of Oxford, UK, May 2023